1   *Review*

The Dark Target algorithm for observing the global aerosol system: Past, present and future

4   **Lorraine A. Remer [1,*], Robert C. Levy [3] , Shana Mattoo [3,4], Didier Tanré [5] , Pawan Gupta [6,7] ,**
5   **Yingxi Shi [1,2,3] , Virginia Sawyer [3,4] , Leigh A. Munchak [3,4,8] , Yaping Zhou [1,2] , Mijin Kim [3,9] ,**
6   **Charles Ichoku [10] , Falguni Patadia [3,6,7] , Rong-Rong Li [11] , Santiago Gassó [3,12] , Richard G.**
7   **Kleidman [3,4], and Brent N. Holben [3]**

8   [1] Joint Center for Earth Systems Technology – UMBC, Baltimore, Maryland 21250, USA. remer@umbc.edu;
9   yingxi.shi@nasa.gov; yaping.zhou-1@nasa.gov
10   [2] Department of Physics, University of Maryland-Baltimore County (UMBC), Baltimore, Maryland 21250,
11   USA. remer@umbc.edu; yingxi.shi@nasa.gov; yaping.zhou-1@nasa.gov
12   [3] NASA-Goddard Space Flight Center (GSFC), Greenbelt, Maryland 20771-0001, USA.
13   robert.c.levy@nasa.gov; shana.mattoo-1@nasa.gov; yingxi.shi@nasa.gov; virginia.r.sawyer@nasa.gov;
14   leigh.munchak@maxar.com; mijin.kim@nasa.gov; falguni.patadia@nasa.gov; santiago.gasso@nasa.gov;
15   richard.g.kleidman@nasa.gov; brent.n.holben@nasa.gov
16   [4] Science Systems and Applications (SSAI), Lanham, Maryland 20706, USA. shana.mattoo-1@nasa.gov;
17   virginia.r.sawyer@nasa.gov; leigh.munchak@maxar.com; richard.g.kleidman@nasa.gov
18   [5] Univ. Lille, CNRS, UMR 8518 - LOA - Laboratoire d'Optique Atmosphérique, Lille F-59000, France.
19   didier.tanre@univ-lille1.fr
20   [6] Science and Technology Institute, Universities Space Research Association (USRA), Huntsville, Alabama
21   35806, USA. pawan.gupta@nasa.gov; falguni.patadia@nasa.gov
22   [7] Marshall Space Flight Center, Huntsville, Alabama 35806, USA. pawan.gupta@nasa.gov;
23   falguni.patadia@nasa.gov
24   [8] Maxar Technologies, Westminster, Colorado 80234, USA. leigh.munchak@maxar.com
25   [9] Universities Space Research Association (USRA), Columbia, Maryland 21046, USA. mijin.kim@nasa.gov
26   [10] College of Arts & Sciences, Howard University, Washington, DC 20059, USA. charles.ichoku@howard.edu
27   [11] Naval Research Laboratory, Code 7231, Washington, DC 20375, USA. rong-rong.li@nrl.navy.mil
28   [12] Earth System Science Interdisciplinary Center (ESSIC), University of Maryland, College Park, Maryland
29   20737, USA. santiago.gasso@nasa.gov

31   *   Correspondence: remer@umbc.edu

33   **Abstract:** The Dark Target aerosol algorithm was developed to exploit the information content
34   available from the observations of the MODerate resolution Imaging Spectroradiometers (MODIS),
35   to better characterize the global aerosol system. The algorithm is based on measurements of the
36   light scattered by aerosols towards a space-borne sensor against the backdrop of relatively dark
37   Earth scenes, thus the name "Dark Target". Development required nearly a decade of research that
38   included application of MODIS airborne simulators to provide test beds for proto-algorithms and
39   analysis of existing data to form realistic assumptions to constrain surface reflectance and aerosol
40   optical properties. This research in itself played a significant role in expanding our understanding
41   of aerosol properties, even before Terra-MODIS launch.   Contributing to that understanding were
42   the observations and retrievals of the growing AERONET network of sun-sky radiometers, which
43   has walked hand-in-hand with MODIS and other aerosol algorithm development, and after launch
44   providing validation of the satellite-retrieved products. The MODIS Dark Target products
45   prompted advances in Earth science and applications across such subdisciplines as climate,
46   transport of aerosols, air quality and data assimilation systems. Then as the Terra and Aqua MODIS
47   sensors aged, the challenge was to monitor the effects of calibration drifts on the aerosol products

48 and to differentiate physical trends in the aerosol system from artifacts introduced by instrument
49 characterization.   Our intention is to continue to adapt and apply the well-vetted Dark Target
50 algorithms to new instruments including both polar orbiting and geosynchronous sensors.   The
51 goal is to produce an uninterrupted time series of an aerosol climate data record that begins at the
52 dawn of the 21st century and continues indefinitely into the future.

53   **Keywords:** aerosol, remote sensing, MODIS, VIIRS
54

1. Introduction

56 The global aerosol system [1] [2] [3] is an integral component of Earth system science [4]. The
57 concept of the global aerosol system brings a holistic perspective to aerosol science, viewing each
58 specific aerosol source, type, transport, transformation, influence and sink as part of a global whole.
59 The concept encourages a far-reaching scope that encompasses aerosol influence on climate,
60 hydrology, biology and health, and how these other systems affect aerosols. The examination of
61 aerosols as a global system, rather than a local one, is only 30 years old[1]. An important factor in
62 creating this shift in perspective from local to global was tied directly to the advent of satellite
63 remote sensing of aerosol.
64

65 Satellites provide the best means of observing and characterizing the global aerosol system [1].
66 These space-borne sensors point at Earth scenes and measure radiation that has been reflected or
67 emitted by the Earth's surface and atmosphere. Satellite aerosol remote sensing requires
68 deconvolving the signal measured by the sensor into a component originating from the Earth's
69 atmosphere from that originating from the surface beneath, and then isolating the aerosol signal
70 from other atmospheric constituents. The process requires extensive knowledge of aerosol optical
71 properties: the degree to which particles emit, absorb or scatter incident radiation. For the purpose
72 of this paper, we will consider only the absorption and scattering of solar radiation, and not
73 emission at longer wavelengths. Particle properties determine the fraction of radiation scattered in a
74 particular direction (i.e. towards the satellite), and this information is wavelength dependent.
75 Higher particle concentrations increase the measurable radiation scattered towards the satellite. The
76 range of radiation levels measured by the sensor are translated into a quantification of aerosol
77 loading in the observed scene. Particle optical properties depend on their chemical composition as
78 well as their size and shape. If the satellite sensor measures sufficient angular and/or spectral
79 information, and if the aerosol signal can be sufficiently separated from the signals due to the
80 surface and other atmospheric constituents, then other information about the aerosol physical
81 properties can be inferred from the measurements.
82

83 Using satellite observations to retrieve quantitative information about aerosols began with the
84 Multi Spectral Scanner (MSS) on board the Earth Resources Technology – 1 (ERTS-1) satellite, a
85 precursor to the modern Landsat missions [5] [6] [7]. These studies from the 1970s proved the

---

[1] Using Google Scholar, no scientific works use the term "global aerosol system" before 1990, only a handful from 1990 to 2000, and then over hundred from 2000 to 2010. [11] is the first use found.

86 concept of quantifying aerosol from space, but the MSS imagery with its nadir-only view and repeat
87 cycle of 18 days could not adequately visualize or quantify aerosol as a global system.   The
88 technique of quantitative retrieval was adapted to the Advanced Very High Resolution Radiometer
89 (AVHRR) on board a series of NOAA polar orbiting satellites that had a larger swath and more
90 frequent repeat cycle [8]. It was this AVHRR-based aerosol product, available only over ocean, that
91 provided the first visualizations of aerosol as a global system [9].
92
93 Motivation was high to expand upon this pioneering work and fully develop a global aerosol
94 product which could characterize aerosol as a global system. NASA had instituted "Mission to
95 Planet Earth"in the early 1990s [10] and was developing a new generation of sensors with expanded
96 capabilities called the Earth Observing System. As part of this effort NASA was investing in science
97 teams that would produce a set of operational products to characterize the many facets of the Earth
98 system.   Aerosols would be one of those products. Producing an operational algorithm that would
99 run automatically, efficiently, globally, and in all aerosol and environmental conditions, was a
100 significant challenge beyond the proof-of-concept studies and the early NOAA AVHRR products.
101 Despite the challenges, the scientific value of a successful product would be high.
102
103 The first operational aerosol algorithm applied to the MODerate resolution Imaging
104 Spectroradiometer (MODIS) data was ready at the time of NASA's Terra satellite launch in late
105 1999, after nearly a decade of development [12] [13]. The algorithm made use of enhanced MODIS
106 instrument capabilities such as a broader spectral range, wide (2330 km) swath, and on-board
107 calibration to characterize the aerosol system in a globally consistent manner.   In parallel to the
108 development of the aerosol algorithm, NASA invested in the development of abilities to validate
109 the products that the algorithm would produce.   Validation efforts included aircraft instruments
110 and airborne campaigns, but the primary suborbital initiative that would dovetail with the MODIS
111 aerosol algorithm for validation was the creation and expansion of the AERosol RObotic NETwork
112 (AERONET: [14]). The combination of the MODIS aerosol product with AERONET to support its
113 development and validation became an irresistible one-two punch that changed our perception of
114 the global aerosol system forever.
115
116 The original algorithm, termed Dark Target (DT) [15] for its use of dark surfaces as targets of
117 opportunity to measure the contrast of the bright aerosol above, has undergone continuous
118 modifications and improvements over the two decades it has been in operation [15] [16] [17] [18]
119 [19] [20] [21] [22] [23] [24].   These changes were implemented as remote sensing science
120 progressed, as validation identified areas of concern that could be remedied, and as the instruments
121 themselves aged.   Change is a necessity in improving a satellite product, and yet change interferes
122 with the goal of being able to use these products to discern trends in the global aerosol system. To
123 maintain consistency in the products there have been major efforts to reprocess the archive of data
124 from the beginnings of missions with more modern computational resources Yet, consistency and
125 continuity remain challenging.
126
127 The impact of the DT aerosol algorithm on remote sensing science, on Earth science and on related
128 applications has been immense. Initially applied to the MODIS sensors on the Terra and Aqua

129   satellites, the algorithm grew to be much more than "the MODIS aerosol algorithm". The algorithm
130   is now retrieving aerosol properties from new sensors such as the Visible Infrared Imaging
131   Radiometer Suite (VIIRS) on the Suomi-National Polar-orbiting Partnership (S-NPP) satellite and
132   has been adapted non-operationally for a fleet of geosynchronous sensors. In addition to direct
133   adaptation the DT algorithm has inspired other algorithm families in a variety of ways. including
134   the introduction of techniques for cloud and snow masking, and the development of best-practices
135   for the validation of satellite-based aerosol products. These influences will be discussed in Section
136   7.5. Meanwhile, many advances in understanding how aerosols affect climate, clouds, biological
137   systems and air quality can be traced directly to research using DT products. We understand the
138   global aerosol system now, much better than we did twenty years ago, in part due to the influence
139   of this one algorithm.
140
141   The purpose of this paper is:
142   (a) to illustrate an evolving algorithm development so as to provide a template for present and
143   future development teams to learn from example,
144   (b) to provide an annotated reference list of a multi-decade body of work
145   (c) to critically examine the concept of continuity with a continuously evolving algorithm applied
146   to aging sensors over a twenty- year period,
147   (d) to preview future characterization of the global aerosol system using the DT algorithm as an
148   example as the community moves forward to new sensors

149   **2. Observing the global aerosol system before MODIS**
150
151   Before the launch of Terra with the first MODIS instrument at the end of 1999, there were already
152   satellite-derived views of the global aerosol system.   Some of these operational and research
153   products from the 1990s proved to be direct predecessors of the MODIS DT product. One of these
154   was the NOAA operational aerosol product that used inputs from the AVHRR instruments aboard
155   NOAA's polar-orbiting satellite series [8] [9] [25] [26] [27] [28]. The NOAA product was based on
156   the "dark target" premise, that aerosol above a dark surface would appear brighter. Furthermore,
157   with appropriate assumptions about the surface reflectance and the properties of the aerosol and
158   atmosphere, the aerosol loading could be quantified as an aerosol optical thickness (AOT) or
159   aerosol optical depth (AOD) through radiative transfer modeling. For the remainder of this paper
160   AOT and AOD will be used interchangeably.   AVHRR had only two reflective bands centered at
161    $0.63\,\mu$m and $0.86\,\mu$m.   The NOAA AVHRR algorithm used one band ($0.63\,\mu$m) and only derived
162   AOD over the ocean where the reflectance of the dark ocean surface was readily characterized. The
163   algorithm was applied to 4 km native pixel resolution data, and clouds were screened using a
164   relatively simple 2x2 pixel spatial variability test, discarding all 4 pixels whenever the difference
165   between the maximum and minimum value exceeded a threshold.   Once determined to be
166   'suitable' for retrieval, the aerosol properties were assumed to be static, set to best represent state-
167   of-the-art understanding of maritime aerosol - a single mode size distribution, with a set value of
168   the real part of the refractive index, and no absorption (imaginary part set to zero). While crude,
169   this AOD product was successfully validated by comparison with ground-based in situ
170   measurements at rare island sites.   Such validation could only be qualitative, as the in-situ
171   measurements did not measure total column aerosol loading [8].   Later when ground-based total

172   column ambient measures of AOD were available from ground sites, the NOAA AVHRR product
173   made use of this sunphotometer-measured AOD for validation [9].

174

175   In addition to NOAA's operational algorithm, there were other research algorithms applied to
176   AVHRR.   These research algorithms also limited retrievals to over oceans, but these algorithms
177   employed both reflective wavelengths from AVHRR.   The added wavelength permitted a retrieval
178   of spectral AOD at two wavelengths [29] [30] [31] [32] [33] or three wavelengths [34] and the
179   Angstrom Exponent. These multi-wavelength algorithms allowed for a more sophisticated
180   representation of the aerosol system. Using [31] as an example, they used fixed bi-modal size
181   distributions and fixed complex refractive index. Validation was also more sophisticated, as they
182   made use of the fledgling AERONET network to directly compare both AOD and Angstrom
183   Exponent. Due to the rarity of validation sites over ocean, the [31] validation data set consisted of
184   only 27 collocation points. Today, nearly 30 years later, the AVHRR data have been reprocessed
185   with modern aerosol algorithms, and a lengthy time series of AOD is available over both land and
186   ocean [35], and there are thousands of validation points.

187

188   While the AVHRR aerosol retrievals provided the theoretical underpinnings for the MODIS DT
189   algorithm, there were also other aerosol retrievals in the 1990s working towards global views of the
190   aerosol system. For example, there were retrievals applied to ultraviolet sensors such as the Total
191   Ozone Monitoring Sensor (TOMS) [36]. Because the TOMS aerosol algorithm was based on
192   different physical principles and did not directly influence the development of the MODIS DT
193   algorithm, it is outside the scope of this paper.

194

195   The algorithms applied to AVHRR in the 1990s provided an unprecedented view of the aerosol
196   system, but they were working with a sensor that was not designed for quantitative aerosol
197   retrieval.   AVHRR had limited spectral range, broad bands that were affected by water vapor
198   absorption, no on-board calibration and a native pixel resolution that made cloud masking a
199   challenge. Furthermore, the NOAA satellites' equator crossing times drifted during each satellite's
200   lifetime, introducing uncertainty in characterizing global systems. Anticipating the need for
201   quantitative observations of the entire Earth System, including aerosol, NASA planned for a series
202   of missions called the Earth Observing System (EOS). The instruments aboard the EOS satellites
203   were designed specifically to meet the requirements of science teams that were responsible for
204   producing science products that would meet the needs of the international science community.
205   MODIS, in particular, was the flagship EOS instrument. Compared to AVHRR, MODIS had 7 times
206   the number of spectral bands, narrower channels in window regions, on-board calibration with an
207   entire calibration team to assure characterization, and pixel resolution as fine as 250 m at nadir. This
208   new hardware would be available to propel aerosol remote sensing into a new age.

209   **3. Developing the first global MODIS aerosol product**

210   The first global MODIS aerosol product made use of the advances provided by the MODIS
211   instrument and permitted operational quantitative aerosol retrieval over land, as well as ocean. This
212   represented a significant challenge as the algorithm must evaluate a number of scenarios and
213   observation conditions, including avoiding pixels with clouds, before carrying out the extraction of
214   aerosol related information. Because there was no prior experience of carrying out aerosol detection

215 using multiple visible and shortwave infrared (SWIR) channels much of this approach had to be
216 created from scratch. Conceptually, the heart of the retrieval was and still remains, the comparison
217 of satellite-measured radiances with pre-calculated Top-of-Atmosphere (TOA) radiances computed
218 with the modeled aerosol properties. The observed and modeled radiances were compared via a
219 cost-function where the best match or matches were reported as the retrieved values for the pixel
220 under observation [12] [13]. This methodology is commonly referred to in the DT algorithm concept
221 as a Look Up Table (LUT) approach. The quantifiable signal was the contrast between a bright
222 aerosol layer over a dark surface, the aerosol brightening the scene because of the particles'
223 scattering properties.
224
225 The primary challenge for the DT algorithm was the separation between the contribution from the
226 surface and the atmosphere. Because the DT algorithm is limited to "dark" scenes where the surface
227 contribution is minimal, most of the satellite-observed radiance originates from the atmosphere and
228 the challenge is mitigated. There are two types of Earth surfaces that offer "dark" scenes, non-glint
229 open ocean (coastal zones require a specific treatment as explained in section 5.1.1) and dark
230 vegetated landscapes over land.   Of the two types of "dark" scenes, the ocean surface is easier to
231 characterize, allowing more aerosol information to be derived from the satellite measurements. The
232 different challenges and opportunities associated with the two types of surfaces led to the
233 development of two independent algorithms, one for over oceans and the other for vegetated land
234 surfaces.   These two algorithms are described in the next two sections.
235

236 *3.1. Retrievals of aerosol loading and particle size over oceans*
237 Over ocean, the operational and research grade AVHRR retrievals provided the necessary
238 inspiration for the MODIS algorithm.   However, a MODIS algorithm having more spectral
239 information than the limited AVHRR, should be able to use this information to better retrieve
240 particle size parameters [13]. MODIS has two bands at 0.25 km and five at 0.50 km spatial
241 resolution, and except for cloud masking, these seven bands provided all the measured information
242 for the algorithm.   With seven bands, it was hoped that there would be seven "pieces of
243 information" and that the algorithm could therefore retrieve seven characteristics of the aerosol
244 particles. This might be AOD plus six constraints on the particle size distribution, shape, absorption
245 and aerosol layer height. In practice this is not the case, as for instance, over ocean, there is variable
246 ocean color due to chlorophyll blooms and other hydrosols. Because this variability so highly
247 affects blue wavelengths, the 0.47 μm channel cannot be used for retrieval. Even with the remaining
248 wavelengths (0.55 μm, 0.66 μm, 0.86 μm, 1.24 μm, 1.63, μm and 2.11 μm) the available pieces of
249 information are fewer than six, as the information from each wavelength is not independent [37].
250 As it turned out, the DT algorithm over ocean is able to retrieve the AOD at one wavelength
251 (chosen to be 0.55 μm) and then provide one or two constraints on the size distribution [13].
252
253 The LUT was created with four fine modes and five coarse modes, each an independent lognormal
254 single mode size distribution with assigned complex refractive index.   The terminology fine and
255 coarse mode indicated modal radii in the submicron (ie. < 1 μm) and supermicron (ie. > 1 μm)
256 ranges, respectively, although noting the tails of each mode would overlap. The aerosol models
257 used to represent the single mode fine and coarse modes for the LUT calculations were based on

258 existing literature [38], modified by field experiment results [39] [40] and early AERONET inversion
259 products [14] [41] [42] [43]. Operationally, the algorithm matches one fine (out of 4) and one
260 coarse mode (out of 5), iterating through each of 20 combinations of fine and coarse modes, while
261 adjusting the number of particles in each mode. The 'solution' is represented by the combination
262 (or combinations) of fine and coarse modes that most closely match(es) the observed spectral
263 reflectances at the top of atmosphere. The two modes and the relative weight between the two
264 constitute the retrieved size distribution. The governing equation in the LUT is shown in
265 Equation (1),
266

$$\rho_\lambda{}^* = \eta\rho_\lambda{}^{*f} + (1-\eta)\rho_\lambda{}^{*c} \tag{1}$$

267 where $\rho_\lambda{}^*$ is the top of atmosphere reflectance at wavelength λ, the superscripts f and c indicate fine
268 mode and coarse mode, respectively.
269

270 The parameter η is the "fine mode weighting" FMW or "fine mode fraction" (FMF). Note that η is
271 defined by *weighting of reflectances*, not by AOD. The LUT is created, indexed by AOD at 0.55 *μ*m for
272 all wavelengths of reflectance. The parameter, η, as defined, is not wavelength dependent. η
273 represents the actual relative sizes of the particle volume in each lognormal mode. [16] show in
274 an Appendix that η is also the ratio of the fine mode AOD at 0.55 *μ*m to the total AOD at 0.55 *μ*m,
275 assuming single scattering. The η parameter has proved to be a useful indicator of particle size and
276 type within the context of the DT products [44] [45] [46], and it correlates with other retrieval
277 products of similar, but not exactly the same definition [47]. However, the parameter is tightly
278 bound to the construction of the DT algorithm. Its climatological statistics vary with nuanced
279 changes in either the algorithm or instrument calibration [48] [49], and the translation of η from a
280 weighting of reflectances to a weighting of AOD will break down as aerosol loading increases and
281 the assumption of single scattering breaks down.
282

283 The conclusions in [37] assuming the single scattering approximation indicate that AOD and η are
284 the two main products of the ocean retrieval, and that if one mode dominates the size distribution,
285 there is sufficient information to also retrieve the effective radius of the dominant mode. The
286 algorithm is not sensitive to all other parameters of the aerosol: other details of the size distribution,
287 complex refractive index, degree of nonsphericity, or aerosol layer height. This does not mean that
288 uncertainty cannot be introduced into the retrieval by these other factors, but it does mean that the
289 algorithm cannot retrieve these other parameters with any skill. Understanding these strengths and
290 weaknesses of the information content and retrieval proved to be essential in constructing a robust
291 operational algorithm. Besides reconciling ourselves to the limitations of information content, we
292 also had to accept that the inversion did not result in a unique solution. There could be multiple
293 combinations of modes that could produce spectral reflectance at the top of the atmosphere that
294 would match satellite-measured values equally well. To choose the best solution that was only
295 slightly better than the second-best solution did not necessarily provide the most useful description
296 of aerosol parameters. Operationally the algorithm reported both the "best" solution and also the
297 "average" of all solutions that met minimum matching requirements. In testing the algorithm and
298 retrieval, the "average" solution was identified as the more robust of the two, and all statistics,

299 climatology and validation of the ocean aerosol algorithm were based on the results of the
300 "average" solution.
301
302 The proto-ocean algorithm was first tested with observations from the MODIS airborne simulator
303 (MAS) [50] where the results showed promising quantification of smoke plumes over the ocean [13]
304 [51]. A few years later the Tropospheric Aerosol Radiative Forcing Observational Experiment
305 (TARFOX) field experiment [52], which took place more than three years before Terra launch,
306 provided a more comprehensive pre-launch test of the ocean aerosol algorithm. In that experiment,
307 the NASA ER-2 aircraft flew at high altitude (20 km) collecting spectral imagery that would mimic
308 MODIS measurements to use as input to the proto-algorithm [39]. Other aircraft flying at low
309 altitude provided ground truth for verifying the retrieval [53] [54]. Of particular importance was
310 the Ames Airborne Tracking Sunphotometer [55] [56] flying on the University of Washington C131-
311 A aircraft that measured the spectral dependence of the AOD over the ocean, but below the aerosol
312 layer. Also there was a ship sailing with an AERONET sunphotometer on board and a station on
313 the island of Bermuda that provided additional validation data [52]. Spectral AOD retrieved from
314 MODIS-like imagery at high altitude could be compared with the low altitude measurements. For
315 a majority of the passes across several days of flights, the proto-algorithm showed that it could
316 match the ground truth across the spectrum [39]. See Figure 1. There were a few situations where
317 the match was less than optimal, which caused us to make modifications to the algorithm, mostly in
318 terms of expanding the glint mask. Masking for clouds, glint, etc., will be addressed in Section 3.4.
319 Assumptions regarding the ocean reflectance are discussed in section 5.5.

320
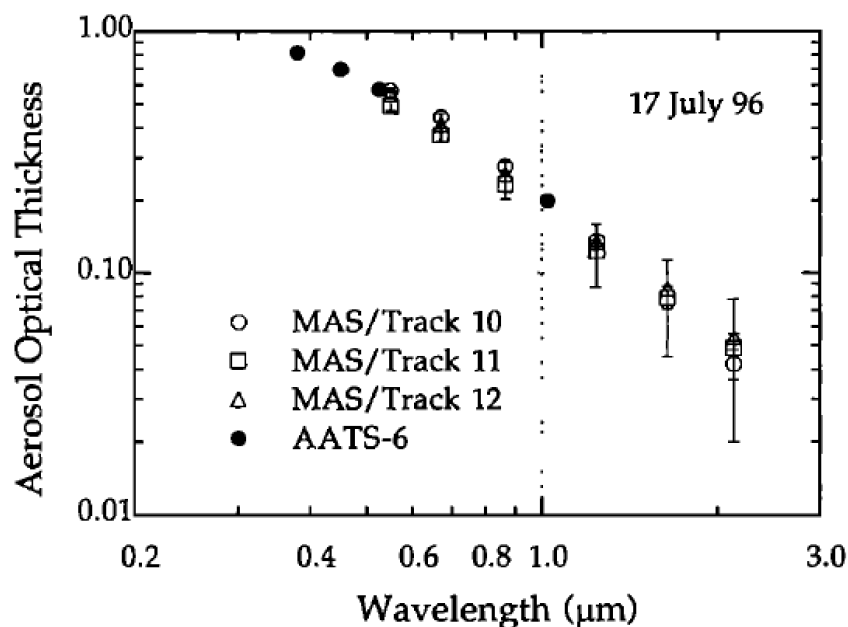
Figure 1. Aerosol optical thickness measured by the Ames Airborne Tracking Sunphotometer
(AATS-6) aboard the low flying C-131A aircraft and derived from the MODIS Airborne Simulator
(MAS) measurements made at high altitude from the ER-2 as a function of wavelength. The
comparison is made over a point located at 37.49°N/74.16°W around 1830 UTC. Three subsequent
tracks of the ER-2/MAS are plotted. Reprinted with permission from John Wiley and Sons.

326 The key elements contributing to a successful aerosol over ocean algorithm were:

327 • Basing the retrieval in physical understanding of aerosols, their environment and radiative
328 transfer.
329 • Avoiding the blue channel in the retrieval to minimize uncertainty introduced by ocean color.
330 • Understanding the limitations of the information content and designing a simplified retrieval
331 based on these limitations, but with sufficient flexibility to find the right solution.
332 • Introducing the new parameter, η, which proved to be the key for many subsequent applications
333 using the MODIS DT product [44] [57]
334 • Accepting that the algorithm produced non-unique solutions and adapting expectations to make
335 use of the multiple solutions.
336 • Using new total, column ambient measures of aerosol optical properties to modify the
337 assumptions in the LUT.
338 • Developing and testing the algorithm from field experiment data, especially making use of over
339 ocean measurements of spectral AOD from sunphotometers on aircraft, ships and islands.

340 The ocean algorithm proved to be exceptionally robust, requiring only cosmetic changes in the
341 20 years since launch.   The same basic algorithm continues to produce highly accurate operational
342 aerosol products over the global oceans from the MODIS instrument aboard NASA's Terra and Aqua
343 satellites, the Visible Infrared Imaging Radiometer Suite (VIIRS) instrument aboard NOAA's Suomi-
344 NPP and NOAA-20 polar orbiting satellites, and has been adapted for non-operational purposes
345 using inputs from instruments on geostationary satellites including NOAA's Advanced Baseline
346 Imager (ABI) on GOES-East and GOES-West and the Advanced Himawari Imager (AHI) on the Japan
347 Meteorological Agency's Himawari-8 satellite.

348 *3.2. Retrievals of aerosol loading over land*

349 Over land, there was no precedent for a global operational aerosol product from AVHRR, as there
350 had been for the ocean retrieval. Instead the new algorithm was inspired by a prior study [58] that
351 made use of dark dense vegetation (DDV) to quantify the aerosol loading. In that early study, both
352 surface reflectance of the DDV targets and the aerosol optical properties were given a priori
353 assumed values. For an operational algorithm to have global validity, those rigid assumptions
354 would require greater flexibility.   There were two significant innovations that made an operational
355 global over land aerosol retrieval possible: (1) parameterization of the land surface reflectance and
356 (2) development of total column, ambient, aerosol optical models [12].

357 3.2.1. Over land surface parameterization

358 The land surface reflectance parameterization was based on an observation that there is a physical
359 connection between light absorption in visible (VIS) wavelengths involved in photosynthesis (blue
360 and red) due to specific pigments, and the light absorbed by liquid water in the shortwave infrared
361 (SWIR) in vegetation.   The pigments are dissolved in liquid water in the plant leaves.   Therefore,
362 where there is photosynthesis occurring, vegetation is green due to absorption in the blue and red
363 by pigments, and dark in the SWIR due to absorption by the corresponding liquid water in the leaf.
364 Furthermore, non-vegetated surfaces appear darker to the eye (in visible) when wet, because of
365 changes to the refractive index when water fills in between the soil or sand grains, again linking
366 light absorption in the visible to the SWIR.   Other factors contribute to reinforcing this relationship
367 between the VIS and SWIR, including shadowing, especially in plant canopies, that darkens the
368 scene throughout the reflective spectrum. This physically-based hypothesis was tested and refined
369 using the 3.75 μm channel on AVHRR for the SWIR wavelength [59], from Landsat Thematic
370 Mapper images and from data collected by the NASA airborne AVIRIS imager now using the 2.2
371 μm for the SWIR[60], and from spectrometer data collected by hand from low-flying light aircraft

372   [61]. The relationship was also supported by theoretical analysis [62]. The result of this work
373   allowed the surface visible reflectance to be parameterized by the surface reflectance in the SWIR.
374   At launch this parameterization was a simple $\rho^{sfc}_{0.47} = 0.25\,\rho^{sfc}_{2.1}$ and $\rho^{sfc}_{0.66} = 0.50\,\rho^{sfc}_{2.1}$, where $\rho^{sfc}_{0.47}$,
375    $\rho^{sfc}_{0.66}$ and $\rho^{sfc}_{2.1}$ are the surface reflectances at 0.47 μm, 0.66 μm and 2.1 μm, respectively.
376
377   Later, we used surface reflectance derived from top-of-atmosphere MODIS measurements
378   atmospherically corrected from collocated AERONET measurements to confirm and modify this
379   simple parameterization [19].   Today we can obtain tens of thousands of ordered pairs (VIS, SWIR)
380   surface reflectances using atmospheric correction at each of hundreds of AERONET stations
381   distributed globally over a broad dynamic range of surface conditions.   Using previously
382   unpublished data, Figure 2 demonstrates the relationship between the surface red (0.66 μm)
383   reflectance and the surface SWIR (2.11 μm) reflectance from atmospherically corrected Aqua-MODIS
384   measurements collocated with AERONET from 2015-2019.   The data covers the range in SWIR
385   Normalized Difference Vegetation Index (NDVI$_{SWIR}$) from highly vegetated (>0.70) to bare surfaces
386   (<0.15).   NDVI$_{SWIR}$ is defined as,

$$NDVI_{SWIR} = \left(\rho^*_{1.24} - \rho^*_{2.11}\right)/\left(\rho^*_{1.24} + \rho^*_{2.11}\right) \tag{2}$$

387   where $\rho^*_{1.24}$ and $\rho^*_{2.11}$ are the top of atmosphere reflectances at 1.24 μm and 2.11 μm. In Figure 2 we
388   see that even when using modern data and a different technique we still arrive at a relationship
389   between VIS and SWIR surface reflectance that is very close to the at-launch parameterization.
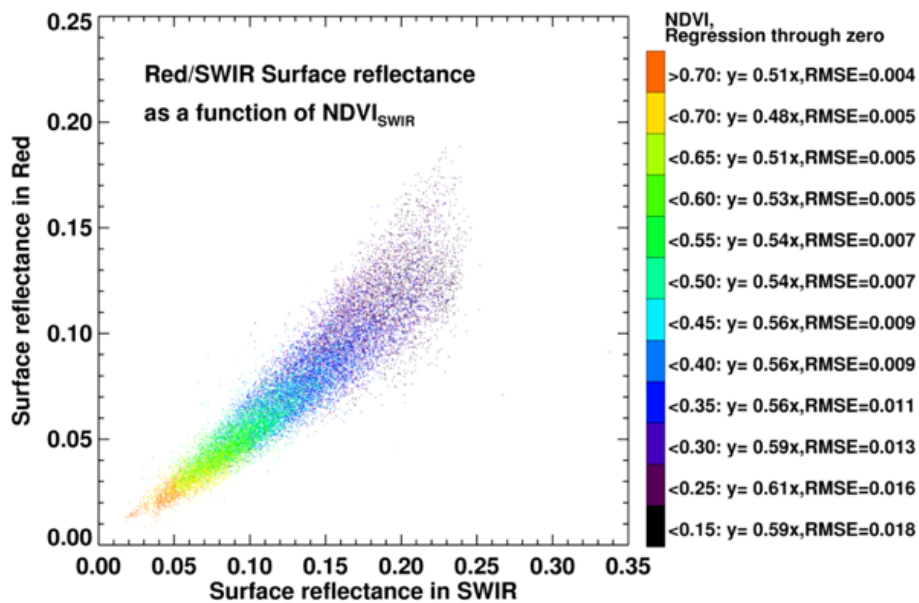
391   **Figure 2.** Surface reflectance in the red (0.66 μm) plotted against surface reflectance in the SWIR (2.11
392   μm) obtained from applying atmospheric correction to top of the atmosphere MODIS observations at
393   collocated AERONET stations from 2015-2019. Over 20,000 collocations are plotted.   Colors denote
394   ranges of NDVI$_{SWIR}$ highest values of NDVI$_{SWIR}$ corresponding to the brightest barest surfaces and the
395   lowest values of NDVI$_{SWIR}$ corresponding to the darkest most vegetated surfaces. Throughout the
396   range of NDVI$_{SWIR}$, the red surface reflectance ranges from 0.48 to 0.61 of the SWIR.

397   The advantage to using the SWIR is that aerosol scattering is much reduced at longer
398   wavelengths for submicron aerosol particles, and even for larger particles such as dust, the
399   wavelength is less sensitive to the aerosol than in the VIS.   The original idea was to use the SWIR
400   band to characterize the surface reflectance, then apply that information to the blue and red bands in
401   the VIS. The algorithm would employ simple single channel retrievals in the blue and red bands,

402   using the surface reflectance derived empirically from the SWIR to act as the bottom boundary
403   condition in the radiative transfer equation.   The second generation over land algorithm replaced
404   the single channel retrievals with a three-channel inversion (0.47 µm, 0.66 µm, 2.1 µm), but it
405   continued to incorporate similar empirical surface reflectance parameterizations.
406
407   At the time of Terra launch, the use of the SWIR to parameterize surface reflectance in the VIS
408   was extremely innovative.   It allowed a global operational retrieval to begin producing aerosol
409   products at launch.   There was no need to acquire a global data base of land surface reflectance over
410   several years, and it automatically corrected for seasonal or land use changes. Although the simple
411   empirical relationships developed from early aircraft measurements and later expanded using
412   atmospherically corrected MODIS reflectance may represent "average" global conditions, they do
413   contain significant scatter around those averages. Applying new dependencies on scattering angle
414   and vegetation index only cut the scatter marginally. Other algorithms that constrain surface
415   reflectance by means of a data base or require temporal stability over a finite time period can
416   outperform the DT land retrieval, suggesting that as we move forward, this method that was highly
417   innovative twenty years ago may not be the best choice for applications where the land surface can
418   be well known using a-priori information.

419   3.2.2. Over land aerosol optical models

420   The second innovation of the original DT aerosol retrieval over land was the development of
421   new dynamic aerosol models for the LUT calculations. These models were based on the fledgling
422   inversions of ground-based radiometer measurements of the angular sky radiance [40] [63] [64] [65].
423   By dynamic we meant that the aerosol optical properties were indexed by a total column parameter,
424   such as AOD, and allowed to vary in optical properties as a function of that index.   In this way the
425   aerosol optical properties for a certain location would be represented by a certain set of properties
426   (size, shape, complex refractive index) for low aerosol loading, and another set of properties for high
427   aerosol loading.   For a site dominated by water soluble sulfates, for example, the optical properties
428   would change as the particle swelled with humidity, becoming larger and more dilute. Because the
429   optical properties were derived from optical measurements of the whole column in ambient
430   conditions, we could avoid all the angst of determining species type, mixing rules, and vertical
431   profiles.   The method side-stepped all of the chemistry and all of the issues of in situ measurements
432   [66] that were irrelevant for creating optical property inputs for radiative transfer calculations of the
433   LUT.

434   3.2.3. Over land algorithm synthesis

435   As with the over-ocean aerosol algorithm, the over-land algorithm was tested from airborne
436   imagery during field experiments.   These were primarily the Smoke/Sulfates, Clouds and Radiation
437   field campaigns, conducted over the Atlantic (SCAR-A), in California (SCAR-C) and in Brazil (SCAR-
438   B) in 1993, 1994 and 1995, respectively, and also during TARFOX in 1996. These experiments
439   combining high altitude imagers to simulate future MODIS measurements with low altitude and
440   ground-based measurements created a rich data base to explore the surface reflectance
441   parameterizations, the dynamic aerosol models and the structure of the new algorithm [12] [13] [39]
442   [60] [64] [65] [66] [67] [68].   There would be a functional operational algorithm for producing AOD
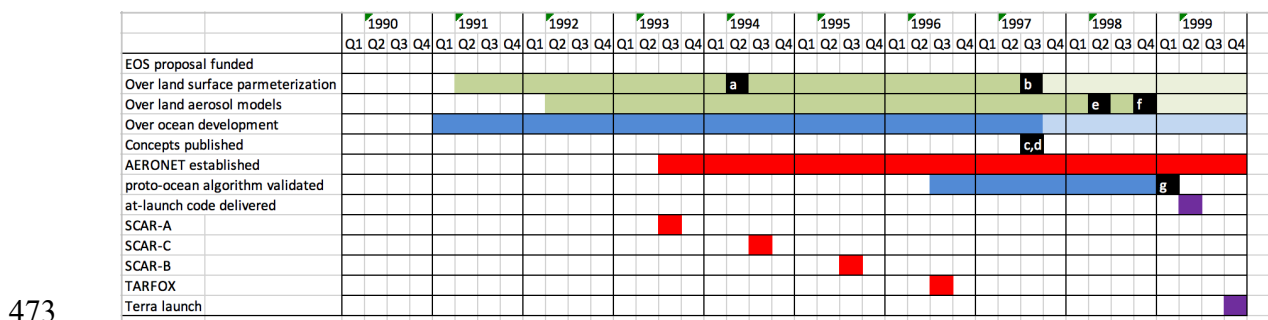443   over global land for the first time at Terra launch. This success was based on the following:

444   •   Basing the retrieval in physical understanding of aerosols, their environment and radiative
445   transfer
446   •   Limiting the retrieval to only dark targets, where contrast with overlaying aerosol was strongest
447   and error propagation of poor surface reflectance assumptions was smallest.
448   •   Avoiding rigid a priori assumptions as much as possible and instead using empirically-derived
449   dynamic relationships for surface reflectance and particle optical properties
450   •   Using new total column ambient measures of aerosol optical properties to create the LUT.

451 • Collecting a test bed of imagery and ground truth from a series of field experiments to derive
452   the dynamic relationships in relevant environments

453   The at-launch over land algorithm was the first of its kind and provided the aerosol and climate
454 community with unprecedented views of the total global aerosol system. It soon caught the eye of
455 the air quality community, as well. However, the product had flaws that slowly became apparent
456 after launch.   It was susceptible to subpixel snow contamination, especially in the Spring thaw of the
457 Northern Hemisphere, and its spectral and particle size information products were not reliable in the
458 same way similar products from the ocean algorithm were. There have been a series of add-ons and
459 changes to the over land algorithm over time, but the basic premise of the algorithm has persisted for
460 twenty years.

461 *3.3. The decade of algorithm development*

462   During the development period (1990 to 1999) previous experience and fundamental
463 understanding of radiative transfer combined to create the concepts that would become the at-launch
464 DT algorithm. The three primary areas of focus were surface parameterization and aerosol models
465 over land, and in producing a comprehensive inversion over ocean.   The AERONET program began
466 at about the same time that work began on the MODIS aerosol algorithm, and the deployment of
467 AERONET stations during the four field experiments in conjunction with the airborne spectral
468 imagers: MODIS Airborne Simulator (MAS) and AVIRIS, played a key role in all aspects of the
469 development including validation of the ocean proto-ocean algorithm following TARFOX.   The
470 major creative periods each leading to a major milestone culminated in a seminal publication, which
471 were followed by a less intense, but continued effort of testing, modifications and adjustments in
472 preparation for Terra launch.   Figure 3 illustrates this first decade of DT development.

	1990				1991				1992				1993				1994				1995				1996				1997				1998				1999			
	Q1	Q2	Q3	Q4	Q1	Q2	Q3	Q4	Q1	Q2	Q3	Q4	Q1	Q2	Q3	Q4	Q1	Q2	Q3	Q4	Q1	Q2	Q3	Q4	Q1	Q2	Q3	Q4	Q1	Q2	Q3	Q4	Q1	Q2	Q3	Q4	Q1	Q2	Q3	Q4
EOS proposal funded																																								
Over land surface parmeterization																	a												b											
Over land aerosol models																																		e	f					
Over ocean development																																								
Concepts published																													c,d											
AERONET established																																								
proto-ocean algorithm validated																																				g				
at-launch code delivered																																								
SCAR-A																																								
SCAR-C																																								
SCAR-B																																								
TARFOX																																								
Terra launch																																								

Figure 3. Timeline of key activities and milestones during the ten years of DT algorithm
development (1990 – 1999).   Green shading indicates land algorithm development elements; blue --
ocean algorithm development elements; red -- validation development or milestones; purple --
mission level milestones. Lighter shading indicates a switch of focus from intense creative work to a
period of testing and modifications. Years divided into quarters. Black squares indicate important
publications. (a) [59] (b) [60] (c) [12] (d) [13] (e) [64] (f) [65] (g) [39].

481   The decade of development ended with Terra launch at the end of 1999. After a commissioning
482 phase, MODIS Terra began sending data and the DT algorithm began producing aerosol products.
483 Figure 4 illustrates the view of the global aerosol system after the first full year of Terra-MODIS DT
484 data production.   The most notable addition from the heritage products was the extension of the
485 aerosol characterization over land, but also the use of the fine mode fraction (η) allowed a clear
486 distinction of dust (greenish hues) from smoke/pollution (red) when aerosol loading rose above
487 background levels. The products were delivered at two levels.   Level 2 offered geolocated but
488 ungridded aerosol products along the orbital swaths of the instrument.   These were the nominal 10
489 km products, available once per day.   Level 3 delivered the statistics of the Level 2 product by

490 aggregating the data to a stable 1-degree equal angle latitude-longitude grid [69]. Level 3 products
491 are available as daily, 8-day or monthly means.   The 1-degree Level 3 data simplified the ability to
492 make use of the data products, and systems set up for on-line visualization, analysis and download
493 encouraged early adoption of the products for a variety of applications [70]. Note that Figure 4 was
494 constructed from Level 2 data and not from Level 3.
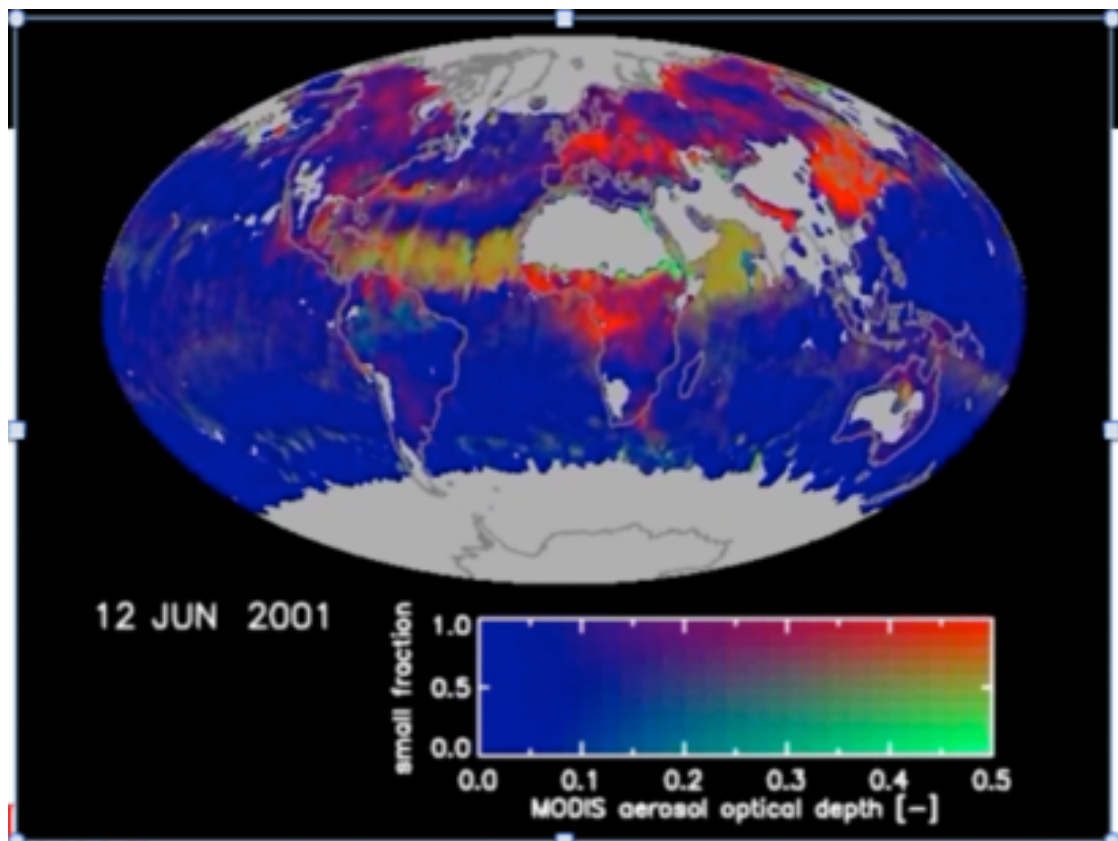
495

496 **Figure 4.** MODIS aerosol optical thickness at 0.55 µm, representing global aerosol distribution on 12
497 June 2001. The two-dimensional color bar describes both magnitude of optical thickness (along
498 bottom axis) and fraction of optical thickness contributed by smaller fine-mode particles (along
499 vertical axis). Blue indicates low aerosol loading. Red indicates heavy loading of small particles such
500 as pollution and smoke. The greener tones indicate a greater percentage of large particles such as
501 desert dust and sea salt. The image was created from the MODIS daily 10-km resolution data after
502 smoothing the raw data with Gaussian filters applied both in the temporal and spatial domains.
503 Visualization produced by Reto Stockli of the NASA Earth Observatory.

504 **4. Validation: Building confidence**

505 *4.1 Validation strategy and infrastructure*

506 Fundamental to the aerosol algorithm developed for the MODIS sensors was the creation of a
507 means to validate the products once they were being produced operationally. The primary form of
508 that validation would prove to be the AERONET network of autonomous upward looking sun/sky
509 radiometers [14] [41] [42] [71] [72] [73] [74]. AERONET began to play a major role in the DT
510 algorithm development even before launch, as the sky inversion parameters provided the
511 information for the algorithms' optical properties in the calculations of the LUTs, and the sun
512 products served as validation for proto-algorithms applied to imagery from high altitude airborne
513 radiometers.

514 The ability to test the algorithm before launch in mission-relevant situations with high quality
515 ground truth allowed us to evaluate the algorithm and to project forward expectations of the final
516 products' uncertainty [75].   Thus, the Dark Target team met the first post-launch products already
517 with expectations of how well those products should match ground-truth. Expectations were based
518 on both theoretical analysis [12] [13] and field experiment results [39] [68] [75]. For AOD, the at-
519 launch expected uncertainty or "error" for ocean was ±(0.03+5% of AOD) and for land ±(0.05+15%
520 of AOD) [16]. To the DT team, this meant that we should expect 66% of the collocations between
521 satellite and ground truth to have differences in AOD within those error bars. Over the years,
522 "expected error" has been invoked by the team in two ways.   First, products produced by new
523 versions of the algorithm are always evaluated against previous expectations.   Percentage falling
524 within expected error (%EE) has become an essential validation metric used by the DT team [15]
525 [16] [76] [77] and adopted by many other aerosol remote sensing teams around the world [78] [79]
526 [80] [81] [82]. Second, the expected error bars themselves have been evaluated and adjusted through
527 the decades as algorithms change and validation data sets expand.   For example, error bars were
528 increased to ±(0.05 + 20% of AOD) over land for the new 3 km product [17], while the standard 10
529 km error bars have maintained consistency over land for 20 years [15] [20], but over ocean the
530 comparison with AERONET AOD is best represented with these error bars: +(0.04 + 10 %); −(0.02 +
531 10 %) that have both increased the relative error from pre-launch estimates and also denote the
532 asymmetrical absolute error.   Retrieved AOD is more likely to be slightly higher than slightly
533 lower.   In the validation we describe below, we will specify the error bars used when reporting the
534 metric, %EE.

535

536 The AERONET direct-sun observations were utilized because of their inherent accuracy (AOD
537 within ±0.02 at most wavelengths) as well as their versatility (could be installed in remote
538 environments and only required minor maintenance).   Note that direct-sun observations can
539 validate spectral AOD and Angstrom Exponent, but the over ocean effective radius and fine mode
540 fraction products would require comparison with inversions of AERONET sky radiance [41] [42]
541 [43] or the AERONET Spectral Deconvolution Algorithm (SDA) [83]. The SDA product provides a
542 parameter inverted from the direct sun measurements similar to, but not exactly the same as, the
543 DT ocean algorithm η parameter or fine mode fraction (FMF).   These AERONET SDA products
544 offer another means to evaluate the DT ocean aerosol size retrieval [47]. We note, though, that both
545 the AERONET sky radiometry retrievals of aerosol particle effective radius and direct-sun SDA
546 FMF parameters are themselves inversions. They can provide valuable constraint on the satellite
547 products but are not the same robust validation as can be achieved by comparing the satellite
548 products to the direct-sun measurements.
549
550 Collocating MODIS-retrieved AOD with measurements from the stationary AERONET instruments
551 required consideration of how the aerosol was observed by each instrument system.   The MODIS
552 product is a snapshot in time, having a spatial resolution of 10x10 km at nadir, but increasing to
553 20x40 km at the edges of the swath. AERONET represents the aerosol at a point on Earth's surface
554 (ignoring the angle of observation) but measures approximately every 15 minutes. Therefore, the
555 validation effort had to assume that there could be a match between the spatial statistics of the
556 MODIS retrieval and the temporal statistics of the AERONET measurements [84]. After comparing

557 average AOD values at different MODIS array sizes with coincident AERONET average AOD for a
558 1-hour time period at representative locations around the globe, we found the most robust solution
559 to be using an array of 5x5 MODIS retrieval boxes (approx. ±25 km from the center box) with ±30
560 minutes of AERONET observations. The physical justification was that since global average wind
561 speeds are approximately 6-7 m/s, aerosol could be traveling ±25 km in the ±30 minutes. Rarely
562 would a collocation occur when all 25 MODIS retrieval boxes in the 5x5 domain reported an AOD
563 value or the AERONET time series consisted of all 4 or 5 observations.   Clouds, inappropriate
564 surfaces, land/ocean coastlines would prevent a DT retrieval or AERONET observation from taking
565 place in particular retrieval boxes within the 5x5 collocation square. A collocation without
566 representative population in either the MODIS spatial domain or AERONET temporal domain
567 would render the match invalid.   A valid match required retrievals from at least 5 of the 25 MODIS
568 retrieval boxes, and reports from at least 2 out the 5 possible AERONET observations. The same
569 match-up criteria could be used for both land and ocean retrievals, as coastal stations would have a
570 good portion of their surrounding 5x5 retrieval boxes over the ocean.   The validation
571 infrastructure, later called Multi-sensor Aerosol Products Sampling System (MAPSS) [85] was a
572 sophisticated investment of resources, requiring nearly as many lines of software code as the
573 algorithm itself.   Initially designed for validation of the DT algorithm, MAPSS evolved into a
574 community resource, expanding to incorporate aerosol retrievals from other satellite sensors [85].
575 Eventually it became part of the Giovanni analysis infrastructure [86]. The validation, more than
576 anything, encouraged the community to embrace the products. Without AERONET, the close
577 collaboration between the MODIS and AERONET teams, and the investment into MAPSS, it would
578 have taken much longer for the MODIS aerosol products to find acceptance across multiple
579 communities and applications.

580 *4.2 Earliest validation*

581   Figure 5 shows the earliest publication of validation for the dark target aerosol algorithm [87]
582 [88]. At that time from the entire global database, there were 315 collocations over land and 64
583 collocations for AOD over ocean but only 25 ocean collocations for effective radius, as we required
584 AOD > 0.15 for a valid retrieval of particle size. The results show high fidelity of the new retrieval to
585 simultaneous AERONET measurements. Over land, correlations (R) were 0.85 to 0.91, depending on
586 wavelength, RMSE = 0.07 to 0.11, regression slopes 0.86 and intercepts 0.02 to 0.06.   This was a
587 remarkable result for the first over land operational aerosol retrieval. Over ocean, the statistics were
588 even better for AOD, and the retrieved effective radius gave indication that it could match AERONET
589 sky inversion products to within ±0.10 μm. We note that for effective radius we are matching one
590 inversion to another inversion, which is different than the validation against direct sun
591 measurements for AOD.   The points shown in Figure 5 represented collocations from all over the
592 globe, in all types of aerosol conditions, and demonstrated the power of MODIS-AERONET match-
593 ups to build confidence in the satellite product.
594
595   There have been dozens of published studies showing validation of the MODIS DT products
596 against AERONET, mostly using a form of the original spatio-temporal collocation methodology. The
597 following list is only a small sample emphasizing some of the earliest and latest papers: [15] [16] [47]
598 [87] [88] [89] [90] [91] [92] [93] [94] [95] [96] [97] [98] [99] [100] [101] [102] [103] [104] [105] [106] [107]
599 [108] [109] [110] [111].   Most recently published validation has become focused on East Asia, China
600 and specific localities within China, with the exception of [98]. That specific paper better resembles
601 the earlier studies and takes a more global perspective.

602
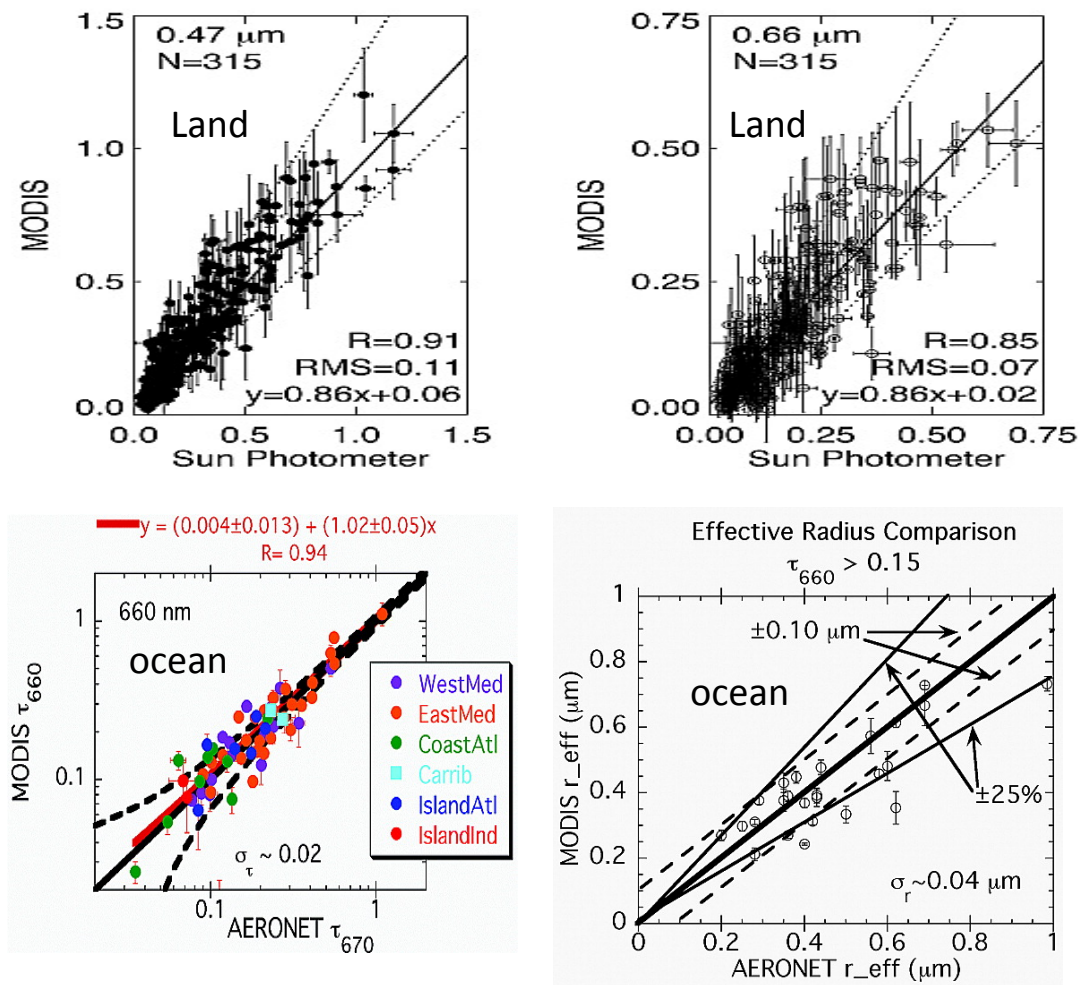
Figure 5. Original validation analysis for the Terra-MODIS product. **Top row**, scatter plot of over land retrieved MODIS AOD at 0.47 μm (left) and 0.66 μm (right) versus the same from collocated AERONET sun observations. The solid line denotes the regression and the dashed lines represent the at-launch expected error ±(0.05+15% of AOD). Regression statistics are given. 315 collocations from the global data base are used in the plots. From [87]. Adapted with permission from Wiley and Sons. **Bottom row**, scatter plot of over ocean retrieved MODIS AOD at 0.66 μm (left) and effective radius (right) versus the same from collocated AERONET sun observations (left) and AERONET sky radiance inversions (right). On the left, the bold solid line denotes the 1:1 line, the solid red line the regression line and the dashed lines denote the at launch expected error ±(0.03 + 5% of AOD). There are 64 collocations represented. On the right, the bold solid line denotes the 1:1 line, the thinner solid lines represent at-launch expected error for size parameters and the dashed lines indicate ±0.10 μm which enclose 72% of the points. Only 25 collocations are plotted, as AOD at 0.66 μm is required to be greater than 0.15 to be included. From [88]. Adapted with permission from Wiley and Sons.

4.3 Present day validation

The network of a few AERONET sensors in 1998 has grown to at least 370 active sites today (August 2020). Coupled with the increase in sites has been improvements regarding calibration and algorithm (gas corrections, sun-pointing accuracy, cloud-screening, etc.) leading to AERONET Version 2 in the mid 2000s [112], and the Version 3 we have today [74]. In addition to improving the network of 'fixed' AERONET sites on land and coastal platforms, the AERONET team has developed the Marine Aerosol Network (MAN), which uses handheld devices on mobile ship (cruise and experiment) platforms [73]. With MAN, we have learned to evaluate the satellite

624 aerosol retrievals in remote oceans by accounting for slowly moving platforms. Before MAN

625 validation, offshore validation efforts relied on airborne sunphotometers during specific short-term

626 field experiments [39] [89] [91] [113] [114] [115], [116] [117].   Besides MAN, AERONET introduced

627 the concept of the Distributed Regional Aerosol Gridded Observation Network (DRAGON). This is

628 an array of relatively short term AERONET stations deployed across a region in a grid with spatial

629 resolution of approximately 10 km [118].   The DRAGONs provide insight to aerosol gradients and

630 process at a mesoscale level, but they also allowed confirmation that the DT product was accurately

631 representing those gradients [76] [78] [102].

632

633 Figure 6 shows the most recent validation of the MODIS DT C6.1 product against AERONET

634 and MAN (unpublished). Validation metrics are shown in Table 1.   The match-up method is slightly

635 different from how it was done in 2002. Now we are still using ±30 minutes of MODIS overpass but

636 defining a circle of 27.5 km radius around the AERONET station for the MODIS spatial statistics

637 instead of using a "square" of 5 x 5 retrieval boxes. Temporal average of AERONET observations

638 within the collocated window and spatial average of MODIS pixels within the spatial collocation are

639 applied. We require that MODIS Quality Assurance Flag (QA) be QA > 0 over ocean, and QA = 3 over

640 land.   The averaging requires that at least 20% of valid MODIS pixels exist within the 27.5 km circle

641 and at least 2 AERONET observations are within the temporal window. In addition to validating the

642 over ocean AOD from coastal ground-based AERONET sites, as we did in 2002, we now can collocate

643 MODIS products with MAN sites over open ocean. The validation against MAN shows the DT AOD

644 over ocean data are almost on the 1 to 1 line.   Correlation coefficients are 0.92 and 0.96, median bias

645 values 0.022 and 0.013, with regression slopes 0.96 and 0.96 and intercepts of 0.036 and 0.021, for

646 Terra and Aqua, respectively.

647 **Table 1.** Validation statistics of MODIS Terra and Aqua DT C6.1 against AERONET and MAN for
648 2000(2002 Aqua)-2019.

		Median Bias	Root Mean Square Error	Correlation Coefficients	Regression Slope	Regression Intercepts	Total Number	%EE
Ocean AERONET	Ter	0.029	0.091	0.89	1.02	0.035	67742	63.9
	Aq	0.019	0.097	0.87	0.93	0.033	65858	71.1
Ocean MAN	Ter	0.022	0.088	0.92	0.96	0.036	27331	75.2
	Aq	0.013	0.050	0.96	0.96	0.021	25681	80.2
Land	Ter	0.016	0.105	0.92	1.04	0.016	238373	74.7
	Aq	-0.001	0.101	0.92	1.02	0.003	193628	76.3
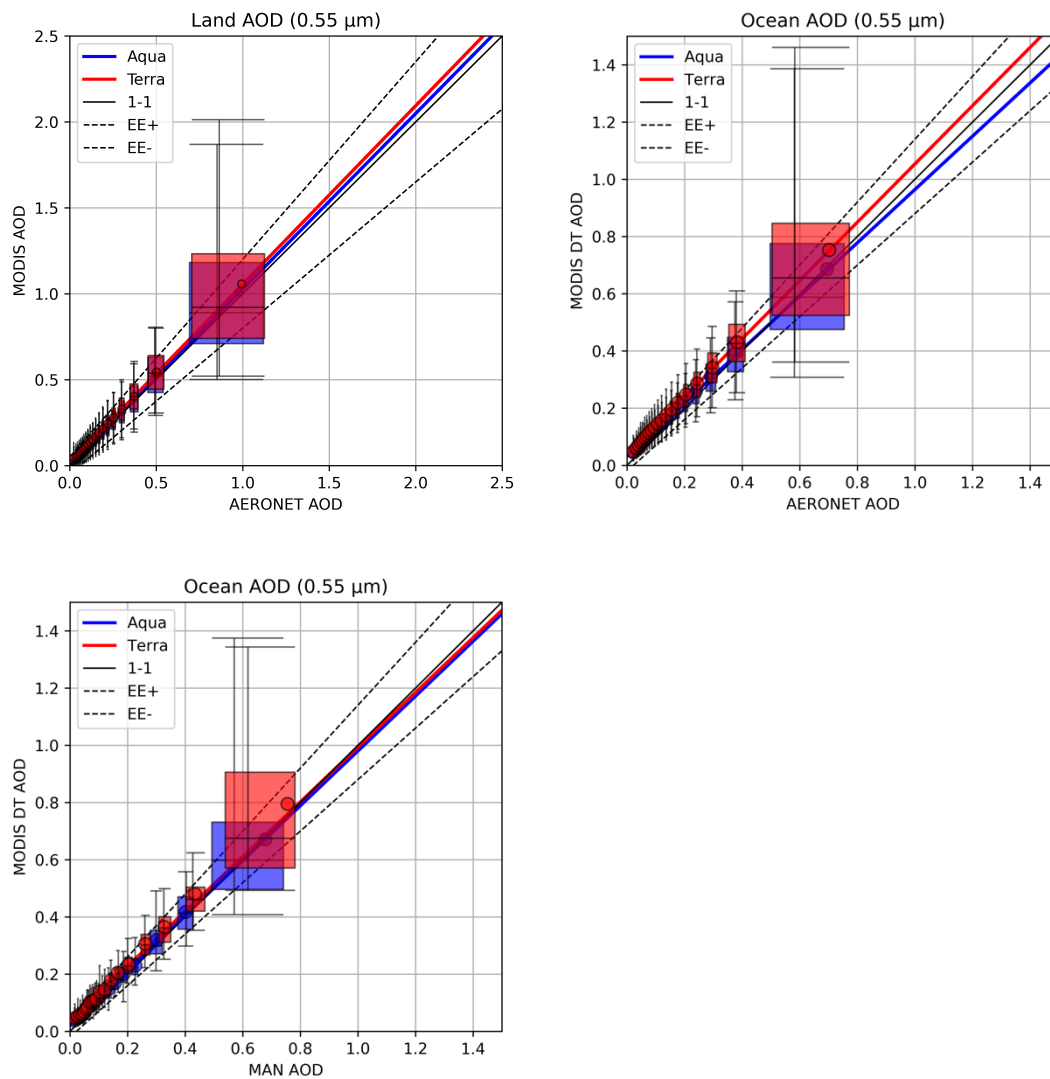
649

650

651 **Figure 6.** Validation of MODIS DT over land (upper left) and ocean (upper right) product against
652 AERONET version 3 level 2.0 AOD at 0.55 μm and MODIS DT over ocean against MAN (lower left)
653 for the entire data record. The solid lines are the linear fitting between the two datasets. The four
654 boundary boxes represent 25% 75% of the data in both x and y directions, the center line is the median,
655 the dot is the mean. The upper and lower whiskers represent the 95% and 5% of MODIS values. Each
656 box represents the statistics from the same number of collocations. The dashed lines are the Expected
657 Error ±(0.05 + 15% of AOD) for land and (+0.04 + 10% of AOD and -0.02 - 10% of AOD) for ocean). The
658 red represents Terra and blue represents Aqua.

659 These results show that the DT AOD product continues to match AERONET values well, with
660 not much overall change in the validation statistics from 2002, despite increasing the number of
661 collocations by three orders of magnitude. The MAN validation provides assurance that coastal
662 stations are not inherently biased from the situation over open ocean. The modern AOD is biased
663 slightly high as compared with AERONET, more so over ocean than land, and Terra is biased high
664 as compared with Aqua.

665

666 While the basic validation methodology has remained the same for 20 years, the analysis has
667 expanded to include bias statistics as functions of various parameters and more emphasis is placed
668 on noting the percentage of retrievals that fall within expected errors. Varying collocation
669 methodology can make a difference to results, but not enough to change overall conclusions, except

670   when attempting to establish accuracy of a finer spatial resolution product to resolve fine resolution
671   variability [17].

672   *4.4 Interannual variation in validation metrics*

673   The expansion of the AERONET network over the past two decades introduces an interesting
674   issue when interpreting validation over time. Because different AERONET stations contribute to
675   the global AERONET database at different points in the time series, the ground truth database is
676   constantly changing. This could result in different validation statistics at different points in the time
677   series, even if the actual satellite product accuracy remained constant [17]. Figure 7 shows time
678   series of annual validation statistics for the operational 3 km product calculated from collocations
679   with AERONET each year from 2000 when 129 stations reported data at least for a part of the year to
680   2015 when 400 stations reported. Note that Figure 7 shows validation statistics for the 3 km product,
681   while Figure 6 shows statistics for the 10 km product. Looking only at the red curve representing
682   MODIS on Terra, the number of collocations grew from about 100 in 2000 to over 8000 in 2012. This
683   reflects the additional stations deployed, but also the fact that stations were operational in the field
684   for longer durations. The decrease after 2012 reflects the lag between the time the data set was
685   acquired for analysis and the process of generating the Quality Assurance for the observations and
686   elevating them to Level 2.0 status. Only AERONET Level 2.0 measurements were used in the
687   analysis. The validation metrics of median and mean bias also exhibit long-term trends in this data
688   set. For Terra, the mean bias of the MODIS AOD against AERONET is about 0.04 during the period
689   2003 to 2005. By 2010 to 2013 that bias has doubled. Has the Terra AOD accuracy degraded by that
690   much over time? It is possible. As will be shown in Section 6.0, there have been drifts in instrument
691   characterization, although most of that has been mitigated for the data analyzed in Figure 7. Figure
692   8 shows that the set of AERONET stations reporting data in 2003-2005 are different from the ones in
693   2015. Not only are there overall more stations in 2015, many stations that were in 2002 no longer exist.
694   There are very few long-term stations, meaning that the representation of the global aerosol system
695   by the AERONET network continuously changes. Biases can be regionally dependent [15] [20] [77],
696   and there could be proportionally more stations in favorable locations in 2003-2005 than there are in
697   2010-2013 or later. Because the ground-truth distribution changes over time, interpreting time series
698   of changing validation statistics is challenging. [77] chose to limit their analysis of interannual
699   validation metrics to just a few long-term locations, widely spaced across the globe in different
700   aerosol regimes.
701

702
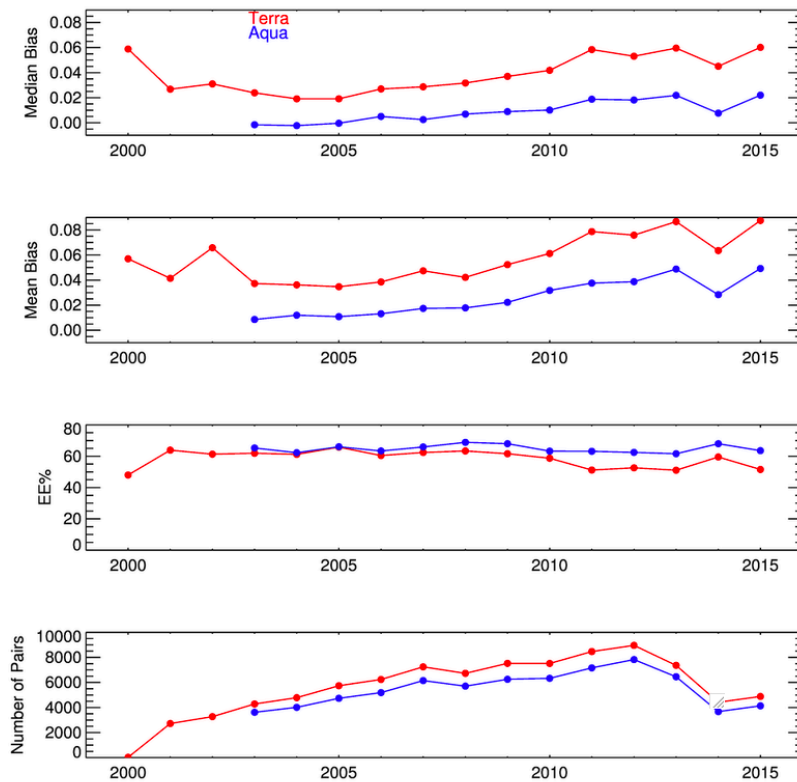
703   **Figure 7.** Time series of validation metrics obtained by collocating MODIS DT 3 km AOD at 0.55 μm
704   with all available AERONET Level 2 Quality Assured from the global database, each year. AERONET
705   AOD was interpolated to 0.55 μm using [119]. Shown are median bias and mean bias against
706   AERONET, percentage within expected error bars given as ± (0.05 + 20% of AOD) and the number of
707   collocations each year. AOD from Terra MODIS in red, and from Aqua MODIS in blue.   Data with
708   only highest quality MODIS retrievals were used.

709
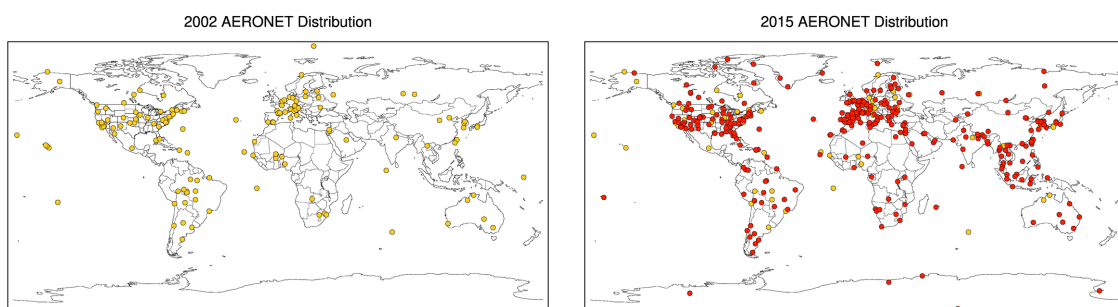
710   **Figure 8.** AERONET global distribution in 2002 (left) and 2015 (right). Yellow dots are stations that
711   existed in 2002 on both maps. Red presents AERONET sites on the 2015 map that did not exist in
712   2002.

713   **5. Twenty years of on-orbit DT aerosol production**

714   *5.1 The first decade (2000 – 2009)*

715   Beginning with Terra-MODIS first light in early 2000 and continuing for roughly a decade, the

716   effort was concentrated on validation, identifying and solving issues that were not encountered

717   during the pre-launch period.   See Figure 9. The products were being produced and there was a

718 sense of urgency to understand apparent problems and to fix the problems that turned out to be
719 real. Early in this period we participated in aerosol-focused field experiments such as the Puerto
720 Rico Dust Experiment (PRIDE) [91] [120], the Chesapeake Lighthouse and Aircraft Measurements
721 for Satellites (CLAMS) [92] [121] and the Southern Africa Regional Science Initiative (SAFARI-2000)
722 [90], but later relied more and more on AERONET's expanding network and improved sky
723 inversions [41] [42] [43], and in the MAPSS system to lead the validation effort. Masking efforts
724 came first, and development of the 2nd generation land algorithm was a close second.   This is the
725 time period when NASA began to invest in major reprocessing efforts to try to maintain a
726 consistent time series of products.   These consistent time series are known as Collections.   During
727 the 2000 to 2009 decade we saw the implementation of five different Collections. This was also the
728 decade when different science and applications communities began to find value in the product and
729 publish their scientific results, using the MODIS DT product as one of their data sources.
730
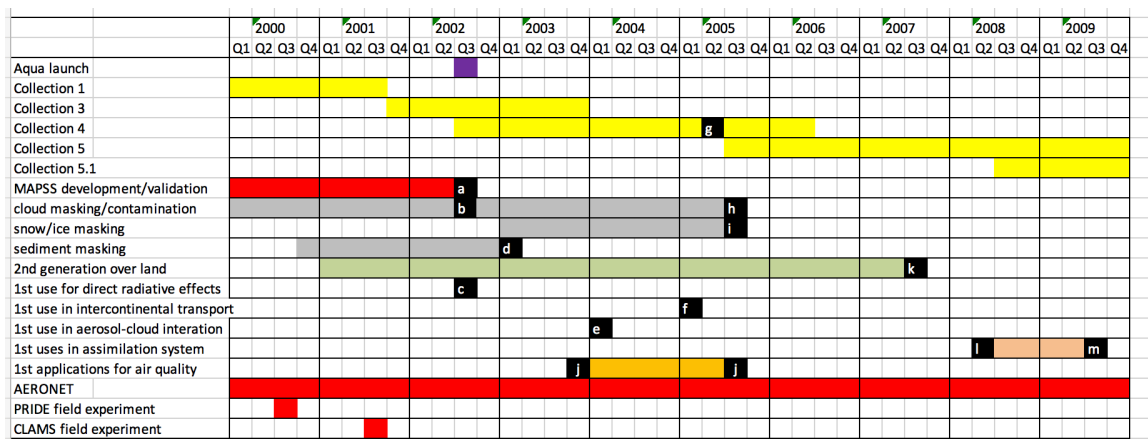
731

732 **Figure 9.** Timeline of key activities and milestones during the first ten years of on orbit DT aerosol
733 production (2000–2009).   Yellow shading indicates forward processing of NASA data Collections.
734 Green shading indicates land algorithm development elements; red – validation development or
735 milestones; gray – masking efforts; purple – mission level milestones; salmon shading links two
736 milestone uses of DT aerosol in assimilation systems. Years divided into quarters. Black squares
737 indicate important publications, including to the best of our knowledge the first publications to use
738 the product in specific applications: (a) [84] [87] [88] (b) [122] (c) [123] (d) [124] (e) [125] (f) [44] (g) [16]
739 (h) [126] (i) [127] (j) [128] [129] [130] (k) [18] [19] (l) [131] (m) [132].

740 5.1.1 Sediment and snow/ice masking

741 At Terra launch, the DT algorithm produced a viable algorithm creating products, as expected from
742 applying the proto-algorithm to imagery from airborne radiometers.   In the first validation, with a
743 limited number of collocations, the AOD products appeared to fall within the error bounds
744 determined from the pre-launch field experiments [39] [68] [75].   These were ±(0.03 + 5% of AOD)
745 for ocean and ±(0.05 + 15% of AOD) for land.   There were a few surprises.   In the ocean algorithm,
746 sediments at the mouth of rivers and shallow shoals created unrealistic, stationary hot spots in the
747 spatial plots of AOD.   A mask making use of the slope between visible (0.47 μm) and SWIR bands
748 (0.86 μm, 1.24 μm and 2.11 μm) was implemented to avoid these locations [124]. In the land
749 algorithm, the first Spring, and especially the month of May produced a band of exceptionally high
750 AOD across the northern hemisphere land masses. This artifact was traced to melting snow that

751   violated the assumptions of the surface reflectance ratios.   Initially the algorithm had relied on
752   ancillary data to identify snow in pixels, which did fine at the onset of northern winter and through
753   the heart of the snowy season but did not adequately identify the snow during the Spring thaw. A
754   mask was developed, again using the reflectance at 0.86 μm and 1.24 μm bands, along with the
755   brightness temperature at 11 μm to identify pixels with subpixel snow amounts, and the artifact
756   was eliminated [127].

757   5.1.2 Cloud mask and critical look at cloud contamination

758   The at-launch algorithm also relied on ancillary inputs to identify and mask cloud pixels.   The
759   ancillary data was the MODIS cloud mask product, MOD35. The initial issue with this mask, was
760   not that it created cloud contamination in the aerosol product, but that it considered heavy aerosol
761   to be a cloud. The product was losing vital heavy aerosol events of importance for climate
762   applications and later for air quality.   We found no way to use just the spectral information from
763   the blue channels through the thermal infrared, to confidently distinguish between all clouds and
764   heavy aerosol. Instead, we turned to spatial variability as the driving factor in a new internal cloud
765   mask, relying on the textural differences between the fractal nature of clouds and the general
766   homogeneity of aerosol layers [122].   The spatial variability test proved to be a strong cloud mask,
767   but it was supplemented by several key individual tests from MOD35 to help with specific cloud
768   types. Thin cirrus had to be dealt with separately, and for that cloud type we used the 1.38 μm
769   channel that was new to MODIS [133] [134] [135] but is now widely used [136].
770
771   Cloud contamination has always been an issue in the Dark Target aerosol product. To avoid losing
772   heavy aerosol events, the algorithm has opted to err on the side of "too much cloud" rather than
773   "not enough aerosol".   However, the construct of the algorithm, especially during the process of
774   aggregating from 0.5 km pixels to 10 km retrieval boxes, eliminates much of the residual cloudy
775   pixels that escape the a priori masking and also helps the algorithm avoid pixels in cloud shadows
776   [137]. During this process, the algorithm eliminates 50% of the non-cloudy pixels over ocean and
777   70% of the non-cloudy pixels over land. This elimination process reduces much residual
778   contamination. Still, some studies began to report strong correlation between the DT retrieved AOD
779   and cloud fraction [138] [139]. Early on we examined the effect these decisions had on the product
780   by making a critical examination of cloud contamination [126].   The study looked at the overall
781   effect on the "global mean" AOD, finding that clouds added 0.020 to 0.025 AOD to the MODIS-
782   derived global mean.   At the time, this would translate to roughly 10 to 17% of the AOD,
783   depending on whether it is over land or ocean [57] [140].   This amount of cloud contamination
784   could be addressed when calculating an observational estimate of aerosol radiative effect [57] from
785   the MODIS product. However, the global value was less useful when considering cloud
786   contamination on a local retrieval-by -retrieval basis. The effect could be much higher at the local
787   level.   It continues to be difficult to impossible to fully assess the effect of true contamination on
788   the product as there are several explanations for the observed increase of retrieved AOD near
789   clouds.   These explanations include the so-called cloud 3D effect, which is an adjacency effect
790   when bright clouds send photons that enter into the field of view of nearby non-cloud, less bright,
791   pixels [141] [142].   Nonetheless, there are physical reasons for AOD to increase near clouds or with
792   cloud fraction including particles swelling with humidity and dissipating cloud droplets in the

793   scene [143] [144]. Different processes take precedence in different situations, but careful

794   examination of specific cases point to 3D effects and physical enhancements as being more common

795   than actually mistaking a cloudy pixel for non-cloudy and including it in the retrieval [145].

796   5.1.3 Second generation land algorithm

797   The at-launch operational aerosol algorithm was unprecedented and very welcomed by the
798   community, even in a qualitative sense. Initial validation suggested that there was also quantitative
799   skill (Figure 5; [87]). However, it became apparent over time as more data was processed and as
800   AERONET expanded into new land and aerosol situations that there was room for major
801   improvements to the algorithm. All assumptions of land surface reflectance parameterization, aerosol
802   models and distribution of aerosol models were re-evaluated and updated [18] [19]. This included
803   turning simple ratios of land surface reflectance into regression models, dependent on view geometry
804   and vegetation index.   The at-launch aerosol models were derived for global conditions from a
805   limited grouping of AERONET stations in only three regions of the globe. In the second-generation
806   algorithm, a formal clustering analysis was made of the global AERONET data set, now expanded to
807   reflect a much more diverse global aerosol system.   The expanded AERONET distribution of stations
808   also allowed us to better apply the different models to the right regions. All of these changes to the
809   assumptions in the land algorithm were important but did not contradict the original assumptions.
810   For example, cluster analysis still resulted in four aerosol model types, with similar particle
811   properties, and placed these four models in roughly the same geographical locations.
812   Specifically, the four models included three that were dominated by fine mode particles and one
813   dominated by a coarse mode.   The three fine mode models had small differences in their size
814   distributions but were distinctive in their light absorption properties.   The model with the most light
815   absorption, with midvisible single scattering albedo (SSA) of 0.85, was found seasonally in tropical
816   and southern hemisphere biomass burning regions and over particular high population density
817   zones of countries with developing economies.   The model exhibiting the least light absorption with
818   SSA = 0.95 was found in the post-industrial countries of the northern hemisphere. The remainder of
819   the globe was assigned a model with a moderate level of light absorption (SSA = 0.90). These three
820   models with dominant fine modes were matched within the retrieval with the one model with
821   dominant coarse mode. As with the over ocean algorithm, the inversion mixed the two models to
822   find a solution that best matched the measured top-of-atmosphere reflectances.   The same coarse-
823   dominant model was applied globally.   In regions with significant coarse mode dust, the inversion
824   mixed in more of the available coarse-dominant model, and regions without dust would minimize
825   the amount of coarse-dominant model mixed into the retrieval. Details of the models and the
826   algorithm are found in [18] and [19].
827   The major difference between the 2nd generation land algorithm and the at-launch algorithm was
828   a structural change that replaced the two individual channel retrievals at 0.47 μm and 0.66 μm with
829   an inversion linking the two channels together by aerosol model.   The inversion used reflectance at
830   0.47 μm, 0.66 μm and 2.1 μm and three radiative transfer equations, one for each wavelength.   The
831   surface reflectances at each wavelength in the radiative transfer equations were linked by the
832   assumed parameterization.   The spectral dependence of AOD was determined by aerosol model.
833   Like the ocean algorithm, values in the new LUT were indexed by AOD at 0.55 μm. The algorithm
834   was given limited flexibility to create an aerosol model by finding the best weighting parameter
835   between two bimodal aerosol models, one dominated by fine mode and one dominated by coarse
836   mode.   In reality this weighting parameter more often than not jumped between $\eta = 0$ for a
837   completely dust dominated scene and $\eta = 1$ for a completely fine mode dominated scene.   The
838   inversion received three pieces of information (top of atmosphere reflectance at 0.47 μm, 0.66 μm and
839   2.1 μm) and returned three outputs (AOD at 0.55 μm, the weighting parameter that defined the
840   aerosol model and thus the spectral dependence of AOD, and the surface reflectance at 2.1 μm). From
841   these three pieces of information one could through the assumptions reconstruct the AOD and
842   surface reflectance at any wavelength.   The inversion never assumed that the atmosphere was

transparent at 2.1 μm, so that top of atmosphere reflectance at 2.1 μm did not equal the surface reflectance at that wavelength.

This second-generation land algorithm with its adjusted surface reflectance parameterization and aerosol models, and with its reconstructed comprehensive inversion, went into operations as part of Collection 5.1 in 2008 (see Figure 9). Subsequent validation showed that these changes did make substantial improvement [15]. However, it was also noted at this point that the aerosol size parameter, which had been used up to this point as a valid quantitative retrieval product, was at best a qualitative indicator of whether small or large particles dominated the scene. Spectral AOD was presented as a product, but spectral dependence accuracy over land is weak, and retrieved AOD at 0.55 μm shows better accuracy in validation on a global basis than does AOD at the other wavelengths. These are global observations. In particular locations where surface reflectance matches assumptions especially well there is a possibility that retrievals of aerosol spectral dependence over land will show greater skill.

5.2 The second decade (2010 – 2020)

The past 10+ years (2010-2020) covers the period of time when Collections 5 and 5.1 were running, and when Collections 6 and 6.1 were started (see Figure 10. In this decade, there were a few important modifications concerning surfaces and the introduction of a 3 km product, but emphasis switched from adding new features to maintaining a consistent product data record. This included identifying temporal drifts in the MODIS data products due to drifting instrument characterization of these aging sensors, which is the main reason Collection 6.1 was implemented in 2017. It also included looking ahead to when the MODIS sensors would finish their missions and the community would need to switch to alternative sensors. In light of that need for continuity the DT algorithm has been successfully ported to the VIIRS sensor [24] and is in the process of being adapted for the current fleet of geosynchronous sensors. Throughout this decade, as was the case for the twenty years previously, AERONET has been an essential partner in the continuous development, validation and maintenance of the DT algorithm.

Activity	2010	2011	2012	2013	2014	2015	2016	2017	2018	2019
Collection 5	a									
Collection 5.1										
Collection 6				c						
Collection 6.1									i	
windspeed dependence			b							
3km product				d						
urban surfaces							g			
DTDB merge					e					
nonspherical coarse model										l
generalized gas corrections									h	
porting to VIIRS for continuity						f				k
porting to GEO sensors										j
AERONET										

Figure 10. Timeline of key activities and milestones during the second ten years of on-orbit DT aerosol production (2010–2020). Yellow shading indicates forward processing of NASA data Collections. Green shading indicates land algorithm development elements; blue – ocean elements; red --validation development or milestones; brown – efforts to adapt the DT element to new sensors. Years divided into quarters. Black squares indicate important publications: (a) [15] (b) [146] (c) [20] (d) [17] (e) [147] (f) [148] (g) [22] (h) [23] (i) [21] (j) [149] (k) [24] (l) [271] [272].

880   5.2.1 Offset between Terra and Aqua

881   The surprise of the Collection 5 version of the Terra and Aqua reprocessed products released in
882   2008 was the unexpected offset between Terra and Aqua AOD. Although there had been a small
883   offset between Terra in Collection 4 and Aqua in Collection 3 [94] when Aqua was upgraded to the
884   Collection 4 inputs and algorithm, Aqua matched the results of Terra nearly perfectly, showing no
885   offset and no discernible "diurnal signature" in the Collection 4 time series [150]. After Collection 5,
886   Terra developed a 0.015 – 0.020 offset from previous values and from Aqua, and this offset
887   continued into Collection 6 and to the present day [20] [140].   The offset is a retrieval artifact, not
888   caused by a temporal component of the aerosol system. The obvious culprit is instrument
889   calibration, but after years of working with the MODIS characterization team and trying alternative
890   calibrations, some mitigation has been achieved, but the basic offset remains [20].

891   5.2.2 Wind speed dependence added to the ocean algorithm

892   The at-launch ocean algorithm used the global mean surface wind speed of 6 m/s as a constant
893   in the [151] surface reflectance parameterization.   This led to a degradation of the ocean retrieval
894   accuracy in areas just outside of the 40 degree glint mask [146]. A change was made to ingest ancillary
895   2-meter wind speed data from the Global Data Assimilation System (GDAS) produced by the
896   National Center for Environmental Prediction (NCEP), and to use this ancillary information to adjust
897   surface reflectance. The change made an important improvement in mostly remote regions of the
898   southern subtropical oceans [146].

899   5.2.3 Introduction of a finer resolution product

900   One interesting post-launch surprise had nothing to do with performance of the algorithm, but
901   in the communities that showed interest in it.   The algorithm was designed with climate applications
902   in mind, but the air quality community also began to use the products for forecasting and mitigation
903   work. To serve that community better we implemented operational production of a 3 km product to
904   supplement the standard 10 km product [17] [76]. The 3 km product serves its purpose with sufficient
905   accuracy but is less accurate than the standard product [77]. The team continues to recommend the
906   10 km product, unless finer resolution is necessary for the application.

907   5.2.4 Creating a merged product from Dark Target and Deep Blue

908   The DT land algorithm, by definition, avoids brighter surfaces because the premise of the algorithm
909   is to deduce the aerosol signal from the aerosol scattering that brightens dark surfaces. A second
910   MODIS product, called Deep Blue [80] [152] initially was developed to produce aerosol products
911   over land surfaces too bright for the DT algorithm.   Subsequently the Deep Blue algorithm has
912   expanded to darker, vegetated surfaces [80]. However, there was continued interest in combining
913   the results of the experienced Dark Target algorithm from darker surfaces with the results of the
914   Deep Blue algorithm from brighter surfaces to produce a more complete, global view.   This has
915   been called the DTDB merge and appears in all MODIS aerosol product files from Collection 6
916   onward [20].   A database of MODIS-derived monthly mean NDVI values was developed for all
917   months of the year at a 0.25° spatial resolution. Over land, pixels with an NDVI value ≤ 0.2 are
918   populated by Deep Blue retrievals, and pixels with an NDVI value ≥0.3 are populated with the DT
919   retrieval. For pixels with an intermediate NDVI value (>0.2 and <0.3), the retrieval with a higher
920   quality flag is chosen, and a simple average of DB and DT is used if both retrievals are present and
921   of highest quality. Because Deep Blue aerosol retrievals are not performed for MODIS over ocean,
922   the product uses DT retrievals for all ocean pixels [20] [147].

923   5.2.5 Expanding gaseous correction

924   To better characterize gaseous absorption and derive consistent atmospheric corrections for
925   retrievals from different sensors, we switched to the HIgh-resolution TRANsmission (HITRAN) gas
926   database and line-by-line radiative transfer model (LBLRTM) to calculate gaseous absorption in
927   each band of each sensor for the LUT.   Previous to Collection 5, the DT algorithm had used the 6S
928   Radiative Transfer code with the MODerate-resolution TRANsmission (MODTRAN) gas database
929   for this purpose. Also, previously only water vapor, ozone and carbon dioxide were considered for
930   atmospheric gas corrections. We have now (starting with MODIS Collection 6) expanded to include
931   additional atmospheric gases (O_3, O_2, N_2O, NO_2, NO, SO_2, CO_2, CO and CH_4) ; however, for bands
932   used in aerosol retrievals, only N_2O, CH_4, O_2, SO_2 are found to have some absorption [23].   This
933   was an important step for preparing the algorithm for adaptation to other sensors. Note that the
934   previously ignored methane is an important absorber in VIIRS band 11 (2.25 μm), whereas it had
935   not been important in any of the MODIS bands.   However, oxygen is an important absorber in
936   MODIS band 5 (1.24 μm) and it had been mistakenly ignored in previous MODIS collections.
937   Although the satellite sensors now have narrower channels in window regions, the absorption from
938   gases is non-negligible and can introduce biases in the AOD retrievals [20] [23].   For creating a
939   consistent long-term climate data record from multiple satellite data sets, such as from MODIS and
940   VIIRS, consistency and accuracy of atmospheric gas correction is critical. The team will continue to
941   revise and update gas corrections with any improvements in gas database [HITRAN] and updates
942   in LBLRTM versions.

943   5.2.6 New surface parameterizations for urban surfaces

944   To support the air quality community, we examined the surface reflectance parameterization in
945   urban centers and found that the parameterization designed for vegetation and natural surfaces is
946   not at all applicable for man-made surfaces [153]. Recently, a more applicable surface
947   parameterization for urban surfaces was implemented, with the algorithm naturally blending the two
948   parameterizations as a function of percentage of urban land cover type from ancillary data [22].

949   5.2.7. Specific LUT with nonspherical coarse mode for dust over ocean

950   To improve the retrieval of dust over ocean, we have recently introduced a new non-spherical
951   coarse mode into the over ocean retrieval and developed a logic tree to identify dust to direct the
952   retrieval to this new coarse mode [271] [272]. Before this modification, over the ocean, the DT
953   algorithm was known to contain scattering-angle-dependent biases in its retrievals of AOD,
954   Angstrom Exponent (AE) and Fine Mode Fraction (FMF) for dust aerosols.   The modification uses a
955   two-step strategy to improve the DT retrieval of dust over ocean. First, a combination of spectral tests
956   using near-UV (deep blue), visible, and thermal infrared (TIR) wavelengths is applied to detect dusty
957   pixels [271].   Second, a new dust model assumes a mixture of spheroid particles to represent global
958   dust optical properties [272], and this new dust model is applied to only those pixels that are
959   identified as dusty. Initial validation with AERONET-identified dusty pixels indicates significant
960   reduction of AOD bias (from 0.06 to 0.02) while improving the fraction of retrievals within expected
961   error (%EE) from 64% to 82%. At the same time, the overall bias in AE is reduced from 0.13 to 0.06,
962   and the scattering-angle-dependent AE bias is largely eliminated. Figure 11 shows the impact of the
963   new retrieval on a two-week average of AOD, AE and fine mode fraction (FMF) during a recent
964   historic dust transport event across the Atlantic Ocean from June 13 to 26, 2020. The reductions in all
965   three parameters in the dust transport route from the coast of west Africa to the Caribbean are
966   significant. The new retrieval suggests the need for a re-estimate of global and regional dust radiative

967   forcing   and   dust   mass   transport   across   Atlantic   and   Pacific   Oceans.
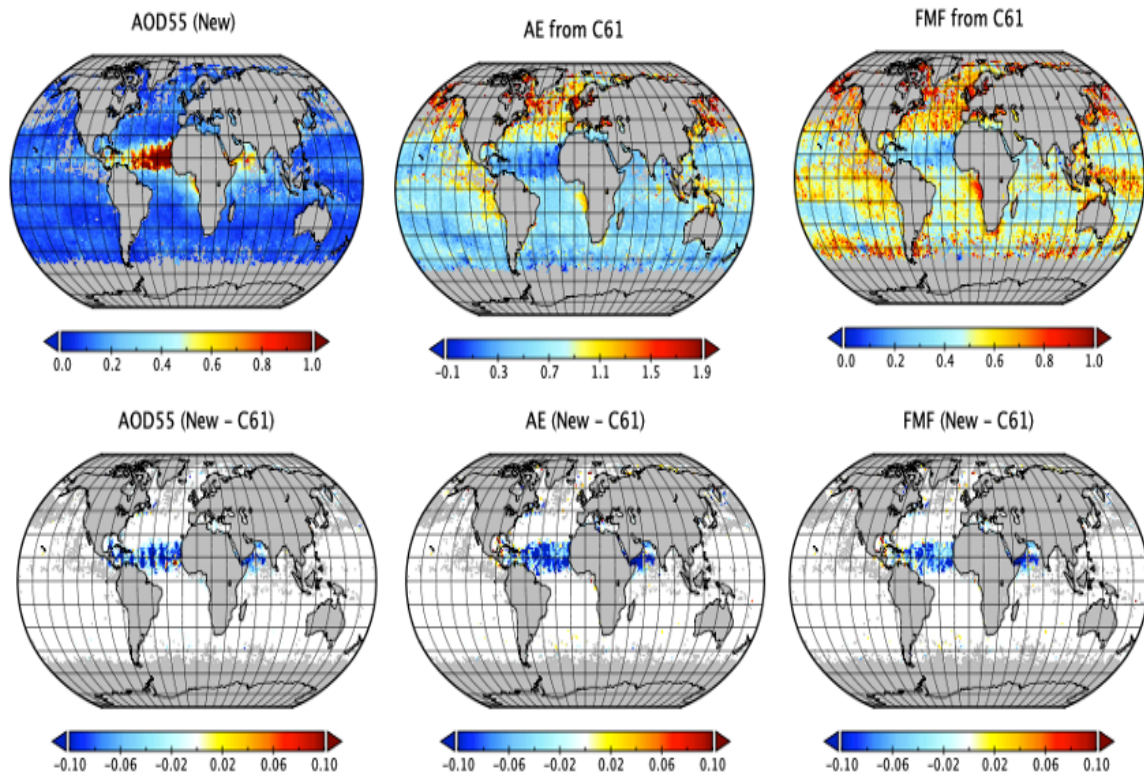
968

969   **Figure 11.**   A two-week average (June 13-26, 2020) of AOD at 0.55μm, Angstrom Exponent (AE) and
970   fine mode fraction (FMF) from the Version C6.1 retrieval (upper panel) and the difference between
971   the new retrieval products and the C6.1 products (lower panel). The new retrieval decreases the mean
972   AOD by about 0.06 and also retrieves coarser particles and more coarse mode aerosol. The late June
973   African dust storm across the Atlantic Ocean is the heaviest one in recent decades.

974   5.2.8. DT product over regions with intense aerosol loading

975   Finally, to support air quality monitoring and hazard response/management as well as to
976   complete our understanding of aerosol regional distributions at the extreme high end of AOD, we
977   analyzed the DT product in circumstances of very high aerosol loading such as over wintertime China
978   and the 2015 Indonesian forest fire event [154].   We increased the DT product data coverage by first
979   identifying these extreme aerosol events and then adjusted masking thresholds to allow more AOD
980   to be retrieved.   As retrieval coverage increased, we modified aerosol model and aerosol layer height
981   assumptions in the retrieval to ensure continued accuracy at high AOD conditions.   These
982   adjustments allow DT to retrieve over heavily polluted regions or retrieve closer to the source of the
983   emissions. This modification to the DT algorithm for heavy aerosol situations is still in research form
984   and has not been adapted for the operational code.

985   **6. Continuity in light of a constantly evolving sensor and algorithm**

986   For twenty years, the DT algorithm has been retrieving aerosol products using inputs from
987   MODIS observations. While the fundamental aspects of the algorithm have remained the same, the
988   algorithm that is running today is not the same algorithm that was implemented at launch.   See
989   Figures 9 and 10. Change is part of the algorithm's success. Change is necessary to react to new
990   information, new opportunities and new user communities. However, since change can also be
991   disruptive of continuity and a consistent climate data record, NASA has implemented a system of
992   Collections, in which the entire data stream is reprocessed from the beginning of the mission to the

993 present using updated algorithms. Currently, we are in the era of Collection 6.1, which was
994 implemented in early 2017. The identical algorithm is run on both Terra and Aqua-MODIS
995 observations, using historical observations prior to 2017 known as re-processing, and new
996 observations (until present) known as forward-processing.
997
998   Prior to launch, MODIS was calibrated to a laboratory source. Through its expected 5-7 year
999 lifetime, the calibration and performance were expected to change with age and exposure – including
1000 degradation of the electronics, the telescope, the mirrors, the onboard calibration source, etc.
1001 [155][156]. All changes affect the electronic signal that is observed, which furthermore impacts the
1002 calibration coefficients and the accuracy of the observation data used in the DT and other retrievals.
1003 Many of these changes are gradual (e.g. degradation) and can be modeled and forecasted. In fact, the
1004 MODIS Calibration and Support team (MCST) has continuously been developing novel techniques
1005 for mitigating some of these degradations and drifts, reducing striping in the imagery, and otherwise
1006 improving the reflectances, radiances, and geolocation information used by the DT and other
1007 algorithms. Each Collection, therefore, also represents a stable implementation of the calibration
1008 algorithm – where there is a continuum between the pre-launch (laboratory) calibration and the
1009 observed calibration at the point of new Collection implementation.
1010
1011   The one caveat in this system is that discontinuity or trends can occur, not from algorithmic
1012 changes nor from physical changes of the Earth system, but from sudden or unexpected changes to
1013 the sensor itself. While MCST may become aware of the problem, it may take until the start of a new
1014 Collection to mitigate and apply a new calibration strategy. Figure 12 shows the time series of
1015 globally averaged, area-weighted and quality flag-weighted AOD for the 0.55 μm AOD product
1016 derived from Terra-MODIS and Aqua-MODIS data. Plotted are three curves for AOD over land and
1017 three curves for AOD over ocean, each corresponding to a different Collection, C5.1, C6 and C6.1.
1018 Over land, Terra Collection 5.1 developed a significant trend in decreasing AOD, on the order of 18%
1019 per decade, but Aqua did not. There was no physical or algorithm-related explanation for this
1020 behavior. Analysis of the Collection 5.1 DT aerosol record, along with comparisons to Aqua [e.g., 20],
1021 showed clear evidence that there was a drift in some of the visible wavelength channels (primarily
1022 the blue band) used in the over-land retrieval. [157] explained how unexpected degradation of the
1023 internal 'Lambertian' source led to the inaccurate calibration, and MCST developed the Earth-View
1024 calibration method [158] to mitigate this artificial drift. This new calibration method was applied
1025 for Collection 6 (starting 2013 and then reprocessed through the full record) and one can observe
1026 from Figure 12 how the -18%/decade trend over land was reduced to near zero. The differences
1027 between Collection 5.1 and Collection 6 in the early years (e.g. prior to 2004) are much smaller, and
1028 we can attribute much of that to the newer retrieval algorithm rather than calibration. The
1029 differences in the later years are due to the de-trending of the calibration.
1030
1031   Rather than algorithm updates, the primary driver for a new Collection 6.1 in 2017 was also
1032 calibration. A known solar flare event affected Terra and caused electronic noise that severely
1033 degraded some of the infrared wavelength bands used for cloud masking. Unchecked, the data
1034 records could have been useless. Instead, our DT algorithm was revised to reduce reliance on the
1035 thermal cloud masking. At the same time MCST introduced a new set of visible/near-IR calibration
1036 coefficients that accounted for drift in additional channels. Potential discontinuities due to the
1037 'Terra anomaly' were reduced, leading to the smooth-looking data record seen in Figure 12.
1038
1039   The point is that the impact of calibration drift has been seen in the MODIS DT aerosol record,
1040 and in fact the DT aerosol record provides a useful 'check' on the calibration. Even a 2% drift in
1041 calibrated reflectance (which still meets required specifications) impacts the aerosol time series.
1042 Through Collection 5, 6, and now 6.1, the differences attributed to the new DT algorithms is generally
1043 less than the impact of calibration updates. Now that we believe that there is general consistency
1044 between Terra and Aqua -MODIS, as well as with other sensors, we are left with little or no significant

1045 trend on the global scale. By reducing the systematic drift on the global scale, we can study whether
1046 there are significant trends on the regional scale, as demonstrated in the right-hand panel of Figure
1047 12.
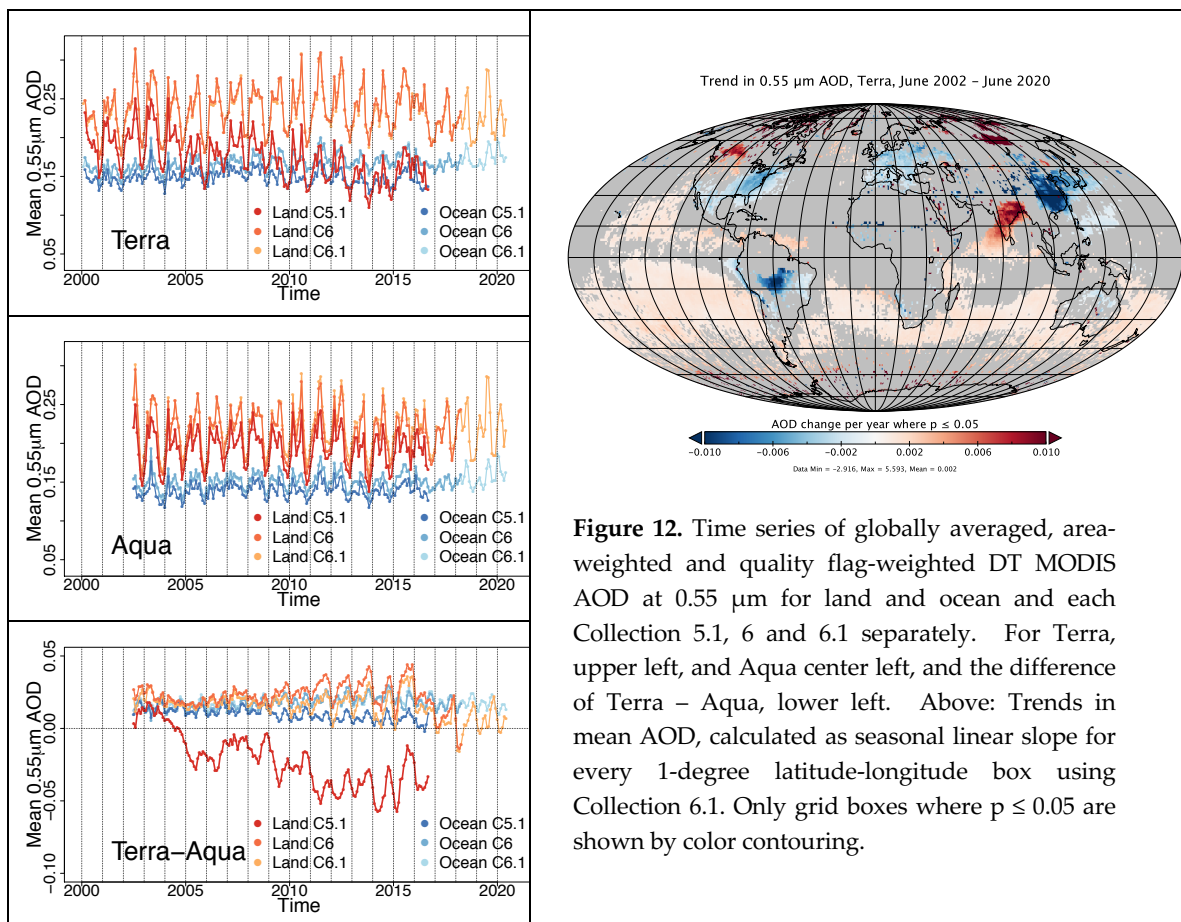
Figure 12. Time series of globally averaged, area-weighted and quality flag-weighted DT MODIS AOD at 0.55 μm for land and ocean and each Collection 5.1, 6 and 6.1 separately. For Terra, upper left, and Aqua center left, and the difference of Terra – Aqua, lower left. Above: Trends in mean AOD, calculated as seasonal linear slope for every 1-degree latitude-longitude box using Collection 6.1. Only grid boxes where $p \leq 0.05$ are shown by color contouring.

1048 **7. Major impacts of the Dark Target algorithm**

1049 The MODIS DT aerosol algorithm was the first operational algorithm to produce nearly daily global
1050 coverage of aerosol products over ocean and land, and it was one of the first to make its debut
1051 during the AERONET era when validation could be demonstrated quickly and easily. The data
1052 processing stream created two levels of aerosol products. Level 2 offered aerosol parameters along
1053 the orbital swath at nominal 10 km resolution, but Level 3 simplified the aerosol product by
1054 aggregating it into an equal angle grid of 1 deg latitude by 1 deg longitude. The Level 3 gridded
1055 product encouraged global analysis and comparison with global models. In addition, NASA
1056 invested in data distribution infrastructure that made acquiring, visualizing and understanding the
1057 products straightforward. The Goddard Distributed Active Archive Center (DAAC), now the Level
1058 1 and Atmosphere Archive and Distribution System (LAADS), made data acquisition easy for bulk
1059 analysis [159]. The GIOVANNI system provided quick data exploration online [160], and the Earth
1060 Observatory, an on-line magazine [161], highlighted new science and innovations made possible by
1061 NASA satellite products. The NASA Earth Data site [162] is a more recent compilation of web-
1062 based visualization tools, including WorldView [163] that continues to introduce and popularize
1063 the aerosol product, among many other satellite-derived products. In addition, the DT group
1064 produced a "stand alone code" for other groups to adopt into their own algorithms and for students
1065 to develop understanding of radiative transfer through the atmosphere from hands-on
1066 experimentation [164]. Soon after the launch of the Terra and Aqua satellites, and the production
1067 of a suite of new satellite products, the aerosol products, in particular, were adopted by multiple

1068   communities early in the mission and have made a lasting impact on science, applications and other
1069   aerosol remote sensing algorithms ever since.

1070   *7.1 Impact on climate prediction and processes*

1071   The initial motivation for proposing an algorithm to produce aerosol characteristics from MODIS
1072   observations was to narrow the uncertainties in climate prediction. The first publication in this
1073   direction made use of MODIS aerosol products and Clouds and the Earth's Radiant Energy System
1074   (CERES)   satellite products of reflected clear-sky solar flux to define the direct radiative efficiency
1075   of the aerosol in a aggregated, global sense [123]. Soon following this paper were several others that
1076   used the MODIS product, sometimes in conjunction with other aerosol measurements or models, to
1077   put observational constraints on the direct radiative effects and anthropogenic direct forcing of the
1078   aerosol either regionally [90] [165] [166] [167] [168] or globally [45] [57] [169] [170] [171] [172] [173]
1079   [174] [175]**.** Another singularly important study is [176] that approached the radiative effect more
1080   holistically, not distinguishing between cloud-free and cloudy skies, and instead used MODIS
1081   aerosol products in conjunction with CERES retrievals of all-sky radiative fluxes.
1082
1083   Other papers pioneered the use of satellite aerosol products, specifically the MODIS DT product,
1084   for evaluating global climate model representation of aerosol characteristics [177] [178] [179]. As the
1085   years passed, it became more common to rely on the DT product among other satellite-derived
1086   aerosol products for observationally-based estimates of direct aerosol effects and forcing, and to use
1087   these products with AERONET to evaluate and constrain different aspects of the global models we
1088   rely on to estimate future climate scenarios [170] [172] [180] [181] [182] [183] [184] [185] [186] [187]
1089   [188] [189] [190] [191].
1090
1091   The MODIS DT aerosol products have influenced one aspect of aerosol in climate prediction that
1092   requires specific attention, and that is the insight into aerosol-cloud relationships and aerosol
1093   indirect effects.   The first paper in this category that used the DT product was [125] that
1094   demonstrated the inverse relationship between smoke loading and cloud cover over the Amazon
1095   basin when AOD was at moderate to high levels, and then showed that the decrease in cloud cover
1096   created a positive radiative effect (warming) that easily overpowered the direct negative effect of
1097   the aerosol itself (cooling). Following [125] many studies made use of the MODIS DT aerosol
1098   product in conjunction with other products, observations and modeling to identify, quantify or
1099   interpret aerosol-cloud associations in these data sets [192] [193] [194] [195] [196] [197] [198] [199]
1100   [200] [201] [202] [203] [204] [205]. Without modeling, identified associations between MODIS DT
1101   AOD and cloud or other parameters may suggest, but does not prove, a physical process. However,
1102   the observed relationships between variables provide a greater challenge for models to duplicate,
1103   than does the challenge of representing each variable independently.
1104
1105   The studies cited above are far from an exhaustive list, and we choose to highlight these few based
1106   on their pioneering contribution or because of their impact, as evidenced by their high number of
1107   citations.   The MODIS DT aerosol products were part of a revolution of satellite observational data
1108   that helped to narrow the uncertainties on some aspects of climate change prediction, such as
1109   aerosol direct radiative effects and forcing.   At the same time, these observations, and especially
1110   documented relationships between different parameters challenged the community to consider

1111   some climate processes in a new light.   The MODIS DT aerosol products, and the studies that made
1112   use of these products, made a contribution to climate change assessment and prediction. The Fourth
1113   IPCC Assessment (AR4) highlighted the product with its own two-panel color figure [206] and
1114   made multiple references to the product and the observationally-based estimates of aerosol
1115   radiative effects and forcing associated with this product. AR4 was the first IPCC report to include
1116   a category of Observation Based in its chart of aerosol direct radiative forcing and cited three
1117   studies that had all used the MODIS DT aerosol products [170] [172] [175].   Six years later, with
1118   the Fifth IPCC Assessment (AR5) [207] the novelty of constraining total column AOD and clear-sky
1119   direct aerosol radiative forcing with global satellite data sets such as the MODIS DT product had
1120   dissipated.   Instead the report emphasizes climate-relevant processes with an expanded section on
1121   aerosol-cloud processes, stating, "satellite-based remote sensing continues to be the primary source
1122   of global data for aerosol-cloud interaction", and then states a concern about the fidelity of the
1123   satellite data sets in proximity to clouds. The section in the AR5 on aerosol-cloud interaction is
1124   supported by dozens of references to both modeling and observational studies.   Included in those
1125   references are many that used the MODIS DT aerosol products to find associations between DT
1126   AOD and other parameters, as cited above.

1127   *7.2 Impact on long-range particle transport*

1128   One important area that the MODIS aerosol product advanced considerably is quantification and
1129   characterization of long-range particle transport. The inspiration to use the product quantitatively
1130   for this purpose came from [208] that showed the potential of using the DT satellite product to
1131   identify dust aerosol over ocean but relied on field data to quantify the dust deposition.   The first
1132   paper to address this geophysical application quantitatively using the MODIS product, estimated
1133   the amount of African dust that crossed the Atlantic ocean [44], suggesting that African dust
1134   brought a significant amount of nutrients to the Amazon basin.   Following that paper the product
1135   has been used multiple times to produce an independent observationally-based estimate of
1136   intercontinental particle transport and deposition [46] [48] [209] [210] [211] [212]. The
1137   observationally-based estimates have provided an important constraint on modeled estimates [213]
1138   [214] [215] [216] [217] [218] and have been used to consider microbial transport on dust particles
1139   [219].

1140   *7.3 Impact on air quality monitoring and mitigation*

1141   Although initially designed for climate applications, the concept of using the satellite-retrieved total
1142   column aerosol loading to infer the particle mass (PM) at ground level has been one of the most
1143   wide-spread applications involving the DT product. A bridge between AOD and PM on the ground
1144   is the total column mass loading, and this was first attempted by [54].   The first studies
1145   investigating the possibility of using MODIS-retrieved AOD for a true air quality application were
1146   [128] and [129]. These papers were published within two weeks of each other. This was quickly
1147   followed by another pioneering study [220], leading to an effort to make the product available and
1148   usable to the operational air quality forecast community [130]. In the fifteen years since these early
1149   efforts, there has been an abundance of increasingly sophisticated attempts to make use of the
1150   MODIS DT and other aerosol products for air quality monitoring, health impact assessment and
1151   mitigation [221] [222] [223] [224] [225] [226] [227] [228][229] [230] [231] [232] [233] [234] [235] [236]
1152   [237] [238]. The cited papers are far from an exhaustive list, but they do represent a sample of

1153 highly cited studies that make use of the MODIS DT aerosol product in the field of air quality and
1154 exposure science.

1155 *7.4 Impact on assimilation systems*

1156 A key development in Earth system science that ran in parallel with the advancements in satellite
1157 remote sensing was the concept and implementation of global data assimilation systems [239].
1158 These are modeling/observational hybrids that use an objective scheme to create physically
1159 consistent fields of different parameters in the Earth system. Originally assimilation was the first
1160 step in numerical weather prediction, in which observations of meteorological variables such as
1161 wind, temperature and humidity fields would be assimilated into 3-dimensional grids and used as
1162 input in a forecast model. As new Earth system parameters became available from satellite remote
1163 sensing, including aerosol, assimilation systems began to ingest these parameters in addition to the
1164 meteorological observations.   The first system to ingest the MODIS DT aerosol product was the
1165 Naval Research Laboratory (NRL) Atmospheric Variational Data Assimilation System (NAVDAS)
1166 [131].   This was followed soon after by the European Centre for Medium-range Weather Forecasts
1167 (ECMWF) integrated forecast system [132]. In both of these cases, the operational AOD product had
1168 to be carefully screened to assure only the highest quality product entered the system, but the
1169 studies reported that ingesting the MODIS DT product significantly improved the aerosol
1170 forecasting ability of the models and reduced variance when comparing with ground truth [131].
1171 Initially only the DT AOD over ocean was used, but after the second-generation DT product over
1172 land was made operational [18] [19], the assimilation systems began using the global land AOD, as
1173 well [240]. Other examples using MODIS DT AOD in assimilation systems include [241] [242] [243].
1174 The success with the MODIS DT AOD product was an encouraging first step and now assimilation
1175 systems have matured to encompass a wide range of different geophysical observations including
1176 AOD from multiple satellites and products [244] [245].
1177
1178 In many ways the original goals in developing the DT aerosol products, which were to provide new
1179 insight into the global aerosol system and help to constrain estimates of climate forcing and change,
1180 are best served by assimilation systems which act to integrate many observations into a single
1181 system. The MODIS DT aerosol product played a significant role in advancing the capabilities of
1182 these important systems.

1183 *7.5 Impact on aerosol remote sensing*

1184 Besides having impact on Earth science and applications, the DT aerosol algorithm has been a major
1185 influence in the field of aerosol remote sensing.   The innovations put into place to create a nearly
1186 global aerosol product, over ocean and land, have been copied, adapted and improved upon by
1187 many other groups over the past 30 years. For example, the MODIS pre-launch algorithm for
1188 atmospheric correction over land [246] intended to use the at-launch MODIS DT aerosol product as
1189 input. Soon after launch the atmospheric correction developers made a few adjustments to the AOD
1190 product, mostly creating a finer resolution product needed by the land community [247], but still
1191 the fundamental algorithm remained the same.   By Collection 5, the atmospheric correction
1192 algorithm had added additional wavelengths to the aerosol retrieval (490 nm, 443 nm, 412 nm) and
1193 changed the wavelengths at which the surface reflectance ratios were calculated [248]. Eventually
1194 the MODIS atmospheric correction algorithm was ported to new sensors (e.g. Landsat-8

1195 Operational Land Imager). At this stage, the aerosol retrieval part of the algorithm was still based
1196 on the original principles of [12], but the aerosol models, the wavelengths used in the inversion, the
1197 surface reflectance ratios had all changed [249].   Most importantly, when the MODIS DT algorithm
1198 moved to the second-generation over land [18] [19], the MODIS atmospheric correction algorithm
1199 and its descendants did not, so the two algorithms now do not use the same inversion method. Yet,
1200 the influence of the original MODIS DT algorithm on the atmospheric correction is apparent in that
1201 the atmospheric correction algorithm still assumes surface reflectance ratios to translate
1202 assumptions about the surface from wavelengths less sensitive to aerosol to wavelengths more
1203 sensitive, and then retrieve where the sensitivity is greatest.
1204
1205 Other algorithms can also trace their heritage back to the MODIS DT algorithm. For example, many
1206 algorithms and groups make use of the dark target concept over land, using relationships between
1207 visible and shortwave infrared bands to separate atmospheric and surface contributions to satellite-
1208 measured reflectance.   These include the family of algorithms connected with the Along Track
1209 Scanning Radiometer (ATSR), Advanced ATSR (AATSR) and ATSR-2 [250] [251] and derivatives
1210 from these original algorithms (e.g. [252]). Other over land algorithms that follow the DT
1211 innovation for surface reflectance include the algorithms developed by the group at Yonsei
1212 University and applied to the Meteorological Imager (MI) [253] Geostationary Ocean Color Imager
1213 (GOCI) [254] [255] [256], Advanced Himawari Imager (AHI) [257] and others [258]   The NOAA
1214 aerosol algorithms over land, both the at-launch algorithm applied to VIIRS [259] and the
1215 Enterprise Processing System (EPS) applied to VIIRS and the Advanced Baseline Imagers [260] are
1216 dark target algorithms that have evolved from the original DT concept described in [12] [60]. The
1217 Deep Blue (DB) aerosol algorithm [152], the DT's sister algorithm on MODIS and VIIRS, turned to a
1218 DT-type land surface parameterization when the previously bright surface algorithm was adapted
1219 for vegetated surfaces [80][261]. Even the third aerosol algorithm on MODIS, the Multi-Angle
1220 Implementation of Atmospheric Correction (MAIAC) [262] makes use of assumed relationships
1221 between the shortwave infrared and the visible channels during its retrieval.
1222
1223 At least two algorithm families have adapted the DT ocean algorithm [13] in nearly its entirety.
1224 These are the MERIS ALAMO [263] [264] and NOAA [259] [260] algorithms. Other algorithms such
1225 as the PARASOL-POLDER algorithm were influenced by the DT ocean algorithm, incorporating a
1226 retrieval that mixes one fine mode and one coarse mode [265] [266], but otherwise deviates from DT
1227 to make use of the multi-angle polarization of POLDER.
1228
1229 We see the influence of DT innovations across the aerosol remote sensing community. Many
1230 algorithms followed the DT lead in turning to total column inversions from AERONET to define
1231 their aerosol models [255] [258] [259] [267], but others continued to use other databases derived
1232 from in situ measurements [252]. The 3x3 spatial variability cloud mask [122] and the subpixel
1233 snow detection [127] have made their way into subsequent algorithms [255] [258] [268]. The fact is
1234 that the innovations that the DT algorithm brought to aerosol remote sensing are now implemented
1235 so widely that they are now standard practice across the community.
1236
1237

8. Discussion

After 30 years, the DT algorithm is well on its path forward, expanding to other sensors beyond MODIS. Currently a version of DT is running operationally using VIIRS observations as inputs [24] [148] and a prototype DT algorithm has been applied to the Advanced Himawari Imager (AHI) [149] and the two Advanced Baseline Imagers (ABI) currently in geosynchronous orbit on the Himawari, GOES-E and GOES-W satellites [269].   The goal is to provide aerosol data users with a comprehensive view of the global aerosol system, combining the global coverage of polar orbiting satellites in Low Earth Orbit (LEO) with the high temporal coverage of sensors in geosynchronous orbit (GEO). Using the same basic algorithm across all sensors and platforms provides a necessary level of consistency for global studies. Even so, differences in sensor characteristics including wavelengths, spatial and temporal resolution, geometries and unresolved calibration offsets makes the task challenging. The DT team intends to homogenize these differences as much as possible and present the data on a common moderate spatial and temporal resolution grid. Figure 13 demonstrates how a DT merged GEO/LEO view of the global aerosol system might look at a single point in time. The combination of DT retrievals from all of these sensors smoothly fills in holes left by any individual sensor. Such spatial coverage will repeat at every time step, likely to be at minimum every 30 minutes.
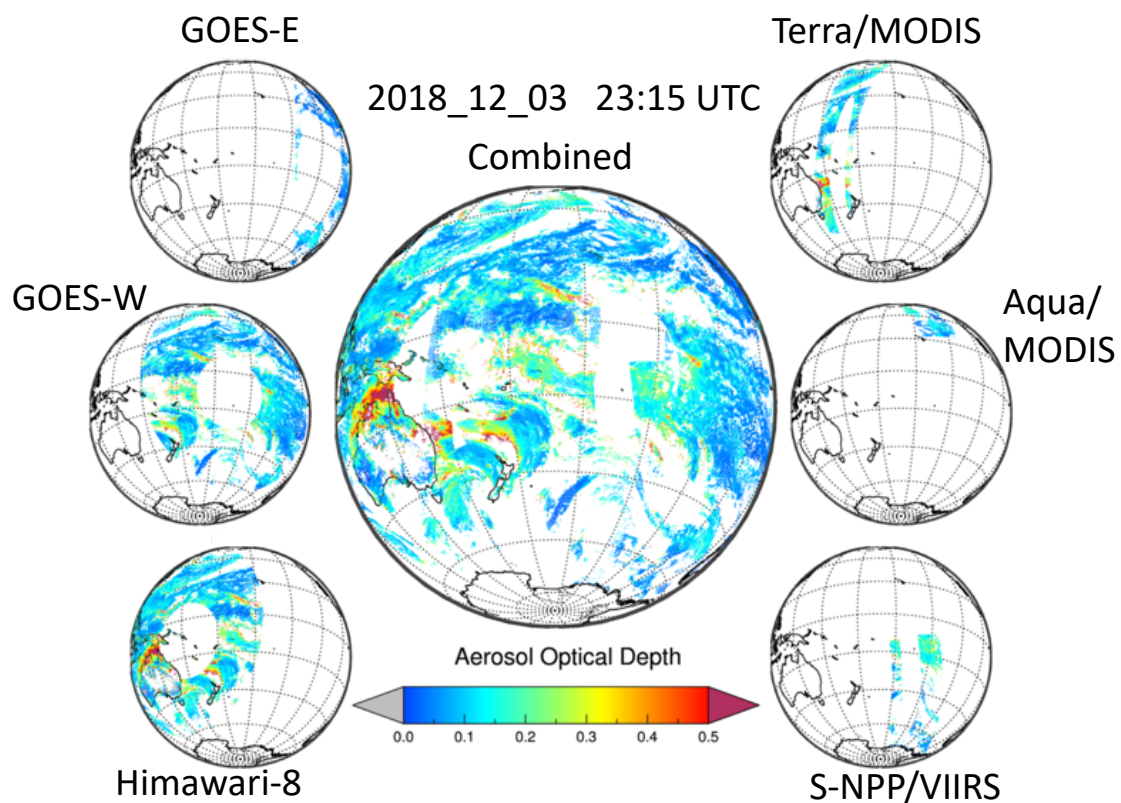
Figure 13. Aerosol optical depth at 0.55 μm, retrieved using the Collection 6.1 aerosol algorithm with inputs from ABI on GOES-E and GOES-W, AHI on Himawari-8, MODIS on Terra and Aqua and VIIRS on S-NPP, and the aggregated combination of the retrievals from all six sensors onto a common 0.1 deg by 0.1 deg spatial grid at 23:15 UTC ± 15 minutes on 03 December 2018.

The Dark Target algorithm can also be applied to more advanced multi-angle polarimeters that have hyperspectral or multi-band wavelengths across the same range as MODIS. Examples of such

sensors include the POLarization and Directionality of Earth Reflectances (POLDER) [266] and the radiometer and polarimeters of the Plankton, Aerosol, Clouds, ocean Ecosystems (PACE) mission [270]. This provides a well-understood baseline for global statistics of aerosol parameters and opportunity to continue and maintain long-term monitoring of the aerosol system into the coming decades.

9. Conclusions

The Dark Target aerosol algorithm produced satellite-derived products that changed our view of the global aerosol system, enabled innovative scientific studies, contributed to new ways of monitoring and forecasting air quality and influenced the field of aerosol remote sensing. By all accounts the DT algorithm has been one of NASA's important contributions to Earth science and applications. Looking back now over three decades we can pinpoint the features of the algorithm and the environment in which it was developed, produced and disseminated that enabled its widespread acceptance and integration into various user communities.

1. The algorithm is based on physical understanding of aerosols, their environment and radiative transfer. The algorithms are not mathematical inversions in the purest sense but are tuned to work within the realities of the physical world. Yet, the algorithm retains as much flexibility as possible, given the information content of multi-wavelength sensors.
2. Extensive pre- and post-launch field experiments with multiple types of measurements including simulations of the future sensor, validation for proto-algorithms and characterization of parameters that would become assumptions in the algorithm were essential elements contributing to the DT success.
3. Concurrent development of a robust ground validation program, involving AERONET, MAN and the MAPSS validation system that automatically linked the ground truth with the satellite products was the single most critical element of success. Characterizing the uncertainty of the aerosol products provided assurance to potential users.
4. Having an "at-launch" algorithm ready to go on Day 1 of the satellite mission required an investment of a decade of development time. It also required an algorithm that could function "on the fly" and not wait for an accumulation of statistics to constrain assumptions, such as a data base of land surface reflectances.
5. The concept of data Collections allowed state-of-the-science algorithms to produce stable time series. This kept the algorithms and calibration fresh and relevant, while guaranteeing consistency to user communities.
6. Investment in easily accessible visualization, analysis and dissemination tools lowered the barrier of entry for users of all levels of ability. Providing the data in $1^o \times 1^o$ gridded Level 3 arrays was key to enticing the global modeling community to use the data in their studies, while providing the 10 km and later the 3 km Level 2 data along the orbital swaths attracted the air quality community. Having a simple, functional data dissemination service, responsive to users, was another important element of success.
7. The products were delivered at multiple levels of difficulty to satisfy multiple needs. The goal was to maintain simplicity in the products, while not sacrificing the quality science behind the algorithm or the variety of retrieved parameters necessary for sophisticated analysis.
8. Continued investment in maintenance of the algorithm was essential, to keep the algorithm relevant as user needs evolved, particularly as the sensors degraded.

We note that many of the elements contributing to the success of the DT algorithm and products lay beyond the scope of the DT team. NASA's investment in AERONET, field experiments, reprocessing, a user-friendly data infrastructure and a long-term commitment to maintaining and improving the algorithm were equally (or more) important than the accomplishments of the team itself.

1310   Now looking forward we have opportunity to take these "lessons learned" and apply them to a
1311 constellation of new opportunities.   Already the DT algorithm has been ported to the polar orbiting
1312 VIIRS sensor and to the geosynchronous AHI sensor.   Each time the algorithm is applied to a new
1313 sensor we face new challenges. Both VIIRS and AHI introduced new viewing geometries, required
1314 adjustments to gaseous absorption and to specific aspects of the traditional algorithm because of
1315 missing wavelengths. However, the future of the DT algorithm and of operational satellite remote
1316 sensing in general is the unification of multiple sensors aboard many satellite platforms in a variety
1317 of orbits. The best way to move forward towards this unification is to apply a single algorithm or
1318 family of algorithms across all the sensors and platforms, managing consistency in the process. In
1319 this way the attempt of characterizing the global aerosol system that began over 30 years ago will
1320 grow closer to reality.

1344 **References**

1345   1. Kaufman, Y.; Tanré, D.; Boucher, O. A satellite view of aerosols in the climate
1346   system. *Nature*, **2002**, *419***,** 215–223, https://doi.org/10.1038/nature01091.
1347   2. Tanré, D.; Kaufman, Y.; Nakajima, T.; Ramanathan, V. Preface to special section on Global
1348   Aerosol System. *J. Geophys. Res.*, **2005**, *110*, D10S01, doi:10.1029/2004JD005724.
1349   3. Stier, P.; Feichter, J.; Roeckner, E.; Kloster, S.; Esch, M. The evolution of the global aerosol
1350   system in a transient climate simulation from 1860 to 2100. *Atmos. Chem. Phys.*, **2006**, *6*, 3059–
1351   3076, https://doi.org/10.5194/acp-6-3059-2006.
1352   4. Lawton, J. Earth System Science.   *Science*, **2001**, *292*, 1965, DOI:10.1126/science.292.5524.1965
1353   5. Griggs, M. Measurements of Atmospheric Aerosol Optical Thickness over Water Using
1354   ERTS-1 Data. *J. Air Poll. Control. Assoc.*, **1975**, *25*, 626, DOI: 10.1080/00022470.1975.10470118
1355   *6.* Fraser, R. S. Satellite measurement of mass of Sahara dust in the atmosphere. *Appl. Opt.*,
1356   **1976**, *15*. 2471–2479.

7. Mekler, Y., H. Quenzel, G. Ohring, and I. Marcus, "Relative atmospheric aerosol content from ERTS observations", J. Geophys. Res., 82 (1977), 967–972.

8. Stowe, L.L.; Carey, R.M.; Pellegrino, P.P. Monitoring the Mt. Pinatubo aerosol layer with NOAA/11 AVHRR data. *Geophys. Res. Lett.*, **1992**,*19,* 159-162, https://doi.org/10.1029/91GL02958

9. 9.Husar, R. B.; Stowe, L. L.; Prospero, J. M. Characterization of tropospheric aerosols over the oceans with the NOAA Advanced Very High Resolution Radiometer optical thickness operational product. *J. Geophys. Res.*, **1997**, *102***,** 16889–16910.

10. 10.Tilford, S. G.; Asrar, G.; Backlund, P.W. Mission to planet earth. *Adv. Space Res.*, **1994**, *14*, 5-9.

11. 11.Bowdle, D.A.; Rothermel, J.; Arnold, J.E.; Williams, S.F. GLObal Backscatter Experiment (GLOBE) Pacific survey mission. NASA, Washington, 4th Airborne Geoscience Workshop; 1991, 107-110, document ID 19910016138.

12. Kaufman, Y. J.; Tanré, D. ; Remer, L. A. ; Vermote, E. ; Chu, A. ; Holben, B. N. Operational remote sensing of tropospheric aerosol over land from EOS moderate resolution imaging spectroradiometer. *J. Geophys. Res.*, **1997**, *102*, 17051-17067, doi:10.1029/96JD03988.

13. Tanré, D.; Kaufman, Y. J.; Herman, M.; Mattoo, S. Remote sensing of aerosol properties over oceans using the MODIS/EOS spectral radiances. *J. Geophys. Res.*, **1997**, *102*, 16971– 16988, doi:10.1029/96JD03437.

14. Holben B.N.; Eck, T.F.; Slutsker, I.; Tanre, D.; Buis, J.P.; Setzer, A.; Vermote, E.; Reagan, J.A.; Kaufman, Y.; Nakajima, T.; Lavenu, F.; Jankowiak, I.; Smirnov, A. AERONET - A federated instrument network and data archive for aerosol characterization. *Rem. Sens. Environ.,* **1998**, *66*, 1-16, https://doi.org/10.1016/S0034-4257(98)00031-5

15. Levy, R.C.; Remer, L.A.; Kleidman, R.G.; Mattoo, S.; Ichoku, C.; Kahn, R.; Eck, T.F. Global evaluation of the Collection 5 MODIS dark-target aerosol products over land. *Atmos. Chem. Phys.*, **2010**, *10*, 10399–10420, https://doi.org/10.5194/acp-10-10399-2010.

16. Remer, L.A.; Kaufman, Y.J.; Tanré, D.; Mattoo, S.; Chu, D.A.; Martins, J.V.; Li, R-R.; Ichoku, C.; Levy, R.C.; Kleidman, R.G.; Eck, T.F.; Vermote, E.; Holben, B.N. The MODIS aerosol algorithm, products and validation. *J. Atmos. Sci.*, **2005**, *62*, 947-973, https://doi.org/10.1175/JAS3385.1

17. Remer, L. A., Mattoo, S., Levy, R. C., and Munchak, L. A. MODIS 3 km aerosol product: algorithm and global perspective. *Atmos. Meas. Tech.,* **2013**, *6*, 1829–1844, https://doi.org/10.5194/amt-6-1829-2013.

18. Levy, R. C.; Remer, L. A.; Dubovik, O. Global aerosol optical properties and application to Moderate Resolution Imaging Spectroradiometer aerosol retrieval over land. *J. Geophys. Res.*, **2007**, *112*, D13210, doi:10.1029/2006JD007815.

19. Levy, R. C.; Remer, L. A. ; Mattoo, S. ; Vermote, E. F.; Kaufman, Y. J. Second-generation operational algorithm: Retrieval of aerosol properties over land from inversion of Moderate Resolution Imaging Spectroradiometer spectral reflectance. *J. Geophys. Res.*, **2007**, 112, D13211, doi:10.1029/2006JD007811.

20. Levy, R. C.; Mattoo, S.; Munchak, L. A.; Remer, L. A.; Sayer, A. M.; Patadia, F.; Hsu, N. C. The Collection 6 MODIS aerosol products over land and ocean. *Atmos. Meas. Tech.*, **2013**, *6*, 2989–3034, https://doi.org/10.5194/amt-6-2989-2013.

1400   21. Levy, R. C.; Mattoo, S.; Sawyer, V.; Shi, Y.; Colarco, P. R.; Lyapustin, A. I.; Wang, Y.; Remer,
1401   L. A. Exploring systematic offsets between aerosol products from the two MODIS sensors.
1402   *Atmos. Meas. Tech.*, **2018**, *11*, 4073–4092, https://doi.org/10.5194/amt-11-4073-2018.
1403   22. Gupta, P; Levy, RC; Mattoo, S; Remer, LA; Munchak, LA. A surface reflectance scheme for
1404   retrieving aerosol optical depth over urban surfaces in MODIS Dark Target retrieval
1405   algorithm. *Atmos. Meas. Tech.*, **2016**, *9*, 3293-3308, doi: 10.5194/amt-9-3293-2016.
1406   23. Patadia, F.; Levy, R. C.; Mattoo, S. Correcting for trace gas absorption when retrieving
1407   aerosol optical depth from satellite observations of reflected shortwave radiation. *Atmos.*
1408   *Meas. Tech.*, **2018**, *11*, 3205–3219, doi:10.5194/amt-11-3205-2018.
1409   24. Sawyer, V.; Levy, R.; Mattoo, S.; Cureton, G.; Shi, Y.; Remer, L.A.   Continuing the MODIS
1410   Dark Target aerosol time series with VIIRS. *Remote Sens.*, **2020**, *12*, 308,
1411   https://doi.org/10.3390/rs12020308.
1412   25. Rao, C. R. N.; Stowe, L. L. ;   McClain, E. P.   Remote sensing of aerosols over the oceans
1413   using AVHRR data Theory, practice and applications, *Int. J. Rem. Sens.*, **1989**, *10*, 743-
1414   749, DOI: 10.1080/01431168908903915.
1415   26. Stowe, L. L.; Ignatov, A. M.; Singh, R. R. Development, validation, and potential
1416   enhancements to the second-generation operational aerosol product at the National
1417   Environmental Satellite, Data, and Information Service of the National Oceanic and
1418   Atmospheric Administration. *J. Geophys. Res. Atmos.*, **1997**, *102*, 16923-16934,
1419   https://doi.org/10.1029/96JD02132.
1420   27. Long, C. S.;Stowe, L. L. Using the NOAA/AVHRR to study stratospheric aerosol optical
1421   thicknesses following the Mt. Pinatubo eruption. *Geophys. Res. Lett.*, 1994,. *21*, 2215-2218, doi:
1422   10.1029/94GL01322.
1423   28. Ignatov, A.; Stowe, L.; Singh, R. Sensitivity study of the Angstrom exponent derived from
1424   AVHRR over oceans. *Adv. Space Res.*, **1998**, *21*, 439–442, https://doi.org/10.1016/S0273-
1425   1177(97)00926-5.
1426   29. Durkee, P. A.;   Pfeil, F.; Frost, E.; Shema, R. Global analysis of aerosol particle
1427   characteristics. *Atmos. Environ. Part A. Gen.Topics*, **1991**, *25*, 2457-2471,
1428   https://doi.org/10.1016/0960-1686(91)90163-2.
1429   30. Nakajima, T.; Higurashi, A.   A use of two-channel radiances for an aerosol characterization
1430   from space, *Geophys. Res. Lett.*, **1998**, *25*, 3815-3818, doi: 10.1029/98GL02151
1431   31. Higurashi, A.; Nakajima, T. Development of a Two-Channel Aerosol Retrieval Algorithm on a
1432   Global Scale Using NOAA AVHRR. *J. Atmos. Sci.*, **1999**, *56*, 924–941, https://doi.org/10.1175/1520-
1433   0469(1999)056<0924:DOATCA>2.0.CO;2.
1434   32. Mishchenko, M. I.; Geogdzhayev, I. V.; Cairns, B.; Rossow, W. B.; Lacis, A. A. Aerosol
1435   retrievals over the ocean by use of channels 1 and 2 AVHRR data: sensitivity analysis and
1436   preliminary results. *Applied Optics*, 1**999**, *38*, 7325-7341, doi: 10.1364/AO.38.007325.
1437   33. Geogdzhayev, I. V.; Mishchenko, M. I.; Rossow, W. B.; Cairns, B.; Lacis, A. A. Global Two-
1438   Channel AVHRR Retrievals of Aerosol Properties over the Ocean for the Period of *NOAA-*
1439   *9*Observations and Preliminary Retrievals Using *NOAA-7* and *NOAA-11* Data. *J. Atmos.*
1440   *Sci.*, **2002**, *59*, 262–278, https://doi.org/10.1175/1520-0469(2002)059<0262:GTCARO>2.0.CO;2.

34. Ignatov, A.; Sapper, J.; Cox, S. ; Laszlo, I.;   Nalli, N. R. ; Kidwell, K. B. Operational Aerosol Observations (AEROBS) from AVHRR/3 On Board NOAA-KLM Satellites. *J. Atmos. Oceanic Technol.*, **2004**, *21*, 3–26, https://doi.org/10.1175/1520-0426(2004)021<0003:OAOAFO>2.0.CO;2.

35. Hsu, N. C.; Lee, J.; Sayer, A. M.; Carletta, N.; Chen, S.-H.; Tucker, C. J.; Holben, B. N.; Tsay, S.-C. Retrieving near-global aerosol loading over land and ocean from AVHRR. *J. Geophys. Res. Atmos.*, **2017**, *122*, 9968– 9989, doi:10.1002/2017JD026932.

36. Herman, J. R.; Bhartia, P. K.; Torres, O.; Hsu, C.; Seftor, C.; Celarier, E.   Global distribution of UV-absorbing aerosols from Nimbus 7/TOMS data, *J. Geophys. Res.*, **1997**, *102*, 16911– 16922, doi:10.1029/96JD03680.

37. Tanré D.; Herman M.; Kaufman Y.J.; Information on the Aerosol Size Distribution contained in the Solar Reflected Spectral Radiances. *J. Geophys. Res.*, **1996**, *101*, 19043-19060, https://doi.org/10.1029/96JD00333.

38. d'Almeida, G. A.   On the variability of desert aerosol radiative characteristics, *J. Geophys. Res.*, **1987**, *92*, 3017– 3026, doi:10.1029/JD092iD03p03017.

39. Tanré, D.; Remer, L. A.; Kaufman, Y. J.; Mattoo, S.; Hobbs, P. V.; Livingston, J. M.; Russell, P. B.; Smirnov, A. Retrieval of Aerosol Optical Thickness and Size Distribution over Ocean from the MODIS Airborne Simulator during TARFOX. *J. Geophys. Res.*, **1999**, *104*, 2261-2278, https://doi.org/10.1029/1998JD200077.

40. Tanré, D.; Kaufman, Y.J.;   Holben, B.N.;   Chatenet, B.;   Karnieli, A.; Lavenu, F.; Blarel, L.; Dubovik, O.; Remer, L.A. ; Smirnov, A. Climatology of dust aerosol size distribution and optical properties derived from remotely sensed data in the solar spectrum. *J. Geophys. Res.*, **2001**, *106*, 18,205-18,218, https://doi.org/10.1029/2000JD900663.

41. Dubovik, O.;   King, M.D. A flexible inversion algorithm for retrieval of aerosol optical properties from sun and sky radiance measurements. *J. Geophys. Res.,* 2000, 105,20673–20696, https://doi.org/10.1029/2000JD900282.

42. Dubovik O.; Smirnov, A. ; Holben, B. N.;   King, M. D. ; Kaufman, Y. J.; Eck, T. F. ; Slutsker, I. Accuracy assessment of aerosol optical properties retrieval from AERONET sun and sky radiance measurements, *J. Geophys. Res.*, **2000**, 105, 9791–9806, https://doi.org/10.1029/2000JD900040.

43. Dubovik, O.; Holben, B. N. ; Eck, T. F. ;   Smirnov, A.; Kaufman, Y. J.; King, M. D.;   Tanré, D; Slutsker, I.   Variability of absorption and optical properties of key aerosol types observed in worldwide locations, *J. Atmos. Sci.*, **2002**, *59*, 590–608, https://doi.org/10.1175/1520-0469(2002)059<0590:VOAAOP>2.0.CO;2.

44. Kaufman, Y. J.; Koren, I.; Remer, L. A.; Tanré, D.; Ginoux, P.; Fan, S. Dust transport and deposition observed from the Terra-Moderate Resolution Imaging Spectroradiometer (MODIS) spacecraft over the Atlantic Ocean, *J. Geophys. Res.*, **2005**, *110*, D10S12, doi:10.1029/2003JD004436.

45. Kaufman, Y. J.; Boucher, O.; Tanré, D.; Chin, M.; Remer, L. A.; Takemura, T. Aerosol anthropogenic component estimated from satellite data., *Geophys. Res. Lett.*, **2005**c, *32*, L17804, doi:17810.11029/12005GL023125.

46. Yu, H.; Remer, L.A.; Chin, M.; Bian, H-S.; Tan, Q.; Yuan,T.; Zhang, Y. Aerosols from Overseas Rival Domestic Emissions over North America. *Science*, **2012**, 337, 566-569, DOI: 10.1126/science.1217576.

47. Kleidman, R. G.; O'Neill, N. T.; Remer, L. A.; Kaufman, Y. J.; Eck, T. F.; Tanré, D.; Dubovik, O.; Holben, B. N. Comparison of MODIS and AERONET remote sensing retrievals of aerosol fine mode fraction over ocean., *J. Geophys. Res.*, **2005**, *110*, D22205, doi:22210.21029/22005/JD005760.

48. Yu, H.; Remer, L. A.; Chin, M. ; Bian, H.; Kleidman, R. G.; Diehl, T. A satellite-based assessment of transpacific transport of pollution aerosol. *J. Geophys. Res.*, **2008**, *113*, D14S12, doi:10.1029/2007JD009349.

49. Yu, H.; Chin, M.; Remer, L.A.; Kleidman, R.G.; Bellouin, N.; Bian, H.S.; Diehl, T. Variability of marine aerosol fine-mode fraction and estimates of anthropogenic aerosol component over cloud-free oceans from the Moderate Resolution Imaging Spectroradiometer (MODIS). *J. Geophys. Res.*, **2009**, *114*, D10206, DOI: 10.1029/2008JD010648.

50. King, M.D.; Menzel, W.P.; Grant, P.S.; Myers, J.S.; Arnold, G.T.; Platnick, S.E.; Gumley, L.E.; Tsay, S-C., Moeller, C.C.; Fitzgerald, M.; Brown, K.S; Osterwisch, F.G. Airborne scanning spectrometer for remote sensing of cloud, aerosol, water vapor and surface properties. *J. Atmos. Ocean. Tech.*, **1996**, *13*, 777-794, https://doi.org/10.1175/1520-0426(1996)013<0777:ASSFRS>2.0.CO;2.

51. Gassó, S.; Hegg, D. A. Comparison of columnar aerosol optical properties measured by the MODIS airborne simulator with in situ measurements. *Rem. Sens. Environ.*, **1998**, *66*, 138–152. https://doi.org/10.1016/S0034-4257(98)00052-2.

52. Russell, P. B.; Hobbs, P. V.; Stowe, L. L. Aerosol properties and radiative effects in the United States East Coast haze plume: An overview of the Tropospheric Aerosol Radiative Forcing Observational Experiment (TARFOX), *J. Geophys. Res.*, **1999**, *104*, 2213– 2222, doi:10.1029/1998JD200028.

53. Hobbs, P. V. An overview of the University of Washington airborne measurements and results from the Tropospheric Aerosol Radiative Forcing Observational Experiment (TARFOX), *J. Geophys. Res.*, **1999**, 104, 2233– 2238, doi:10.1029/98JD02283.

54. Gassó, S., ;Hegg, D. A., On the retrieval of columnar aerosol mass and CCN concentration by MODIS, *J. Geophys. Res.*, **2003**, *108*, 4010, doi:10.1029/2002JD002382.

55. Matsumoto, T.; Russell, P. ; Mina, C. ; Van Ark, W. ; Banta, V. Airborne Tracking Sunphotometer. *J. Atmos. Ocean . Tech.*, **1987**, *4*, 336-339, https://doi.org/10.1175/1520-0426(1987)004<0336:ATS>2.0.CO;2

56. Russell, P. B.; Livingston, J. M.; Hignett, P.; Kinne, S.; Wong, J.; Chien, A.; Bergstrom, R.; Durkee, P.; Hobbs, P. V. Aerosol-induced radiative flux changes off the United States mid-Atlantic coast: Comparison of values calculated from sunphotometer and in situ data with those measured by airborne pyranometer. *J. Geophys. Res.*, **1999**b, *104*, 2289– 2307, doi:10.1029/1998JD200025.

57. Remer, L. A.; Kaufman, Y. J. Aerosol direct radiative effect at the top of the atmosphere over cloud free ocean derived from four years of MODIS data. *Atmos. Chem. Phys.*, **2006**, *6*, 237–253, https://doi.org/10.5194/acp-6-237-2006.

58. Kaufman, Y.J.; Sendra, C. Algorithm for atmospheric corrections. *Int. J. Remote Sensing,* **1988**, *9*, 1357–1381, DOI: 10.1080/01431168808954942.

59. Kaufman, Y. J.; Remer, L. A. Detection of Forests Using Mid-IR Reflectance: An Application for Aerosol Studies. *IEEE Trans. Geoscience Rem. Sens.*, **1994**, *32*, 672-683, doi: 10.1109/36.297984.

60. Kaufman, Y. J.; Wald, A. E.; Remer, L. A.; Gao, B.-C.; Li, R.-R.; Flynn, L. The MODIS 2.1 μm Channel - Correlation with visible reflectance for use in remote sensing of aerosol. *IEEE Trans. Geo*, **1997**b, *35*, 1286-1298, doi; 10.1109/36.628795.

61. Remer, L. A.; Wald, A. E.; Kaufman, Y. J. Angular and Seasonal Variation of Spectral Surface Reflectance Ratios: Application to the Remote Sensing of Aerosol Over Land. *IEEE Trans. Geosci. Rem. Sens.*, **2001**, *39*, 275-283, doi: 10.1109/36.905235.

62. Kaufman, Y. J. ; Gobron, N. ; Pinty, B. ; Widlowski, J.-L. ; Verstraete, M. M. Relationship between surface reflectance in the visible and mid-IR used in MODIS aerosol algorithm - theory, *Geophys. Res. Lett.*, **2002**, *29*, 2116, doi:10.1029/2001GL014492.

63. Kaufman, Y. J.; Gitelson, A.; Karnieli, A.; Ganor, E.; Fraser, R. S.; Nakajima, T.; Mattoo, S.; Holben, B. N. Size distribution and scattering phase function of aerosol particles retrieved from sky brightness measurements, *J. Geophys. Res.*,**1994**, *99*, 10341– 10356, doi:10.1029/94JD00229.

64. Remer, L. A.; Kaufman, Y. J. Dynamical Aerosol Model: Urban/industrial Aerosol. *J. Geophys. Res.*, **1998**, *103*, 13859-13871, doi: 10.1029/98JD00994.

65. Remer, L. A.; Kaufman, Y. J. ; Holben, B. N. ; Thompson, A. M. ; McNamara, D. A model of tropical biomass burning smoke aerosol size distribution. *J. Geophys. Res.*, **1998**, *103*, 31879-31891. doi: /10.1029/98JD00271.

66. Remer, L. A.; Gassó, S.; Hegg, D. A. ;Kaufman, Y. J.; Holben, B. N. Urban/industrial aerosol: Ground-based sun/sky radiometer and airborne in situ measurements. *J. Geophys. Res.*, **1997**, *102*, 16849-16859, doi:10.1029/96JD01932.

67. Yamasoe, M.A.; Kaufman, Y.J.; Dubovik, O.; Remer, L.A.; Holben, B.N.; Artaxo, P. Retrieval of the real part of the refractive index of aerosols from sun/sky radiometers during SCAR-B. *J. Geophys. Res.*, **1998**, *103*, 31,893-31,902, https://doi.org/10.1029/98JD01211.

68. Chu, D. A.; Kaufman, Y. J. ; Remer, L. A. ; Holben, B. N. Remote sensing of smoke from MODIS airborne simulator during the SCAR-B experiment. *J. Geophys. Res,*, **1998**: *103*, 31 979–31 988, https://doi.org/10.1029/98JD01148.

69. King, M.D. ; Menzel, W.P.; Kaufman, Y. J.; Tanré, D.; Gao, B.-C.; Platnick, S.E.; Ackerman, S.A.; Remer, L.A.; Pincus, R.; Hubanks, P.A. Cloud and aerosol properties, precipitable water, and profiles of temperature and water vapor from MODIS. *IEEE Trans. Geo. Rem. Sens.*, **2003**, *41*, 442-458, doi: 10.1109/TGRS.2002.808226.

70. Berrick, S. W.; Leptoukh, G.; Farley, J. D.; Rui, H. Giovanni: A Web Service Workflow-Based Data Visualization and Analysis System, *IEEE Trans. Geo. Rem. Sens.*, **2009**, *47*, 106-113. doi: 10.1109/TGRS.2008.2003183.

71. Holben, B.N.; Tanre, D.; Smirnov, A.; Eck, T.F.; Slutsker, I.; Abuhassan, N.; Newcomb, W.W.; Schafer, J.; Chatenet, B.; Lavenue, F.; Kaufman, Y.J.; Vande Castle, J.; Setzer, A.; Markham, B.; Clark, D.; Frouin, R.; Halthore, R.; Karnieli, A.; O'Neill, N.T.; Pietras, C.; Pinker, R.T.; Voss, K.; Zibordi, G. An emerging ground-based aerosol climatology: Aerosol Optical Depth from AERONET, *J. Geophys. Res.*, **2001**, *106*, 12 067-12 097.

72. Smirnov A.; Holben, B.N.; Eck, T.F.; Dubovik, O.; Slutsker, I. Cloud screening and quality control algorithms for the AERONET database, *Rem.Sens.Env.*, **2000**, *73*, 337-349, https://doi.org/10.1016/S0034-4257(00)00109-7.

73. Smirnov, A.; Holben, B. N. ; Slutsker, I.; Giles, D. M.; McClain, C. R.; Eck, T. F.; Sakerin, S. M.; Macke, A.; Croot, P.; Zibordi, G.; Quinn, P. K.; Sciare, J.; Kinne, S.; Harvey, M.; Smyth, T. J.; Piketh, S.; Zielinski, T.; Proshutinsky, A.; Goes, J. I.; Nelson, N. B.; Larouche, P.; Radionov, V. F. ; Goloub, P.; Krishna Moorthy, K.; Matarrese, R.; Robertson, E. J.; Jourdin, F. Maritime Aerosol Network as a component of Aerosol Robotic Network, *J. Geophys. Res.*, **2009**, *114*, D06204, doi:10.1029/2008JD011257.

74. Giles, D. M.,; Sinyuk, A.; Sorokin, M. G.; Schafer, J. S.; Smirnov, A.; Slutsker, I.,; Eck, T. F.; Holben, B. N.; Lewis, J. R.,; Campbell, J. R.; Welton, E. J.,; Korkin, S. V.; Lyapustin, A. I. Advancements in the Aerosol Robotic Network (AERONET) Version 3 database – automated near-real-time quality control algorithm with improved cloud screening for Sun photometer aerosol optical depth (AOD) measurements, *Atmos. Meas. Tech.*, **2019**, *12*, 169-209, https://doi.org/10.5194/amt-12-169-2019.

75. King, M. D.; Kaufman, Y. J.; Tanré, D.; Nakajima, T. Remote Sensing of Tropospheric Aerosols from Space: Past, Present, and Future. *Bull. Amer. Meteor. Soc.*, **1999**, *80*, 2229–2260, doi.org/10.1175/1520-0477(1999)080<2229:RSOTAF>2.0.CO;2.

76. Munchak, L. A.; Levy, R. C.; Mattoo, S.; Remer, L. A.; Holben, B. N.; Schafer, J. S.; Hostetler, C. A.; and Ferrare, R. A. MODIS 3 km aerosol product: applications over land in an urban/suburban region. *Atmos. Meas. Tech.*, **2013**, *6*, 1747–1759, https://doi.org/10.5194/amt-6-1747-2013.

77. Gupta, P.; Remer, L.A ; Levy, R.C.; Mattoo, S. Validation of MODIS 3 km land aerosol optical depth from NASA's EOS Terra and Aqua missions. *Atmos. Meas. Tech.*, **2018**, *11*, 3145-3159, doi: 10.5194/amt-11-3145-2018.

78. Xiao, Q.; Zhang, H.; Choi, M.; Li, S.; Kondragunta, S.; Kim, J.; Holben, B.; Levy, R.C.; Liu, Y. Evaluation of VIIRS, GOCI, and MODIS Collection 6 AOD retrievals against ground sunphotometer observations over East Asia. *Atmos. Chem. Phys.*, **2016**, *16*, 1255–1269, https://doi.org/10.5194/acp-16-1255-2016.

79. Xie, Y.; Zhang, Y.; Xiong, X.; Qu, J.J.; Che, H. Validation of MODIS aerosol optical depth product over China using CARSNET measurements. *Atmos. Environ.*, **2011**, *45*, 5970-5978, https://doi.org/10.1016/j.atmosenv.2011.08.002.

80. Hsu, N. C.; Jeong, M.-J. ; Bettenhausen, C. ; Sayer, A. M. ; Hansell, R. ; Seftor, C. S.; Huang, J. ; Tsay, S.-C. Enhanced Deep Blue aerosol retrieval algorithm: The second generation. *J. Geophys. Res. Atmos.*, **2013**, *118*, 9296–9315, doi:10.1002/jgrd.50712.

81. Liu, H.; Remer, L. A.; Huang, J.; Huang, H.-C.; Kondragunta, S.; Laszlo, I.; Oo, M.; Jackson, J. M. Preliminary evaluation of S-NPP VIIRS aerosol optical thickness, *J. Geophys. Res. Atmos.*, **2014**, *119*, 3942– 3962, doi:10.1002/2013JD020360.

82. Nichol, J.E.; Bilal, M. Validation of MODIS 3 km resolution aerosol optical depth retrievals over Asia. *Rem. Sens.*, **2016**, *8*, 328, doi: 10.3390/rs8040328.

83. O'Neill, N. T.; Eck, T. F.; Smirnov, A.; Holben, B. N.; Thulasiraman, S. Spectral discrimination of coarse and fine mode optical depth, *J. Geophys. Res.*, **2003**, *108*, 4559-4573, 1doi:0.1029/2002JD002975.

84. Ichoku, C.; Chu, D. A.; Mattoo, S.; Kaufman, Y. J.; Remer, L. A.; Tanré, D.; Slutsker, I.; Holben, B. N. A spatio-temporal approach for global validation and analysis of MODIS aerosol products. *Geophys. Res. Lett.*, **2002**, 29, doi:10.1029/2001GL013206.

85. Petrenko, M.; Ichoku, C.; Leptoukh, G. Multi-sensor Aerosol Products Sampling System (MAPSS). *Atmos. Meas. Tech.*, **2012**, *5*, 913–926, https://doi.org/10.5194/amt-5-913-2012.

86. MAPSS: Multi-sensor Aerosol Products Sampling System. Available on-line at https://giovanni.gsfc.nasa.gov/mapss/   Accessed: 28 July 2020.

87. Chu, D. A.; Kaufman, Y. J.; Ichoku, C.; Remer, L. A.; Tanré, D.; Holben, B. N. Validation of MODIS aerosol optical depth retrieval over land. *Geophys. Res. Lett.*, **2002**, *29*, doi:10.1029/2001GL013205.

88. Remer, L. A.; Tanré, D.; Kaufmann, Y. J.; Ichoku, C.; Mattoo, S.; Levy, R.; Chu, D. A.; Holben, B.; Dubovik, O.; Smirnov, A.; Martins, J. V.; Li, R.-R.; Ahmad, Z. Validation of MODIS aerosol retrieval over ocean. *Geophys. Res. Lett.*, **2002**, 29, doi:10.1029/2001GL013204.

89. Chu, D. A., et al. Evaluation of aerosol properties over ocean from Moderate Resolution Imaging Spectroradiometer (MODIS) during ACE-Asia, *J. Geophys. Res.*, **2005**, *110*, D07308, doi:10.1029/2004JD005208.

90. Ichoku, C.; Remer, L.A. ; Kaufman, Y.J. ; Levy, R. ; Chu, D.A. ; Tanré , D. ; Holben, B.N. MODIS observation of aerosols and estimation of aerosol radiative forcing over southern Africa during SAFARI 2000. *J. Geophys. Res.*, **2003**, *108*, 8499, 10.1029/2002JD002366.

91. Levy, R.C.; Remer, L.A. ; Tanré, D. ; Kaufman, Y.J.; Ichoku, C. ; Holben, B.N. ; Livingston,   J.M.; Russell, P.B.; Maring, H. Evaluation of the MODIS retrievals of dust aerosol over the ocean during PRIDE. *J. Geophys. Res.*, **2003**, *108*, 10.1029/2002JD002460.

92. Levy, R.C., Remer, L.A. ; Martins, J.V. ; Kaufman, Y.J. ; Plana-Fattori, A.,   Redemann, J. ; Russell, P.B.; Wenny, B.   Evaluation of the MODIS aerosol retrievals over ocean and land during CLAMS. *J. Atmos. Sci.*, **2005**, *62*, 974-992, 10.1175/JAS3391.1

93. Xia XA; Chen HB; Wang PC. Validation of MODIS aerosol retrievals and evaluation of potential cloud contamination in East Asia. *J. Environ. Sci. (China*), **2004**, *16*, 832-837.

94. Ichoku, C.; Remer, L. A. ; Eck, T. F.   Quantitative evaluation and intercomparison of morning and afternoon Moderate Resolution Imaging Spectroradiometer (MODIS) aerosol measurements from Terra and Aqua. *J. Geophys. Res.*, **2005**, *110*, D10S03, doi:10.1029/2004JD004987.

95. Tripathi, S.N.; Dey, S.; Chandel, A.; Srivastava, S.; Singh, R.P.; Holben, B.N. Comparison of MODIS and AERONET derived aerosol optical depth over the Ganga Basin, India.   *Ann. Geophys.*, **2005**, *23*, 1093–1101, https://doi.org/10.5194/angeo-23-1093-2005.

96. Sayer, A.M.; Hsu, N.C.; Eck, T.F.; Smirnov, A.; Holben, B.N. AERONET-based models of smoke-dominated aerosol near source regions and transported over oceans, and implications for satellite retrievals of aerosol optical depth. *Atmos. Chem. Phys*, **2014**, *14*, 11493–11523, 10.5194/acp-14-11493-2014.

97. Wang, Y.,; Yuan, Q.; Li, T.; Shen, H.; Zheng, L.; Zhang, L. Evaluation and comparison of MODIS Collection 6.1 aerosol optical depth against AERONET over regions in China with multifarious underlying surfaces. *Atmos. Environ.*, **2019**, *200*, 280-301, https://doi.org/10.1016/j.atmosenv.2018.12.023.

98. Wei, J.; Li, Z.; Peng, Y.; Sun, L. MODIS Collection 6.1 aerosol optical depth products over land and ocean: validation and comparison. *Atmos. Environ.*, **2019**, *201*, 428-440, https://doi.org/10.1016/j.atmosenv.2018.12.004.

99. Bilal, M.; Nazeer, M.; Nichol, J.; Qiu, Z.; Wang, L.; Bleiweiss, M.P.; Shen, X.; Campbell, J.R.; Lolli, S. Evaluation of Terra-MODIS C6 and C6. 1 Aerosol Products against Beijing, XiangHe, and Xinglong AERONET Sites in China during 2004-2014. *Remote Sensing*, **2019,** *11*, 486, doi:10.3390/rs11050486.

100. Bright, J.M.; Gueymard, C.A. Climate-specific and global validation of MODIS Aqua and Terra aerosol optical depth at 452 AERONET stations. *Solar Energy*, **2019**, *183*, 594-605, https://doi.org/10.1016/j.solener.2019.03.043.

101. Zhang, M.; Liu, J.; Li, W.; Bilal, M.; Zhao, F.; Zhang, C.; Yuan, B.; Khedher, K.M. Evaluation of the Aqua-MODIS C6 and C6. 1 Aerosol Optical Depth Products in the Yellow River Basin, China. *Atmosphere*, **2019**, *10*, 426, DOI:10.3390/atmos10080426.

102. Choi, M.; Lim, H.; Kim, J.; Lee, S.; Eck, T.F.; Holben, B.N.; Garay, M.J.; Hyer, E.J.; Saide, P.E.; Liu, H. Validation, comparison, and integration of GOCI, AHI, MODIS, MISR, and VIIRS aerosol optical depth over East Asia during the 2016 KORUS-AQ campaign. *Atmos. Meas. Tech.*, **2019**, *12*, 4619-4641, https://doi.org/10.5194/amt-12-4619-2019

103. Tian, X.; Gao, Z. Validation and Accuracy Assessment of MODIS C6. 1 Aerosol Products over the Heavy Aerosol Loading Area. *Atmosphere*, 2019, *10,* 548, https://doi.org/10.3390/atmos10090548.

104. Fan, X.; Xia, X.; Chen, H. Intercomparison of Multiple Satellite Aerosol Products against AERONET over the North China Plain. *Atmosphere*, **2019**, *10*, 480, https://doi.org/10.3390/atmos10090480.

105. Che, H.; Yang, L.; Liu, C.; Xia, X.; Wang, Y.; Wang, H.; Wang, H.; Lu, X.; Zhang, X. Long-term validation of MODIS C6 and C6. 1 Dark Target aerosol products over China using CARSNET and AERONET. *Chemosphere*, **2019**, *236*, 124268, https://doi.org/10.1016/j.chemosphere.2019.06.238.

106. Mei, L.; Zhao, C.; de Leeuw, G.; Che, H.; Che, Y.; Rozanov, V.; Vountas, M.; Burrows, J.P.; Understanding MODIS dark-target collection 5 and 6 aerosol data over China: Effect of surface type, aerosol loading and aerosol absorption. *Atmos. Res.*, **2019**, *228*, 161-175. DOI:10.1016/J.ATMOSRES.2019.05.023.

107. Huang, J.; Kondragunta, S.,; Laszlo, I.,; Liu, H.; Remer, L. A.,; Zhang, H.; Superczynski, S.; Ciren, P.; Holben, B. N.; Petrenko, M.   Validation and expected error estimation of Suomi-NPP VIIRS aerosol optical thickness and Ångström exponent with AERONET. *J. Geophys. Res. Atmos.*, **2016**, *121*, 7139– 7160, doi:10.1002/2016JD024834.

108. Huang, Y.; Zhu, B.,; Zhu, Z.; Zhang, T.; Gong, W.; Ji, Y.; Xia, X.; Wang, L.; Zhou, X. ; Chen, D. Evaluation and Comparison of MODIS Collection 6.1 and Collection 6 Dark Target Aerosol Optical Depth over Mainland China Under Various Conditions Including Spatiotemporal Distribution, Haze Effects, and Underlying Surface. *Earth and Space Sci.*, **2019**, *6*, 2575-2592, https://doi.org/10.1029/2019EA000809

109. Li, Y.; Shi, G. ; Sun, Z. Evaluation and improvement of MODIS aerosol optical depth products over China. *Atmos. Environ.*,   **2020**, *223*, 117251, doi: 10.1016/j.atmosenv.2019.117251

110. You, Y.,; Zhao, T.,; Xie, Y.; Zheng, Y.; Zhu, J.; Xia, J.; Cao, L.; Wang, C.; Che, H.; Liao, Y.; Duan, J. Variation of the aerosol optical properties and validation of MODIS AOD products over the eastern edge of the Tibetan Plateau based on ground-based remote sensing in 2017. *Atmos. Environ.*, **2020**, *223*, 117257, https://doi.org/10.1016/j.atmosenv.2019.117257.

111. Yang, X.; Zhao, C.; Luo, N.; Zhao, W.; Shi, W.; Yan, X. Evaluation and Comparison of Himawari-8 L2 V1. 0, V2. 1 and MODIS C6. 1 aerosol products over Asia and the oceania regions. *Atmos. Environ.*, **2020**, *220*, 117068, https://doi.org/10.1016/j.atmosenv.2019.117068.

112. Holben, B. N.; Eck, T. F.; Slutsker, I.; Smirnov, A. ; Sinyuk, A; Schafer, J. ; Giles, D. ; Dubovik, O. Aeronet's Version 2.0 quality assurance criteria, *Proc. SPIE 6408, Remote Sensing of the Atmosphere and Clouds*, **2006**, *64080Q*, doi:10.1117/12.706524.

113. Schmid, B., et al. Coordinated airborne, spaceborne, and ground-based measurements of massive thick aerosol layers during the dry season in southern Africa, *J. Geophys. Res.*, **2003**, 108, 8496, doi:10.1029/2002JD002297.

114. Livingston, J. M., et al. Airborne Sun photometer measurements of aerosol optical depth and columnar water vapor during the Puerto Rico Dust Experiment and comparison with land, aircraft, and satellite measurements, *J. Geophys. Res.*, **2003**, *108*, 8588, doi:10.1029/2002JD002520.

115. Redemann, J.; Zhang, Q.; Livingston, J.; Russell, P.; Shinozuka, Y.; Clarke, A.; Johnson, R.; Levy, R. Testing aerosol properties in MODIS Collection 4 and 5 using airborne sunphotometer observations in INTEX-B/MILAGRO. *Atmos. Chem. Phys.***, 2009**, *9*, 8159–8172, doi: 10.5194/acp-9-8159-2009.

116. Redemann, J.; Schmid, B.; Eilers, J.A.; Kahn, R.; Levy, R.C.; Russell, P.B.; Livingston, J.M.; Hobbs, P.V.; Smith Jr, W.L.; Holben, B.N. Suborbital measurements of spectral aerosol optical depth and its variability at subsatellite grid scales in support of CLAMS 2001. *J. Atmos. Sci.*, **2005**, *62*, 993-1007, doi: 10.1175/JAS3387.1

117. Russell, P. B., et al. Multi-grid-cell validation of satellite aerosol property retrievals in INTEX/ITCT/ICARTT 2004. *J. Geophys. Res.*, **2007**, *112*, D12S09, doi:10.1029/2006JD007606.

118. Holben, B.N.; Kim, J.; Sano, I.,; Mukai, S.; Eck, T.F.; Giles, D.M.,; Schafer, J.S.,; Sinyuk, A.; Slutsker, I.,; Smirnov, A.; Sorokin, M. and co-authors. An overview of mesoscale aerosol processes, comparisons, and validation studies from DRAGON networks. *Atmos. Chem. Phys.*, **2018**, *18*, 655–671, https://doi.org/10.5194/acp-18-655-2018.

119. Eck, T.F.,;.Holben, B.N ; Reid, J.S.; Dubovik, O.; Smirnov, A.; O'Neill, N.T.; Slutsker, I.; Kinne, S. Wavelength dependence of the optical depth of biomass burning, urban and desert dust aerosols, *J. Geophys. Res.*, **1999**, *104*, 31333-31350, https://doi.org/10.1029/1999JD900923.

120. Reid, J. S. ; Maring, H. B. Foreword to special section on the Puerto Rico Dust Experiment (PRIDE). *J. Geophys. Res.*, **2003**, *108*, D19, 8585, doi:10.1029/2003JD0035102003

121. Charlock, T.P.; Smith, W.L. PREFACE. *J. Atmos. Sci.*, **2005**, *62*, 901–902, https://doi.org/10.1175/JAS9001.1.

122. Martins, J. V.; Tanré, D.; Remer, L.; Kaufman, Y.; Mattoo, S.,; Levy, R, MODIS Cloud screening for remote sensing of aerosols over oceans using spatial variability. *Geophys. Res. Lett.*, **2002**, *29*, doi:10.1029/2001GL013252.

123. Christopher, S.A.; Zhang, J. Shortwave aerosol radiative forcing from MODIS and CERES observations over the oceans. *Geophys. Res. Lett.,* **2002**, *29*, 6-1, **https://doi.org/10.1029/2002GL014803**.

124. Li, R-R.; Kaufman, Y.J.; Gao,B-C.; Davis, C.O. Remote Sensing of Suspended Sediments and Shallow Coastal Waters, *IEEE Trans. Geosci. Rem. Sens.,* **2003**, *41*, 559 - 566, doi: 10.1109/TGRS.2003.810227

125. Koren, I.; Kaufman, Y.J.; Remer, L.A.; Martins, J.V. Measurement of the effect of Amazon smoke on the inhibition of cloud formation. *Science*, **2004**, *303*, 1342-1345, DOI: 10.1126/science.1089424.

126. Kaufman, Y.J.; Remer, L.A.; Tanré, D.; Li, R-R.; Kleidman, R.; Mattoo, S.; Levy, R.C.; Eck, T.F.; Holben, B.N.; Ichoku, C.; Martins, J.V.; Koren, I. A critical examination of the residual cloud contamination and diurnal sampling effects on MODIS estimates of aerosol over ocean.   *IEEE Trans. Geosci. Rem. Sens.,* **2005**, *43*, 12, 2886-2897, doi: 10.1109/TGRS.2005.858430.

127. Li, R.-R.; Remer, L.; Kaufman, Y. J.; Mattoo, S.; Gao, B.-C.; Vermote, E. Snow and ice mask for the MODIS aerosol products. *IEEE Geosc.i Rem. Sens. Lett.,* **2005**, *2*, 306-310, doi: 10.1109/LGRS.2005.847755.

128. Wang, J. ; Christopher, S.A. Intercomparison between satellite-derived aerosol optical thickness and PM2. 5 mass: Implications for air quality studies. *Geophys. Res. Lett.,* **2003**, *30*, 2095, doi:10.1029/2003GL018174.

129. Chu, D. A.; Kaufman, Y. J.; Zibordi, G.; Chern, J. D.; Mao, J.; Li, C.; Holben, B. N. Global monitoring of air pollution over land from the Earth Observing System-Terra Moderate Resolution Imaging Spectroradiometer (MODIS), *J. Geophys. Res.-Atmos.,* **2003**, *108*, 4661, doi:10.1029/2002JD003179.

130. Al-Saadi, J., and Coauthors. Improving National Air Quality Forecasts with Satellite Aerosol Observations. *Bull. Amer. Meteor. Soc* **2005.**, *86*, 1249-1262, https://doi.org/10.1175/BAMS-86-9-1249.

131. Zhang, J.; Reid, J.S.; Westphal, D.L.,; Baker, N.L.; Hyer, E.J. A system for operational aerosol optical depth data assimilation over global oceans. *J. Geophys. Res. Atmos.,* **2008**, *113,* D10208, doi:10.1029/2007JD009065.

132. Benedetti, A.; Morcrette, J.J.; Boucher, O.; Dethof, A.; Engelen, R.J.; Fisher, M.; Flentje, H.; Huneeus, N.; Jones, L.; Kaiser, J.W.; Kinne, S. Aerosol analysis and forecast in the European centre for medium-range weather forecasts integrated forecast system: 2. Data assimilation. *J. Geophys. Res.: Atmos.,* **2009** *114*, D13205, doi:10.1029/2008JD011115.

133. Gao, B-C.; Goetz, A.F.H.; Wiscombe, W.J. Cirrus cloud detection from Airborne Imaging Spectrometer data using the 1.38 μm water vapor band. *Geophys. Res. Lett.,* **1993**, *20*, 301-304, https://doi.org/10.1029/93GL00106

134. Gao, B.C. ; Kaufman, Y.J.. Selection of the 1.375-μm MODIS channel for remote sensing of cirrus clouds and stratospheric aerosols from space. *J. Atmos. Sci.* **1995,** *52*, 4231-4237, https://doi.org/10.1175/1520-0469(1995)052<4231:SOTMCF>2.0.CO;2

135. Gao, B.C.; Kaufman, Y.J.; Tanre, D. ; Li, R.R. Distinguishing tropospheric aerosols from thin cirrus clouds for improved aerosol retrievals using the ratio of 1.38-μm and 1.24-μm channels. *Geophys. Res. Lett.,* **2002**, *29*, 36-1, https://doi.org/10.1029/2002GL015475

1778 136. Gao, B-C.; Li, R.-R. Removal of Thin Cirrus Scattering Effects in Landsat 8 OLI Images Using
1779   the Cirrus Detecting Channel. *Rem. Sens.*, **2017**, *9*, 834, doi:10.3390/rs9080834

1780 137. Remer, L. A.; Mattoo, S.; Levy, R. C.; Heidinger, A.; Pierce, R. B.,; Chin, M. Retrieving aerosol
1781   in a cloudy environment: aerosol product availability as a function of spatial resolution.
1782   *Atmos. Meas. Tech.*, **2012**, *5*, 1823–1840, https://doi.org/10.5194/amt-5-1823-2012.

1783 138. Zhang, J.; Reid, J.S.; Holben, B.N. An analysis of potential cloud artifacts in MODIS over
1784   ocean aerosol optical thickness products. *Geophys. Res. Lett.*, **2005**, *32*, L15803,
1785   doi:10.1029/2005GL023254.

1786 139. Shi, Y.; Zhang, J.; Reid, J.S.; Holben, B.; Hyer, E.J.; Curtis, C. An analysis of the collection 5
1787   MODIS over-ocean aerosol optical depth product for its implication in aerosol
1788   assimilation. *Atmos. Chem. Phys.*, **2011**, *11*, 557–565, doi: 10.5194/acp-11-557-2011.

1789 140. Remer, L.A.; Kleidman, R.G.; Levy, R.C.; Kaufman, Y.J.; Tanré, D.; Mattoo, S.; Martins, J.V.;
1790   Ichoku, C.; Koren, I.; Yu, H.; Holben, B.N. Global aerosol climatology from the MODIS
1791   satellite sensors, *J. Geophys. Res.*, **2008**, *113*, D14S07, doi:10.1029/2007JD009661.

1792 141. Wen, G.; Marshak, A.; Cahalan, R. F.; Remer, L. A.; Kleidman, R. G. 3D aerosol-cloud
1793   radiative interaction observed in collocated MODIS and ASTER images of cumulus cloud
1794   fields. *J. Geophys. Res.*, **2007**, *112*, D13204, doi:10.1029/2006JD008267.

1795 142. Várnai, T.;Marshak, A. MODIS observations of enhanced clear sky reflectance near
1796   clouds. *Geophys. Res. Lett.*, **2009**, *36*, L06807, doi:10.1029/2008GL037089.

1797 143. Koren, I.; Remer, L. A.; Kaufman, Y. J.; Rudich, Y.; Martins, J. V. On the twilight zone
1798   between clouds and aerosols. *Geophys. Res. Lett.*, **2007**, *34*, L08805, doi:10.1029/2007GL029253.

1799 144. Charlson, R.J.; Ackerman, A.S.; Bender, F.A-M.; Anderson, T.L.; Liu, Z.   On the climate
1800   forcing consequences of the albedo continuum between cloudy and clear air. *Tellus B: Chem.*
1801   *Phys. Meteorol.*, **2007**, *59*, 715-727, DOI: 10.1111/j.1600-0889.2007.00297.x

1802 145. Spencer, R. S.; Levy, R. C.; Remer, L. A.; Mattoo, S.; Arnold, G. T.; Hlavka, D. L.; et al.
1803   Exploring aerosols near clouds with high-spatial-resolution aircraft remote sensing during
1804   SEAC[4]RS. *J. Geophys. Res. Atmos.*, **2019**,
1805   *124*, 2148– 2173, https://doi.org/10.1029/2018JD028989.

1806 146. Kleidman, R. G.; Smirnov, A.; Levy, R. C.; Mattoo, S.; Tanre, D. Evaluation and Wind Speed
1807   Dependence of MODIS Aerosol Retrievals Over Open Ocean. *IEEE Trans. Geosci. Rem. Sens.*,
1808   **2012**, *50*, 429– 435, doi:10.1109/TGRS.2011.2162073.

1809 147. Sayer, A. M.; Munchak, L. A.; Hsu, N. C.; Levy, R. C.; Bettenhausen, C.; Jeong, M.-J. MODIS
1810   Collection 6 aerosol products: Comparison between Aqua's e-Deep Blue, Dark Target, and
1811   "merged" data sets, and usage recommendations, *J. Geophys. Res. Atmos.*,
1812   **2014**, *119*, 13,965– 13,989, doi:10.1002/2014JD022453.

1813 148. Levy, R.C.; Munchak, L.A. ; Mattoo, S. ;   Patadia, F. ; Remer, L.A.; Holz, R.E.   Towards a
1814   long-term global aerosol optical depth record: applying a consistent aerosol retrieval
1815   algorithm to MODIS and VIIRS-observed reflectance. *Atmos. Meas. Tech.*, **2015**. *8*, 4083-
1816   4110, doi: 10.5194/amt-8-4083-2015.

1817 149. Gupta, P.; Levy, R. C.; Mattoo, S.,; Remer, L. A.; Holz, R. E.; Heidinger, A. K. Applying the
1818   Dark Target aerosol algorithm with Advanced Himawari Imager observations during the
1819   KORUS-AQ field campaign, *Atmos. Meas. Tech.*, **2019**,   *12*, 6557–6577,
1820   https://doi.org/10.5194/amt-12-6557-2019.

150. Remer, L.A.; Kaufman, Y.J.; Kleidman, R.G. Comparison of Three Years of Terra and Aqua MODIS Aerosol Optical Thickness Over the Global Oceans. *IEEE Geosci. Rem. Sens. Lett.*, **2006**, *3*, 537-540, doi: 10.1109/LGRS.2006.879562.

151. Cox, C.; Munk, W. Measurement of the Roughness of the Sea Surface from Photographs of the Sun's Glitter. *J. Opt. Soc. Am.*, **1954**, *44*, 838-850, •https://doi.org/10.1364/JOSA.44.000838

152. Hsu, N.C.; Tsay, S.C.; King, M.D.; Herman, J.R. Deep blue retrievals of Asian aerosol properties during ACE-Asia. *IEEE Trans. Geosci. Rem. Sens.*, **2006**, *44*, 3180-3195, doi: 10.1109/TGRS.2006.879540.

153. Dark Target Aerosol Retrieval Algorithm: ATBD Land Algorithm, Available on-line at https://darktarget.gsfc.nasa.gov/atbd/land-algorithm. Accessed: 28 July 2020.

154. Shi, Y.R.; Levy, R.C.; Eck, T.F.; Fisher, B.; Mattoo, S.; Remer, L.A.; Slutsker, I; Zhang, J. Characterizing the 2015 Indonesia fire event using modified MODIS aerosol retrievals. *Atmos. Chem. Phys.*, **2019**, *19*, 259–274, https://doi.org/10.5194/acp-19-259-2019.

155. Barnes, W.L; Pagano, T. S.; Salomonson, V. V. Prelaunch characteristics of the Moderate Resolution Imaging Spectroradiometer (MODIS) on EOS-AM1. *IEEE Trans. Geo. Rem. Sens.* **1998**, *36*, 1088-1100, doi: 10.1109/36.700993.

156. Xiong, X.; Chiang, K,; Esposito, J.; Guenther, B.; Barnes, W. MODIS on-orbit calibration and characterization. *Metrologia*, **2003**, *40*, S89, https://doi.org/10.1088/0026-1394/40/1/320.

157. Lyapustin, A.; Wang, Y.; Xiong, X.; Meister, G.; Platnick, S.; Levy, R.; Franz, B.; Korkin, S.; Hilker, T.; Tucker, J.,; Hall, F.; Sellers, P.,; Wu, A.; Angal, A. Scientific impact of MODIS C5 calibration degradation and C6+ improvements,. *Atmos. Meas. Tech.*, **2014**, *7*, 4353–4365, https://doi.org/10.5194/amt-7-4353-2014.

158. Sun, J.; Angal, A.; Xiong, X.; Chen, H.; Geng, X.; Wu, A.; Choi, T.; Chu, M. MODIS reflective solar bands calibration improvements in Collection 6. *Earth Observing Missions and Sensors: Development, Implementation, and Characterization II*, **2012**, *8528*, 85280N, https://doi.org/10.1117/12.979733

159. LAADS DAAC. Available on-line at https://ladsweb.modaps.eosdis.nasa.gov. Accessed 18 July 2020.

160. Giovanni The bridge between data and science. Available on-line at https://giovanni.gsfc.nasa.gov/giovanni/. Accessed 18 July 2020.

161. Earth Observatory. Available on-line at https://earthobservatory.nasa.gov. Accessed 18 July 2020.

162. Earth observation data. Available on-line at https://earthdata.nasa.gov/earth-observation-data. Accessed 18 July 2020.

163. World View. Available on-line at https://worldview.earthdata.nasa.gov. Accessed 18 July 2020.

164. Levy, R. C.; Pinker, R. T. Remote Sensing of Spectral Aerosol Properties: A Classroom Experience. *Bull. Amer. Meteor. Soc.*, **2007**, *88*, 25–30, doi:10.1175/BAMS-88-1-25.

165. Zhang, J.; Christopher, S.A. Longwave radiative forcing of Saharan dust aerosols estimated from MODIS, MISR, and CERES observations on Terra. *Geophys. Res. Lett.*, **2003**, *30*, 2188, doi:10.1029/2003GL018479, 23.

1862 166. Li, F.; Vogelmann, A.M.; Ramanathan, V.   Saharan dust aerosol radiative forcing measured
1863   from space. *J. Climate*,   **2004**, *17*, 2558-2571, doi: 10.1175/1520-
1864   0442(2004)017<2558:SDARFM>2.0.CO;2
1865 167. Ramanathan, V.; Ramana, M.V. Persistent, widespread, and strongly absorbing haze over
1866   the Himalayan foothills and the Indo-Gangetic Plains. *Pure Appl. Geophys.*, **2005**, *162*,1609-
1867   1626, doi: 10.1007/s00024-005-2685-8.
1868 *168.* Satheesh, S.K.; Moorthy, K.K.; Kaufman, Y.J.; Takemura, T. Aerosol optical depth, physical
1869   properties and radiative forcing over the Arabian Sea. *Meteorol. Atmos. Phys.* , **2006**. *91*, 45-62,
1870   doi: 10.1007/s00703-004-0097-4
1871 169. Yu, H.; Dickinson, R. E.; Chin, M.; Kaufman, Y. J.; Zhou, M.; Zhou, L.; Tian, Y.; Dubovik,
1872   O.; Holben, B. N.   Direct radiative effect of aerosols as determined from a combination of
1873   MODIS retrievals and GOCART simulations, *J. Geophys. Res.*,   **2004**,   *109*, D03206,
1874   doi:10.1029/2003JD003914.
1875 170. Yu, H.; Kaufman, Y. J.; Chin, M.; Feingold, G.; Remer, L. A.; Anderson, T. L.; Balkanski, Y.;
1876   Bellouin, N.; Boucher, O.; Christopher, S.; DeCola, P.; Kahn, R.; Koch, D.; Loeb, N.; Reddy,
1877   M. S.; Schulz, M.; Takemura, T.; Zhou, M. A review of measurement-based assessment of the
1878   aerosol direct radiative effect and forcing., *Atmos. Chem . Phys.*, **2006**, *6*, 613-
1879   666, https://doi.org/10.5194/acp-6-613-2006
1880 171. Zhang, J.; Christopher, S. A.; Remer, L. A.,;Kaufman, Y. J.   Shortwave aerosol radiative
1881   forcing over cloud-free oceans from Terra: 2. Seasonal and global distributions, *J. Geophys.
1882   Res.*,   **2005**,   *110*, D10S24, doi:10.1029/2004JD005009.
1883 172. Bellouin, N.; Boucher, O.; Haywood, J.; Reddy, M.S. Global estimate of aerosol direct
1884   radiative forcing from satellite measurements. *Nature*, **2005**, *438*, 1138-1141, doi:
1885   10.1038/nature04348.
1886 173. Abel, S. J.; Highwood, E. J.;, Haywood, J. M.; and Stringer, M. A. The direct radiative effect
1887   of biomass burning aerosols over southern Africa. *Atmos. Chem. Phys.* **2005**, *5*, 1999–2018.
1888   https://doi.org/10.5194/acp-5-1999-2005.
1889 174. Loeb, N.G.; Manalo-Smith, N. Top-of-Atmosphere Direct Radiative Effect of Aerosols over
1890   Global Oceans from Merged CERES and MODIS Observations. *J. Climate,* **2005**, *18*, 3506–
1891   3526, doi:10.1175/JCLI3504.1
1892 175. Chung, C. E.; Ramanathan, V.; Kim, D.; Podgorny, I. A.   Global anthropogenic aerosol
1893   direct forcing derived from satellite and ground-based observations, *J. Geophys.
1894   Res.*, 2005, *110*, D24207, doi:10.1029/2005JD006356.
1895 176. Quaas, J.; Boucher, O.; Bellouin, N.;Kinne, S.   Satellite-based estimate of the direct and
1896   indirect aerosol climate forcing. *J. Geophys. Res.*, **2008**, *113*, D05204,
1897   doi:10.1029/2007JD008962.
1898 177. Kinne, S., et al. Monthly averages of aerosol properties: A global comparison among models,
1899   satellite data, and AERONET ground data, *J. Geophys. Res.*, **2003**, *108*, 4634,
1900   doi:10.1029/2001JD001253.
1901 178. Reddy, M. S.; Boucher, O.; Bellouin, N.; Schulz, M.; Balkanski, Y.; Dufresne, J.-L.; Pham,
1902   M.   Estimates of global multicomponent aerosol optical depth and direct radiative
1903   perturbation in the Laboratoire de Météorologie Dynamique general circulation model, *J.
1904   Geophys. Res.*,   **2005**,   *110*, D10S16, doi:10.1029/2004JD004757.

179. Quaas, J.; Boucher, O. Constraining the first aerosol indirect radiative forcing in the LMDZ GCM using POLDER and MODIS satellite data. *Geophys. Res. Lett.*, **2005**, *32*, L17814, doi:10.1029/2005GL023850.

180. Bellouin, N.; Jones, A.; Haywood, J.; Christopher, S. A. Updated estimate of aerosol direct radiative forcing from satellite observations and comparison against the Hadley Centre climate model. *J. Geophys. Res.*, **2008**, *113*, D10205, doi:10.1029/2007JD009385.

181. Bellouin, N.; Quaas, J.; Gryspeerdt, E.;, Kinne, S.; Stier, P.; Watson-Parris, D.; et al. Bounding global aerosol radiative forcing of climate change. *Reviews of Geophysics*, **2020**, *58*, e2019RG000660. https://doi.org/10. 1029/2019RG000660

182. Stier, P.; Feichter, J.; Kinne, S.; Kloster, S.; Vignati, E.; Wilson, J.; Ganzeveld, L.; Tegen, I.; Werner, M.; Balkanski, Y.; Schulz, M. The aerosol-climate model ECHAM5-HAM. *Atmos. Chem. Phys.*, **2005**. *5*, 1125-1156, https://doi.org/10.5194/acp-5-1125-2005.

183. Ramanathan, V., et al. Atmospheric brown clouds: Hemispherical and regional variations in long-range transport, absorption, and radiative forcing, *J. Geophys. Res.*, **2007**, *112*, D22S21, doi:10.1029/2006JD008124.

184. Myhre, G.; Berglen, T.F.; Johnsrud, M.; Hoyle, C.; Berntsen, T.K.; Christopher, S.A.; Fahey, D.W.; Isaksen, I.S.; Jones, T.A.; Kahn, R.A.; Loeb, N. Modelled radiative forcing of the direct aerosol effect with multi-observation evaluation. *Atmos. Chem. Phys.*, **2009**, *9*,1365-1392, doi: 10.5194/acp-9-1365-2009.

185. Jaeglé, L.; Quinn, P.K.; Bates, T.S.; Alexander, B.; Lin, J.T. Global distribution of sea salt aerosols: new constraints from in situ and remote sensing observations. *Atmos. Chem. Phys.*, **2011**. *11*, 3137–3157, doi.org/10.5194/acp-11-3137-2011

186. Lu, Z.; Streets, D.G.; Zhang, Q.; Wang, S.; Carmichael, G.R.; Cheng, Y.F.; Wei, C.; Chin, M.; Diehl, T.;Tan, Q. Sulfur dioxide emissions in China and sulfur trends in East Asia since 2000. *Atmos. Chem. Phys,*, **2010**, *10*, 6311–6331, doi:10.5194/acp-10-6311-2010

187. Lu, Z.; Zhang, Q.; Streets, D. G. Sulfur dioxide and primary carbonaceous aerosol emissions in China and India, 1996–2010, *Atmos. Chem. Phys.*, **2011**,*11*, 9839–9864, doi:10.5194/acp-11-9839-2011, 2011.

188. Zhang, K.; O'Donnell, D.; Kazil, J.; Stier, P.; Kinne, S.; Lohmann, U.; Ferrachat, S.; Croft, B.; Quaas, J.; Wan, H,; Rast, S. The global aerosol-climate model ECHAM-HAM, version 2: sensitivity to improvements in process representations. *Atmos. Chem. Phys.*, **2012**, *12*, 8911-8949, https://doi.org/10.5194/acp-12-8911-2012

189. Shindell, D. T.; Lamarque, J.-F.; Schulz, M.; Flanner, M.; Jiao, C.; Chin, M.; Young, P. J.; Lee, Y. H.; Rotstayn, L.; Mahowald, N.; Milly, G.; Faluvegi, G.; Balkanski, Y.; Collins, W. J.; Conley, A. J.; Dalsoren, S.; Easter, R.; Ghan, S.; Horowitz, L.; Liu, X.; Myhre, G.; Nagashima, T.; Naik, V.; Rumbold, S. T.; Skeie, R.; Sudo, K.; Szopa, S.; Takemura, T.; Voulgarakis, A.; Yoon, J.-H.; Lo, F. Radiative forcing in the ACCMIP historical and future climate simulations. *Atmos. Chem. Phys.*, **2013**, *13*, 2939–2974, https://doi.org/10.5194/acp-13-2939-2013.

190. Chin, M.; Diehl, T.; Tan, Q.; Prospero, J.M.; Kahn, R.A.; Remer, L.A.; Yu, H.; Sayer, A.M.; Bian, H.; Geogdzhayev, I.V.; et al. Multi-decadal aerosol variations from 1980 to 2009: observations and a global model. *Atmos. Chem. Phys.*, **2014** *14*, 3657-3690, DOI: 10.5194/acp-14-3657-2014.

191. Pan, X.; Chin, M.; Gautam, R.; Bian, H.; Kim, D.; Colarco, P.R.; Diehl, T.L.; Takemura, T.; Pozzoli, L.; Tsigaridis, K.; Bauer, S.E. A multi-model evaluation of aerosols over South Asia: common problems and possible causes. *Atmos. Chem. Phys.*, **2015**, *15*, 5903–5928, doi:10.5194/acp-15-5903-2015.

192. Kaufman, Y.J.; Koren, I.; Remer, L.A.; Rosenfeld, D.; Rudich, Y. The effect of smoke, dust, and pollution aerosol on shallow cloud development over the Atlantic Ocean. *Proc. Nat. Acad. Sci.*, **2005**, *102*, 11207-11212; DOI:10.1073/pnas.0505191102

193. Koren, I.; Kaufman, Y. J.; Rosenfeld, D.; Remer, L. A.; Rudich, Y. Aerosol invigoration and restructuring of Atlantic convective clouds. *Geophys. Res. Lett.*, **2005**, *32*, L14828, doi:10.1029/2005GL023187.

194. Koren, I.; Martins, J.V.; Remer, L.A.; Afargan, H. Smoke invigoration versus inhibition of clouds over the Amazon. *Science*, **2008**. *321*, 946-949, doi: 10.1126/science.1159185

195. Koren, I.; Remer, L.A. ; Altaratz, O.; Martins, J.V.; Davidi, A. Aerosol-induced changes of convective cloud anvils produce strong climate warming. *Atmos. Chem. Physics*, **2010**, *10*, 5001-5010, doi.org/10.5194/acp-10-5001-2010

196. Matsui, T.; Masunaga, H.; Kreidenweis, S. M.; Pielke Sr., R. A.; Tao, W.-K.; Chin, M.; Kaufman, Y. J. Satellite-based assessment of marine low cloud variability associated with aerosol, atmospheric stability, and the diurnal cycle, *J. Geophys. Res.*, **2006**, *111*, D17204, doi:10.1029/2005JD006097.

197. Chylek, P.; Dubey, M.K.; Lohmann, U.; Ramanathan, V.,; Kaufman, Y.J.; Lesins, G.; Hudson, J.; Altmann, G.; Olsen, S. Aerosol indirect effect over the Indian Ocean. *Geophys. Res. Lett.*, **2006**, *33*, L06806, doi:10.1029/2005GL025397.

198. Myhre, G.; Stordal, F. ; Johnsrud, M.; Kaufman, Y. J.; Rosenfeld, D. et al. Aerosol-cloud interaction inferred from MODIS satellite data and global aerosol models. *Atmos. Chem. Phys.*, **2007**, *7*, 3081-3101, doi: 10.5194/acp-7-3081-2007

199. Yuan, T.,; Li, Z.,; Zhang, R.; Fan, J. Increase of cloud droplet size with aerosol optical depth: An observation and modeling study, *J. Geophys. Res.*, **2008**, *113*, D04201, doi:10.1029/2007JD008632.

200. Yuan, T-L.,; Remer, L.A.; Pickering, K.E.; Yu, H-B. Observational evidence of aerosol enhancement of lightning activity and convective invigoration. *Geophys. Res. Lett*, **2011**, *38*, L04701, DOI: 10.1029/2010GL046052.

201. Yuan, T.,; Remer, L.; Yu, H. Microphysical, macrophysical and radiative signatures of volcanic aerosols in trade wind cumulus observed by the A-Train. *Atmos. Chem. Phys.,* **2011** *11*, 7119-7132, DOI: 10.5194/acp-11-7119-2011.

202. Ten Hoeve, J.E.; Remer, L.A.; Jacobson, M.Z. Microphysical and radiative effects of aerosols on warm clouds during the Amazon biomass burning season as observed by MODIS: impacts of water vapor and land cover. *Atmos. Chem. Phys.*, **2011**, *11*, 3021–3036, https://doi.org/10.5194/acp-11-3021-2011.

203. Manoj, M.G.; Devara, P.C.S.; Safai, P.D.; Goswami, B.N. Absorbing aerosols facilitate transition of Indian monsoon breaks to active spells. *Climate Dynamics*, **2011**, *37*,2181-2198, doi: 10.1007/s00382-010-0971-3.

204. Wang, M.; Ghan, S.; Liu, X.; L'Ecuyer; T.S.; Zhang, K.; Morrison, H.; Ovchinnikov, M.; Easter, R.; Marchand, R.; Chand, D.; Qian, Y.; Penner, J.E. Constraining cloud lifetime

effects of aerosols using A-Train satellite measurements. *Geophys. Res. Lett*, **2012**, *39*, L15709, doi:10.1029/2012GL052204.

205. Costantino, L.; Bréon, F.M. Aerosol indirect effect on warm clouds over South-East Atlantic, from co-located MODIS and CALIPSO observations. *Atmos. Chem. Phys*, **2013**, *13*, 69-88. doi;10.5194/acp-13-69-2013.

206. Solomon, S.; Qin, D.; Manning, M.; Chen, Z.; Marquis, M.; Averyt, K.B.; Tignor, M.; Miller, H.L. (eds.) Contribution of Working Group I to the Fourth Assessment Report of the Intergovernmental Panel on Climate Change, **2007**. Cambridge University Press, Cambridge, United Kingdom and New York, NY, USA.

207. Boucher, O.; Randall, D.; Artaxo, P.; Bretherton, C.; Feingold, G.; Forster, P.; Kerminen, V.-M.;. Kondo, Y; Liao, H.; Lohmann, U.; Rasch, P.; Satheesh, S.K.; Sherwood, S.; Stevens, B.; Zhang, X.Y. Clouds and Aerosols. In: Climate Change 2013: The Physical Science Basis. Contribution of Working Group I to the *Fifth Assessment Report of the Intergovernmental Panel on Climate Change*. Stocker, T.F.; Qin, D.; Plattner, G.-K.; Tignor, M.; Allen, S.K.; Boschung, J.; Nauels, A.; Xia, Y.; Bex, V.; Midgley, P.M., Eds.,. Cambridge University Press, Cambridge, United Kingdom and New York, NY, USA. 2013.

208. Gao, Y.; Kaufman, Y. J.; Tanré, D.; Kolber, D.; Falkowski, P. G. Seasonal distributions of aeolian iron fluxes to the global ocean. *Geophys. Res. Lett.*, **2001**. *28*, 29–32. https://doi.org/10.1029/2000GL011926.

209. Lin, I-I.; Chen, J-P.; Wong, G.T.F.; Huang, C-W.; Lien, C-C. Aerosol input to the South China Sea: Results from the MODerate Resolution Imaging Spectro-radiometer, the Quick Scatterometer, and the Measurements of Pollution in the Troposphere Sensor, Deep Sea Research Part II: Topical Studies in Oceanography, **2007**, *54*, 1589-1601, doi: 10.1016/j.dsr2.2007.05.013.

210. Yu, H.; Remer, L.A.; Kahn, R.A., Chin, M.; Zhang, .Y. Satellite perspective of aerosol intercontinental transport: From qualitative tracking to quantitative characterization. *Atmos. Res.*, **2013**, *124*, 73-100, DOI: 10.1016/j.atmosres.2012.12.013.

211. Yu, H.; Tan, Q.; Chin, M.; Remer, L. A.; Kahn, R. A.; Bian, H.; et al. Estimates of African dust deposition along the trans-Atlantic transit using the decadelong record of aerosol measurements from CALIOP, MODIS, MISR, and IASI. *J. Geophys. Res. Atmos.*, **2019**, 124, 7975– 7996, https://doi.org/10.1029/2019JD030574.

212. Gassó, S.; Stein, A.; Marino, F.; Castellano, E.; Udisti, R.; Ceratto, J. A combined observational and modeling approach to study modern dust transport from the Patagonia desert to East Antarctica. *Atmos. Chem. Phys.*, **2010**, *10*, 8287–8303, https://doi.org/10.5194/acp-10-8287-2010.

213. Heald, C. L.; Jacob, D. J.; Park, R. J.; Alexander, B.; Fairlie, T. D.; Yantosca, R. M.; Chu, D. A. Transpacific transport of Asian anthropogenic aerosols and its impact on surface air quality in the United States, *J. Geophys. Res.*, **2006**, *111*, D14310, doi:10.1029/2005JD006847.

214. Stohl, A.; Berg, T.; Burkhart, J.F.; Fjæraa, A.M.; Forster, C.; Herber, A.; Hov, Ø.;, Lunder, C.; McMillan, W.W.; Oltmans, S.; Shiobara, M. Arctic smoke record air pollution levels in the European Arctic during a period of abnormal warmth, due to agricultural fires in eastern Europe. *Atmos. Chem. Phys*, **2007**, *7*, 511–534, https://doi.org/10.5194/acp-7-511-2007.

215. Mahowald, N.M.; Engelstaedter, S.; Luo, C.; Sealy, A.; Artaxo, P.; Benitez-Nelson, C.; Bonnet,

S.; Chen, Y.; Chuang, P.Y.; Cohen, D.D.; Dulac, F. Atmospheric iron deposition: global distribution, variability, and human perturbations. *Annual Review of Marine Science*, **2009**, *1*, 245-278, doi: 10.1146/annurev.marine.010908.163727.

216. Ridley, D. A.;Heald, C. L.; Ford, B. North African dust export and deposition: A satellite and model perspective. *J. Geophys. Res.*, **2012**, *117*, D02202, doi:10.1029/2011JD016794.

217. Kim, D., et al. Sources, sinks, and transatlantic transport of North African dust aerosol: A multimodel analysis and comparison with remote sensing data, *J. Geophys. Res. Atmos.*, **2014**, *119*, 6259– 6277, doi:10.1002/2013JD021099.

218. Yu, H.; Yang, Y.; Wang, H.; Tan, Q.; Chin, M.; Levy, R. C.; Remer, L. A.; Smith, S. J.; Yuan, T.; Shi, Y. Interannual variability and trends of combustion aerosol and dust in major continental outflows revealed by MODIS retrievals and CAM5 simulations during 2003– 2017. *Atmos. Chem. Phys.*, **2020**, *20*, 139–161, https://doi.org/10.5194/acp-20-139-2020.

219. Schuerger, A.C.; Smith, D.J.; Griffin, D.W. *et al.* Science questions and knowledge gaps to study microbial transport and survival in Asian and African dust plumes reaching North America. *Aerobiologia,***2018**, *34*, 425–435, https://doi.org/10.1007/s10453-018-9541-7.

220. Engel-Cox, J.A.; Holloman, C.H.; Coutant, B.W.; Hoff, R.M. Qualitative and quantitative evaluation of MODIS satellite sensor data for regional and urban scale air quality. *Atmos. Environ.*, **2004**. *38*, 2495-2509, https://doi.org/10.1016/j.atmosenv.2004.01.039.

221. Edwards, D. P., et al. Observations of carbon monoxide and aerosols from the Terra satellite: Northern Hemisphere variability, *J. Geophys. Res.*, **2004**, *109*, D24202, doi:10.1029/2004JD004727.

222. van Donkelaar, A.; Martin, R. V.; Park, R. J.   Estimating ground-level $PM_{2.5}$ using aerosol optical depth determined from satellite remote sensing, *J. Geophys. Res.*, **2006**, *111*, D21201, doi:10.1029/2005JD006996.

223. Van Donkelaar, A.; Martin, R.V.; Brauer, M.; Kahn, R.; Levy, R.; Verduzco, C.; Villeneuve, P.J. Global estimates of ambient fine particulate matter concentrations from satellite-based aerosol optical depth: development and application. *Environ. Health Persp.*, **2010**. *118*, 847-855,   DOI: 10.1289/ehp.0901623.

224. Van Donkelaar, A.; Martin, R.V.; Brauer, M.; Hsu, N.C.; Kahn, R.A.; Levy, R.C.; Lyapustin, A.; Sayer, A.M.; Winker, D.M. Global estimates of fine particulate matter using a combined geophysical-statistical method with information from satellites, models, and monitors. *Environ. Sci. Tech.*, **2016**, *50*, 3762-3772, https://doi.org/10.1021/acs.est.5b05833.

225. . Koelemeijer, R.B.A.; Homan, C.D.; Matthijsen, J. Comparison of spatial and temporal variations of aerosol optical thickness and particulate matter over Europe. *Atmos. Environ.*, **2006**. *40*, 5304-5315, doi.org/10.1016/j.atmosenv.2006.04.044.

226. Engel-Cox, J.A.; Hoff, R.M.; Rogers, R.; Dimmick, F.; Rush, A.C.; Szykman, J.J.;, Al-Saadi, J.; Chu, D.A.; Zell, E.R. Integrating lidar and satellite optical depth with ambient monitoring for 3-dimensional particulate characterization. *Atmos. Environ.*, **2006**, *40*, 8056-8067.

227. Gupta, P.; Christopher, S.A.; Wang, J.; Gehrig, R.,; Lee, Y.C. ; Kumar, N. Satellite remote sensing of particulate matter and air quality assessment over global cities. *Atmos. Environ.*, **2006**, *40*, 5880-5892.

228. Kumar, N.; Chu, A.; Foster, A. An empirical relationship between PM2. 5 and aerosol optical depth in Delhi Metropolitan. *Atmos. Environ.*, **2007**. *41*, 4492-4503, doi: 10.1016/j.atmosenv.2007.01.046.

229. Schaap, M.; Apituley, A.; Timmermans, R.M.A.; Koelemeijer, R.B.A.; De Leeuw, G. Exploring the relation between aerosol optical depth and PM 2.5 at Cabauw, the Netherlands. *Atmos. Chem. Phys.*, **2009**, *9*, 909–925, 10.5194/acp-9-909-2009.

230. Guo, J.P.; Zhang, X.Y.; Che, H.Z.;, Gong, S.L.;, An, X.; Cao, C.X.; Guang, J.; Zhang, H.; Wang, Y.Q.; Zhang, X.C.; Xue, M. Correlation between PM concentrations and aerosol optical depth in eastern China. *Atmos. Environ.*, **2009**, *43*, 5876-5886.

231. Gupta, P.; Christopher, S. A. Particulate matter air quality assessment using integrated surface, satellite, and meteorological products: Multiple regression approach, *J. Geophys. Res.*, **2009**, *114*, D14205, doi:10.1029/2008JD011496.

232. Gupta, P.; Christopher, S. A. Particulate matter air quality assessment using integrated surface, satellite, and meteorological products: 2. A neural network approach, *J. Geophys. Res.*, **2009**, *114*, D20205, doi:10.1029/2008JD011497.

233. Zhang, H.; Hoff, R.M.; Engel-Cox, J.A. The relation between Moderate Resolution Imaging Spectroradiometer (MODIS) aerosol optical depth and PM2. 5 over the United States: a geographical comparison by US Environmental Protection Agency regions. *J. Air Waste Man. Assoc.*, **2009**, *59*, 1358-1369, https://doi.org/10.3155/1047-3289.59.11.1358.

234. Wang, Z.; Chen, L.; Tao, J.; Zhang, Y.; Su, L. Satellite-based estimation of regional particulate matter (PM) in Beijing using vertical-and-RH correcting method. *Rem. Sens. Environ.*, **2010**, *114*, 50-63, https://doi.org/10.1016/j.rse.2009.08.009.

235. Lee, J.; Kim, J.; Song, C. H.; Ryu, J. H.; Ahn, Y. H.; Song, C. K. Algorithm for retrieval of aerosol optical properties over the ocean from the Geostationary Ocean Color Imager. *Rem. Sens. Environ.*, **2010**, *114*, 1077-1088, doi: 10.1109/IGARSS.2016.7730061.

236. Philip, S.; Martin, R.V.; van Donkelaar, A.; Lo, J.W.H.; Wang, Y.; Chen, D.; Zhang, L.; Kasibhatla, P.S.; Wang, S.; Zhang, Q.; Lu, Z. Global chemical composition of ambient fine particulate matter for exposure assessment. *Environ. Sci. Tech.*, **2014**, *48*, 13060-13068, doi: 10.1021/es502965b

237. Xin, J.; Zhang, Q.; Wang, L.; Gong, C.; Wang, Y.; Liu, Z.; Gao, W. The empirical relationship between the PM2. 5 concentration and aerosol optical depth over the background of North China from 2009 to 2011. *Atmos. Res.*, **2014**, *138*, 179-188, https://doi.org/10.1016/j.atmosres.2013.11.001.

238. McClure, C. D.; Jaffe, D.A. US particulate matter air quality improves except in wildfire-prone areas. *Proc. Nat. Acad. Sci.*, **2018**, *115*, 7901-7906; DOI:10.1073/pnas.1804353115.

239. Lahoz, W. A.; Schneider, P. Data assimilation: making sense of Earth Observation. *Frontiers Environ. Sci.*, **2014**, *2*, 16, DOI=10.3389/fenvs.2014.00016.

240. Hyer, E.J.; Reid, J.S. ; Zhang, J. An over-land aerosol optical depth data set for data assimilation by filtering, correction, and aggregation of MODIS Collection 5 optical depth retrievals. *Atmos. Meas. Tech*, **2011**, *4*, 379-408, https://doi.org/10.5194/amt-4-379-2011.

241. Liu, Z.; Liu, Q.; Lin, H.-C.; Schwartz, C. S.; Lee, Y.-H.; Wang, T. Three-dimensional variational assimilation of MODIS aerosol optical depth: Implementation and application to a dust storm over East Asia, *J. Geophys. Res.*, **2011**, *116*, D23206, doi:10.1029/2011JD016159.

242. Schutgens, N.A.J.; Miyoshi, T.; Takemura, T.; Nakajima, T. Applying an ensemble Kalman filter to the assimilation of AERONET observations in a global aerosol transport model. *Atmos. Phys. Chem.*, **2010**, *10*, 2561–2576, doi: 10.5194/acp-10-2561-2010.

243. Huneeus, N.; Chevallier, F.; Boucher, O. Estimating aerosol emissions by assimilating observed aerosol optical depth in a global aerosol model. *Atmos. Chem. Phys.*, **2012**,*12*, 4585–4606, https://doi.org/10.5194/acp-12-4585-2012.

244. Lynch, P.; Reid, J. S.; Westphal, D. L.; Zhang, J.; Hogan, T. F.; Hyer, E. J.; Curtis, C. A.; Hegg, D. A.; Shi, Y.; Campbell, J. R.; Rubin, J. I.; Sessions, W. R.; Turk, F. J.; Walker, A. L. An 11-year global gridded aerosol optical thickness reanalysis (v1.0) for atmospheric and climate sciences. *Geosci. Model Dev.*, **2016**, *9*, 1489–1522, doi:10.5194/gmd-9-1489-2016, 2016.

245. Gelaro, R. and Coauthors. The Modern-Era Retrospective Analysis for Research and Applications, Version 2 (MERRA-2). *J. Climate*, **2017**, *30*, 5419–5454, https://doi-org.proxy-bc.researchport.umd.edu/10.1175/JCLI-D-16-0758.1.

246. Vermote, E. F.; El Saleous, N.; Justice, C. O.; Kaufman, Y. J.; Privette, J. L.; Remer, L.; Roger, J. C.; Tanré, D. Atmospheric correction of visible to middle-infrared EOS-MODIS data over land surfaces: Background, operational algorithm and validation, *J. Geophys. Res.*, **1997**, *102*, 17131– 17141, doi:10.1029/97JD00201.

247. Vermote, E. F.; El Saleous, N. Z.; Justice, C. O. Atmospheric correction of MODIS data in the visible to middle infrared: first results, *Rem. Sens. Environ.*, **2002**, *83*, 97-111, doi: 10.1016/S0034-4257(02)00089-5.

248. Vermote, E. F.; Kotchenova, S. Atmospheric correction for the monitoring of land surfaces. *J. Geophys. Res.*, **2008**, *113*, D23S90, doi:10.1029/2007JD009662.

249. Vermote, E.; Justice, C. ; Claverie, M. Preliminatry analysis of the performance of the Landsat 8/OLI land surface reflectance product. *Rem. Sens. Environ.*, **2016**, *185*, 46-56, https://doi.org/10.1016/j.rse.2016.04.008.

250. Veefkind, J.P.; De Leeuw, G. ; Durkee, P.A. Retrieval of aerosol optical depth over land using two-angle view satellite radiometry during TARFOX. *Geophys. Res. Lett.*, 1998, *25*, 3135-3138, doi:10.1029/98GL02264.

251. Gonzalez, C.R.,; Veefkind, J.P. ; de Leeuw, G. Aerosol optical depth over Europe in August 1997 derived from ATSR-2 data. *Geophys. Res. Lett.*, **2000**, *27*, 955-958, doi:10.1029/1999GL010962.

252. Holzer-Popp, T.; Schroedter, M.; Gesell, G. Retrieving aerosol optical depth and type in the boundary layer over land and ocean from simultaneous GOME spectrometer and ATSR-2 radiometer measurements, 1, Method description. *J. Geophys. Res.*, **2002**, *107*, 4578, doi:10.1029/2001JD002013.

253. Kim, M.; Kim, J.; Jeong, U.; Kim, W.; Hong, H.; Holben, B.; Eck, T. F.; Lim, J. H.; Song, C. K.; Lee, S.; Chung, C.-Y. Aerosol optical properties derived from the DRAGON-NE Asia campaign, and implications for a single-channel algorithm to retrieve aerosol optical depth in spring from Meteorological Imager (MI) on-board the Communication, Ocean, and Meteorological Satellite (COMS). *Atmos. Chem. Phys.*, **2016**, *16*, 1789–1808, doi.org/10.5194/acp-16-1789-2016.

254. Lee, H.J.; Liu, Y., Coull, B.A.; Schwartz, J.; Koutrakis, P. A novel calibration approach of MODIS AOD data to predict PM 2.5 concentrations. *Atmos. Chem. Phys.*, **2011** *11*, doi:

2161   10.5194/acp-11-7991-2011.

2162   255. Choi, M.; Kim, J.,; Lee, J.; Kim, M.; Park, Y.-J.; Jeong, U.; Kim, W.; Hong, H.; Holben, B.; Eck,

2163   T. F.; Song, C. H.; Lim, J.-H.; Song, C.-K. GOCI Yonsei Aerosol Retrieval (YAER) algorithm

2164   and validation during the DRAGON-NE Asia 2012 campaign. *Atmos. Meas. Tech.*, **2016,** *9*,

2165   1377–1398, https://doi.org/10.5194/amt-9-1377-2016.

2166   256. Choi, M.; Kim, J.; Lee, J.; Kim, M.; Park, Y. J.; Holben, B.; Song, C. H. GOCI Yonsei aerosol

2167   retrieval version 2 products: an improved algorithm and error analysis with uncertainty

2168   estimation from 5-year validation over East Asia. *Atmos. Meas. Tech.*, **2018**,*11*, 385–408,

2169   https://doi.org/10.5194/amt-11-385-2018.

2170   257. Lim, H.; Choi, M.; Kim, J.; Kasai, Y.; Chan, P. W. AHI/Himawari-8 Yonsei aerosol retrieval

2171   (YAER): Algorithm, validation and merged products. *Rem. Sens.*, **2018**, *10*, 699 doi:

2172   10.3390/rs10050699

2173   258. Kim, J.; Yoon, J.-M. ; Ahn, M. H. ; Sohn, B. J.; Lim, H. S. Retrieving aerosol optical depth

2174   using visible and mid-IR channels from geostationary satellite MTSAT-1R, *Int. J. Rem.*

2175   *Sens.*, **2008**, *29*, 6181-6192, doi: 10.1080/01431160802175553.

2176   259. Jackson, J. M.; Liu, H. Q. ; Laszlo, I. ;   Kondragunta, S. ;   Remer, L. A. ; Huang, J. F. ;

2177   Huang, H. C.   Suomi-NPP VIIRS aerosol algorithms and data products. *J. Geophys. Res.-*

2178   *Atmos.*, **2013**, *118***,** 12673-12689, doi:10.1002/2013JD020449.

2179   260. Laszlo, I.;   Liu, H. EPS Aerosol Optical Depth (AOD) Algorithm Theoretical Basis

2180   Document. Version 3.0.1 NOAA NESDIS Center for Satellite Applications and Research.

2181   **2016**, Available on-line at

2182   https://www.star.nesdis.noaa.gov/jpss/documents/ATBD/ATBD_EPS_Aerosol_AOD_v3.0.1.

2183   pdf.   Accessed 28 July 2020.

2184   261. Hsu, N. C.; Lee, J.,; Sayer, A. M.; Kim, W.; Bettenhausen, C.;   Tsay, S.-C. VIIRS Deep Blue

2185   aerosol products over land: Extending the EOS long-term aerosol data records. *J.Geophys.*

2186   *Res. Atmos.*, **2019**,*124*, 4026-4053, https://doi.org/10.1029/2018JD029688.

2187   262. Lyapustin, A.; Wang, Y.; Laszlo, I.; Kahn, R.; Korkin, S.; Remer, L.; Levy, R.; Reid, J.

2188   S. Multiangle implementation of atmospheric correction (MAIAC): 2. Aerosol algorithm, *J.*

2189   *Geophys. Res.*, **2011**, *116*, D03211, doi:10.1029/2010JD014986.

2190   263. Holzer-Popp, T.; de Leeuw, G.,; Griesfeller, J.; Martynenko, D.; Klüser, L.; Bevan, S.; Davies,

2191   W.; Ducos, F.; Deuzé, J. L.; Graigner, R. G.; Heckel, A.; von Hoyningen-Hüne W.;

2192   Kolmonen, P.; Litvinov, P.,; North, P.; Poulsen, C. A.; Ramon, D.; Siddans, R.; Sogacheva, L.;,

2193   Tanre, D.; Thomas, G. E.; Vountas, M.; Descloitres, J.,; Griesfeller, J.; Kinne, S.; Schulz, M.;

2194   Pinnock, S. Aerosol retrieval experiments in the ESA aerosol cci project. *Atmos. Meas. Tech.*,

2195   **2013**, *6*, 1919–1957, https://doi.org/10.5194/amt-6-1919-2013.

2196   264. De Leeuw, G.; Holzer-Popp, T.; Bevan, S.; Davies, W.H.; Descloitres, J.; Grainger, R.G.;

2197   Griesfeller, J.; Heckel, A.; Kinne, S.; Klüser, L.; Kolmonen, P. Evaluation of seven European

2198   aerosol optical depth retrieval algorithms for climate analysis. *Rem. Sens.   Environ.*, **2015**,*162*,

2199   295-315. https://doi.org/10.1016/j.rse.2013.04.023.

2200   265. Herman, M.; Deuze, ́ J.-L.; Marchant, A.; Roger, B.,; Lallart, P. Aerosol remote sensing from

2201   POLDER/ADEOS over the ocean: Improved retrieval using a nonspherical particle model. *J.*

2202   *Geophys. Res.*, **2005**, *110*, D10S02, doi:10.1029/2004JD004798.

266. Tanre ́,D.; Breón,F.M.; Deuze ́,J.L.; Dubovik,O.; Ducos,F.;   Francois, P.; Goloub, P.; Herman, M.; Lifermann, A.; Waquet, F. Remote sensing of aerosols by using polarized, directional and spectral measurements within the A-Train: the PARASOL mission. *Atmos. Meas. Tech.*, **2011**, *4*, 1383–1395, https://doi.org/10.5194/amt-4-1383-2011.

267. Torres, O.; Tanskanen, A.; Veihelmann, B.; Ahn, C.; Braak, R.; Bhartia, P. K.; Veefkind, P.; Levelt, P.   Aerosols and surface UV products from Ozone Monitoring Instrument observations: An overview, *J. Geophys. Res.*,   **2007**,   *112*, D24S47, doi:10.1029/2007JD008809.

268. Huang, J.; Laszlo, I.; Remer, L.A.;, Liu, H.; Zhang, H.; Ciren, P.; Kondragunta, S. Screening for snow/snowmelt in SNPP VIIRS aerosol optical depth algorithm. *Atmos. Meas. Tech.*, **2018**, *11*, 5813–5825, doi: 10.5194/amt-11-5813-2018.

269. Schmit, T. J.; Gunshor, M. M.; Menzel, W. P. ; Gurka, J. J.; Li, J.; Bachmeier, A. S. Introducing the next-generation Advanced Baseline Imager on GOES-R. *Bull. Amer. Meteor. Soc.*, **2005**, *86*, 1079–1096, https://doi.org/10.1175/BAMS-86-8-1079.

270. Werdell, P.J.; Behrenfeld, M.J.;   Bontempi, P.S.; Boss, E.; Cairns, B.; Davis, G.T.;   Franz, B.A.; Gliese, U.B.; Gorman, E.T.; Hasekamp, O.; Knobelspiesse, K.D.; Mannino, A.; Martins, J.V.; McClain, C.R.;   Meister, G.; Remer, L.A. The Plankton, Aerosol, Cloud, ocean Ecosystem (PACE) mission: Status, science, advances. *Bull. Amer. Meteor. Soc.*, **2019**, *100*, 1775-1794, doi:10.1175/BAMS-D-18-0056.1.

271. Zhou, Y., R. Levy, L. Remer, S. Mattoo, Yingxi Shi, Chengxi Wang (2020), Dust aerosol retrieval over the oceans with the MODIS/VIIRS Dark Target algorithm. Part I: Dust detection. Earth and Space Science, in review

272. Zhou, Y., R. Levy, L. Remer, S. Mattoo, R. Espinosa (2020), Dust aerosol retrieval over the oceans with the MODIS/VIIRS Dark Target algorithm. Part II: Non-spherical dust model, Earth and Space Science, in review.